RENEWABLE FEEDSTOCKS TOWARDS A SUSTAINABLE FUTURE FOR POLYMERS

A DISSERTATION
SUBMITTED TO THE FACULTY OF
THE UNIVERSITY OF MINNESOTA
BY

HUSSNAIN SAJJAD

IN PARTIAL FULFILLMENT OF THE REQUIREMENTS
FOR THE DEGREE OF
DOCTOR OF PHILOSOPHY

THERESA M. REINEKE & WILLIAM B. TOLMAN, ADVISORS

February 2021

Acknowledgements

I would first like to extend my sincere gratitude to my advisors, Profs. Theresa Reineke and Bill Tolman. Theresa, for always being a kind and encouraging mentor who offers unrestrictive freedom of exploration to her students; and Bill, for leading by example when it comes to thinking like a scientist and "digging deep" in order to find solutions to tough problems. Next, I would like to thank Prof. Tom Hoye, David Giles, Prof. Jane Wissinger, Letitia Yao, and Prof. Chris Ellison for their helpful feedback and mentorship, both in formal and informal ways, which has helped me immensely throughout this program.

Graduate school would have felt incomplete without the friends and acquaintances I have made along the way. I especially am grateful to the past and present members of the Reineke and Tolman groups for their scientific and non-scientific conversations, encouragement and assistance during times when obstacles seem impassable, and for the countless positive memories I have gained over the years. I am grateful to all my friends, mentors, peers, and collaborators who have been a part of my scientific journey thus far.

Furthermore, my family, especially my parents, has never wavered in their support for me. I thank them for the inspiration, encouragement, and motivation they have unconditionally provided to me.

Of course, the research I have performed would not have been possible without funding from the Department of Chemistry, the Graduate Program at The University of Minnesota, and the NSF Center for Sustainable Polymers. Cheers to new scientific discoveries!

Abstract

Biomass has tremendous potential to serve as a sustainable replacement for the limited resources we currently exploit to manufacture polymeric materials. Identifying and testing novel, renewable feedstocks for polymer synthesis is a grand challenge which the topic of this thesis aims to address. The first area of research focuses on utilizing fatty acid derivatives and bio-derivable triacetic acid lactone to produce new acrylic triblock copolymers for pressure-sensitive adhesives. The findings reveal that it is possible to utilize renewable, long-chained alkyl-acrylates with high M_e to create useful elastomers. The second area of reach explores the ring opening polymerizations of di-substituted valerolactones derived from triacetic acid lactone. The findings provide valuable insights towards the thermodynamics and kinetics of polymerization of substituted valerolactones. Finally, the third area of research details the synthesis of novel anhydride-like monomers obtained from bio-derived itaconic acid. The monomers were polymerized via photoinitiated thiol-ene chemistry to obtain thermosets that were found to be degradable in aqueous environments.

Table of Contents

List of Tables

List of Figures

List of Schemes

Abbreviations

%	Percent
°C	Degrees Celsius
AcLa	Acrylated Lactone
AcPy	Acrylated Pyrone
AIBN	Azobis(Isobutyronitrile)
AMM	Activated Monomer Mechanism
BCE	Before Common Era
BnOH	Benzyl Alcohol
BTCBA	3,5-Bis(2-Dodecylthiocarbonothioylthio-1-Oxopropoxy)Benzoic Acid
CDCl3	Deuterated Chloroform
cm	Centimeter
CNTs	Carbon Nano Tubes
CPD	Cyclopentadiene
CPP	1,3-Bis(P-Carboxyphenoxy)Propane
CSP	Center For Sustainable Polymers
CTA	Chain Transfer Agent
Đ	Dispersity
DBU	1,8-Diazabicyclo[5.4.0]Undec-7-Ene
DI	Deionized
DMA	Dynamic Mechanical Anlysis
DMAP	4-(Dimethylamino)Pyridine
DMF	Dimethyl Formamide
DPEHMP	Dipentaerythritol Hexakis(3-Mercaptopropionate)
DPP diphenyl phosphate	Diphenyl Phosphate
DSC	Differential Scanning Calorimetry
E	Young's Modulus
E'	Plateau Modulus
EPR	Electron Paramagnetic Resonance
FT-IR	Fourier-Transform Infrared
g	Gram
G'	Storage Modulus
G"	Loss Modulus
G^0_N	Plateau Modulus
Gsm	Grams Per Square Inch
h	Hour
HRMS high res mass spectrometry	High Resolution Mass Spectrometry
i-Pr	*Iso*-Propyl
K	Kelvin
kDa	Kilodalton
Kg	Kilogram
*k*obs	Observed Rate Constant

La	Lactone
LauAc	Lauryl Acrylate
LiBr	Lithium Bromide
m/z	Mass-To-Charge Ratio
M_c	Molecular Mass Between Crosslinks
M_e	Entanglement Molar Mass
mg	Milligram
MHz	Megahertz
min	Minute
mL	Milliliter
mmol	Millimole
M_n	Average Molar Mass
Mt	Million Metric Tons
mW	Milliwatt
nBA	N-Butyl Acrylate
Nm	Nanometer
NMR	Nuclear Magnetic Resonance
Pa	Pascal
PBS	Phosphate Buffer Saline
p_c	Gel Point
PE	Poly(Ethylene)
PET	Poly(Ethylene Terephthalate)
PETMP	Pentaerythritol Tetrakis(3-Mercaptopropionate)
pH	Power Of Hydronium
PLA	Poly(Lactide)
PP	Poly(Propylene)
PS	Poly(Styrene)
PSA	Pressure Sensitive Adhesive
PSI	Pressure Per Square Inch
PSTC	Pressure Sensitive Tape Council
PUR	Poly(Urethane)
PVC	Poly(Vinylchloride)
Py	Pyrone
RAFT	Reversible Addition-Fragmentation Chain Transfer
RE	Rosin Ester
ROMP	Ring Opening Metathesis Polymerization
ROP	Ring Opening Polymerization
RT	Room Temperature
RT FTIR	Real-Time Fourier Transform Infrared
s	Second
SA	Sebacic Acid
SBS	Styrene Butadiene Styrene
SEC	Size Exclusion Chromatography

SEC MALLS	Size Exclusion Chromatography Multiangle Laser Light Scattering
SIS	Styrene Isoprene Styrene
$Sn(Oct)_2$	Tin(II) Bis(2-Ethylhexanoate)
TAL	Triacetic Acid Lactone
Tan δ	Ratio Of Loss/Storage Modulii
TBD	Triazabicyclodecene
T_c	Crystallization Temperature
TEM	Transmission Electron Microscopy
T_g	Glass Transition Temperature
TGA	Thermogravimetric Analysis
THF	Tetrahydrofuran
T_m	Melting Temperature
TPE	Thermoplastic Elastomer
δ	Chemical Shift
ΔG	Gibbs Free Energy
ΔH	Enthalpy Of Reaction
ΔS	Entropy Of Reaction
v	Crosslink Density
ρ	Density

Chapter 1.

Introduction

1.1 An Age of Plastics

In 2015 a report published in *Nature* unveiled the discovery of 3.3-million-year-old stone tools that were unearthed from the shores of Lake Turkana in Kenya.[1] The tools are believed to have been created and used for cutting and hammering by the extinct hominin species *Australopithecus afarensis* or *Kenyanthropus platyops*, who are among the closest relatives of modern-day humans. The creation of such tools ushered in a new era of technological advancement for early hominins, whose later evolution brought into existence the most intelligent, adaptive, and dominant species in the 4.5-billion-year history of this planet – *Homo sapiens.* The so-called "three-age system" divides the history of *Homo sapiens* into three time-periods, generally referred to as the Stone Age (3.4 million years ago – 2000 BCE (before common era)), the Bronze Age (3300 – 300 BCE), and the Iron Age (1200 – 550 BCE).[2] Through those ages, we humans created innumerable tools and technologies from stone, bronze, and iron, successively, towards the evolutionary and societal progression of our species.

Now, one may propose that a new era in human history has been initiated with the advent and widespread use of polymeric materials – the Plastics Age. Use of polymeric materials (plastics) can be dated as far back as 1600 BCE, when mesoamericans used natural rubber, now more commonly referred to as polyisoprene, harvested from rubber trees to make balls, bands, and figurines.[3] It was not until the early- to mid-20th century, however, more than 3000 thousand years after the mesoamericans used synthetic rubber balls for sporting games, did use of polymeric materials achieve an exponential growth on a global scale. To showcase this point, we can quantify the production of the most

prevalent polymers in circulation today – polyethylene (PE), polyethylene terephthalate (PET), polypropylene (PP), polystyrene (PS), polyurethanes (PURs), and polyvinylchloride (PVC) – over the past 50 years. We find that global manufacturing of these polymers has increased from 2 million metric tons (Mt) to more than 380 Mt, with cumulative totals that exceed 7800 Mt and are steadily growing.[4] These massive figures may be unsurprising, as polymeric materials are ubiquitously used in nearly every contemporary enterprise, such as food packaging to mitigate and prevent spoilage, lightweight vehicles for transpiration to reduce fuel consumption, commodity products like adhesives and clothing, and medical devices that can make the difference between life and death. The use of polymeric materials has become so prevalent that some geologists argue that the presence of plastic waste in the Earth's crust may be used as an indicator of the proposed Anthropocene epoch.[5]

Yet, we must reconcile with two undeniable facts in our obsession and professed love for plastics; (1) the resources that we predominantly use today to create and manufacture polymeric materials are finite and limited, and (2) the processes by which we obtain those resources are inherently unsustainable. Almost all of the plastic we use today are derived from petroleum-based feedstocks (fossil fuels), with nearly 10% of the total annual oil production directly dedicated towards monomer synthesis and almost the same amount consumed in polymer manufacturing processes.[6] Fossil fuels are formed via anaerobic decomposition pathways of dead organisms, processes which occur over millions to tens of millions of years.[7] Such timescales are vastly longer than the rate at which polymeric materials are made, used, and discarded. Accounting for the quantity of

currently known extractable fuel reserves and the rate at which we are expending those sources, it is estimated that we will deplete coal, oil, and gas supplies in 50-100 years.[8] Furthermore, fossil fuel production and use generates an enormous amount of carbon dioxide and other greenhouse gases, accounting for more than 75% of yearly emissions.[9] The global warming effect caused by the presence of such gases in the Earth's atmosphere is responsible for the disastrous effects on the delicate ecosystem of our planet, including the extinction of many species as their environments change,[10] reduced crop yields causing hunger and malnutrition,[11] and rising sea levels and oceanic temperatures[12] to name a select few examples.

These statistics prompt us to ask, "What can be done to ensure that the polymeric materials we have become so reliant upon and benefit from continue to remain as an integral part of our daily lives?" One proposed solution is to supplant current petroleum-derived feedstocks with renewable, biomass-derived alternatives that can be used to create novel polymeric materials with mechanical and thermal properties that are competitive with those currently in use.[13,14] Replacing fossil fuels with biomass may be a promising, sustainable paradigm for polymer synthesis as the relative timescales of biomass production and its subsequent utilization are orders of magnitude smaller than that of petroleum oil, as depicted in Figure 1.1.

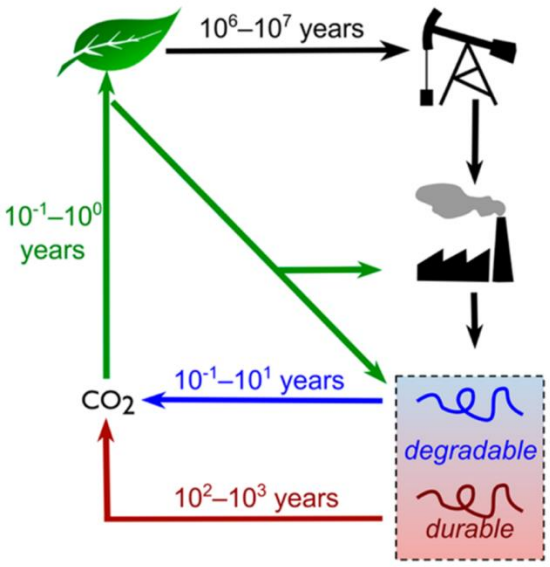

Figure 1. 1. Schematic depicting the time scale of polymer production from fossil fuels versus directly from biomass. Reprinted with permission from Schneiderman, D. K.; Hillmyer, M. A. *Macromolecules* **2017**, *50*, 3733-3749. Copyright 2017 American Chemical Society.

Adoption of such a model, that is, reducing our dependency on fossil fuels and instead relying directly on biomass for feedstocks to synthesize polymers, is exemplified by the commercial success of polylactide (PLA), a thermoplastic polyester that is degradable under select conditions. Lactide can be derived from the fermented plant starch of corn, cassava, sugarcane, and sugar beet pulp and then used to synthesize PLA via ring opening polymerization (ROP).[15,16] Although widespread applicability of PLA is currently hindered by the polymer's physical shortcomings, such as lower glass transition temperatures (T_g) (55 – 60 °C) compared to competitor products such as PET (T_g = 67 – 81 °C),[17] its definitive commercial success in niche industries like 3-D printing lends credibility to the notion that biomass can indeed be used to obtain polymerizable

compounds. Inspired and motivated by the commercial success of polymers like PLA, we turn our attention towards the exploration and identification of other biomass-derived precursors in order to expand the repertoire of renewable feedstocks that can yield polymeric materials. Ideally, such precursors should yield new materials that match (or even out-perform) the thermal and mechanical properties of the petroleum-derived counterparts they aim to replace. Numerous review articles published in recent years highlight on-going work towards achieving a sustainable paradigm for polymers.[13,14,16,18] The following sections of this thesis introduce renewable, bio-derived feedstocks that are emerging as promising candidates for such an end goal, and warrant further investigation for their viability in producing sustainable polymeric materials.

1.2 Platform Chemicals from Biomass

1.2.1 Triacetic Acid Lactone

Triacetic acid lactone (TAL), as shown in Figure 1.2, is a heterocyclic, di-substituted "pyrone," a classification of unsaturated 6-membered lactones, which can be obtained through a variety of methods. Its chemical synthesis was first reported over century ago, involving the pyrolysis of acetic acid to TAL.[19] Since that initial report, the five-step synthetic pathway has been refined to optimize and increase yields.[20,21]

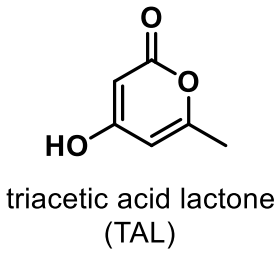

Figure 1. 2. Chemical structure of triacetic acid lactone (TAL).

More recently, research efforts are underway to obtain TAL via the biological pathways of select microbes that can synthesize and excrete the compound as a secondary metabolite of glucose and fatty acids.[22–24] The successful genetic bioengineering of organisms such as *Escherichia coli* and *Saccharomyces cerevisiae* has been performed with the objective to increase the titer levels of TAL.[25–29] Highlighting one notable study, a strain of *Yarrowia lipolytica* was genetically modified to increase the production of various enzymes, such as 2-pyrone synthase (2-PS), which function as catalysts in the

cellular metabolic pathways that ultimately lead to TAL production (Figure 1.3).[29] The work demonstrated that such genetic bioengineering can result in a marked increase in titer levels of TAL, up to 35% in this particular case, compared to the native fungal variant.

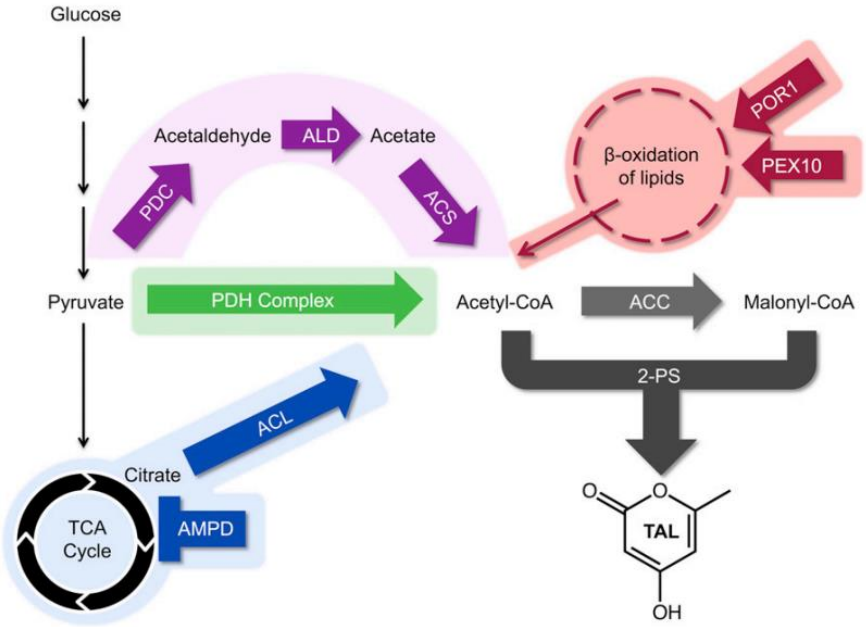

Figure 1. 3. Scheme showing the various metabolic pathways in *Yarrowia lipolytica* that may be bioengineered to increase its production of TAL. Reprinted with permission from Markham *et al*, *PNAS,* **2018**.[29]

By exploiting the rich functionality "built-in" to the molecule, such as the internal alkene bonds, the ester moiety, and the free hydroxyl group, TAL has been used as an initial chemical building block to synthesize a variety of downstream compounds for a myriad of applications. Commodity feedstocks such as acetyl acetone and 1-pentene,

food preservatives including sorbitol and sorbic acid, as well as more specialty chemicals like katsumadain and dehydroacetic acid derivatives which have been studied for their antimicrobial and antifungal properties, have all been synthesized from TAL (Figure 1.4).[21,30–34]

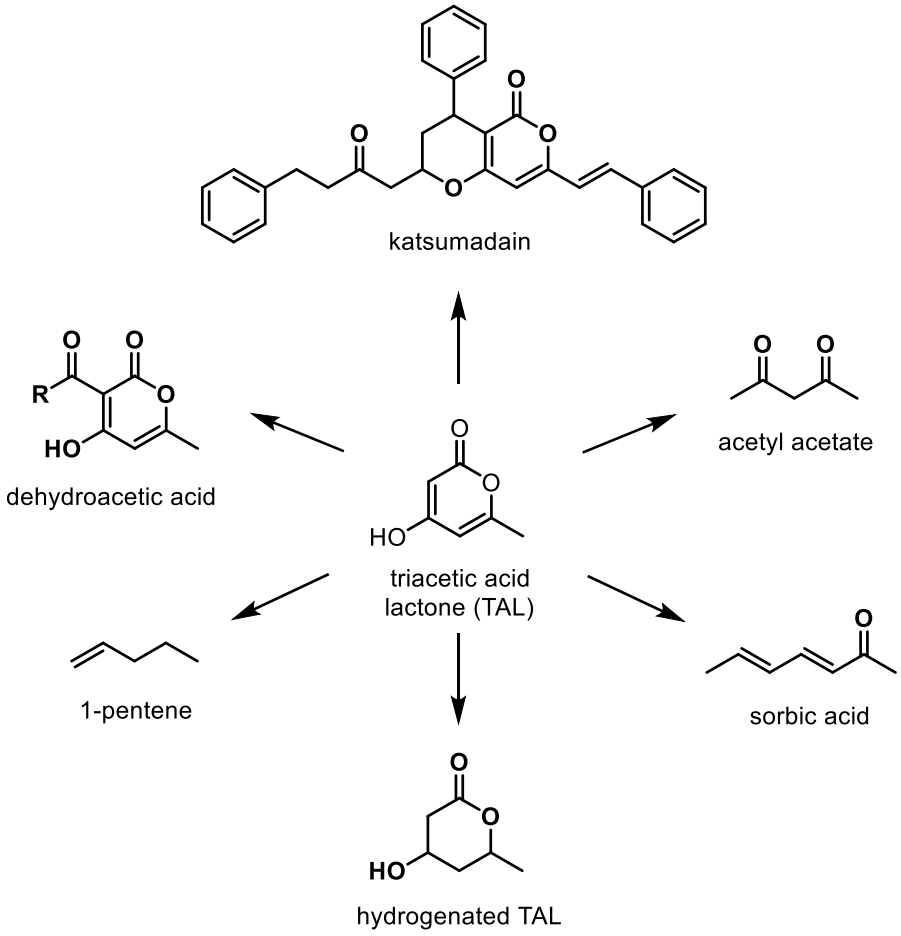

Figure 1. 4. Useful platform chemicals derived from triacetic acid lactone.

The use of TAL as an emerging biomass-derived compound for such diverse applications prompted us to investigate the viability of using it as a precursor for monomers that may be suitable for the synthesis of new polymeric materials. Prior to the work described herein, there existed only one example in the literature demonstrating the incorporation of TAL into polymers. Post-polymerization modification of poly(epichlorohydrin) via S_N2 chemistry using the hydroxyl group of TAL, obtained from genetically modified *Yarrowia lipolytica*, was performed.[29] The results showed an increase in T_g of the material from -30 °C up to 70 °C, depending on the degree of substitution. Chapters 2 and 3 of this text respectively detail the use of TAL in the formulation of triblock polymers that serve as useful commodity products like elastomers and pressure-sensitive adhesives, and novel polyesters that can be obtained via ROP of TAL derivatives.

1.2.2 Fatty Acids

The implementation of biosynthetic fatty acids in the polymer manufacturing industry is another favorable strategy to reduce our dependency on fossil fuels. Fatty acids are the chemical building blocks of abundant triglycerides found in vegetable oils like soybean oil, palm kernel oil, and coconut oil. These fatty acids can be isolated from vegetable oils by separation from the glycerin component via hydrolysis, a process that is currently done on industrial scales for biodiesel manufacturing (Figure 1.5). Subsequent hydrogenation of the fatty acids can yield long-chain alcohols. Such vegetable oils and

their fatty acid and glycerin components and derivatives have a wide variety of applications from foods, biofuels, cosmetics, lubricants, paints, and pharmaceuticals.[35,36]

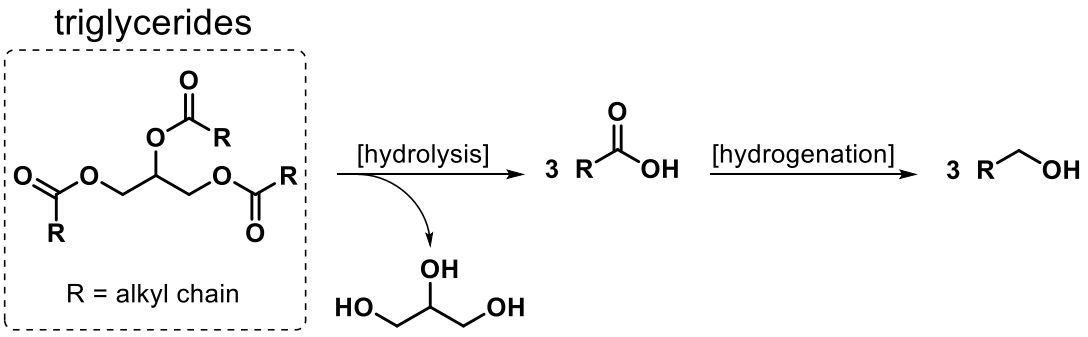

Figure 1. 5. Schematic showing the hydrolysis of triglycerides obtainable from vegetable oils to yield long alkyl-chain fatty acids and their subsequent reduction to yield alcohols.

One alcohol of particular interest that is obtainable from the fatty acids of palm kernel oil and coconut oil is lauryl alcohol (dodecanol). Thousands of tons of lauryl alcohol are produced annually from the hydrogenation of oil-derived fatty acids and used to make surfactants, lubricants, pharmaceuticals, and as a food additive.[37,38] Acrylation of the hydroxyl group of lauryl alcohol yields lauryl acrylate, a useful chemical building block for the synthesis of polymers (Figure 1.6). Although acrylic precursors are currently industrially manufactured from petrochemical sources, research efforts in academia are focused on obtaining bio-based acrylates,[39] bringing us one step closer towards the realization of a fully sustainable model for such common precursors.

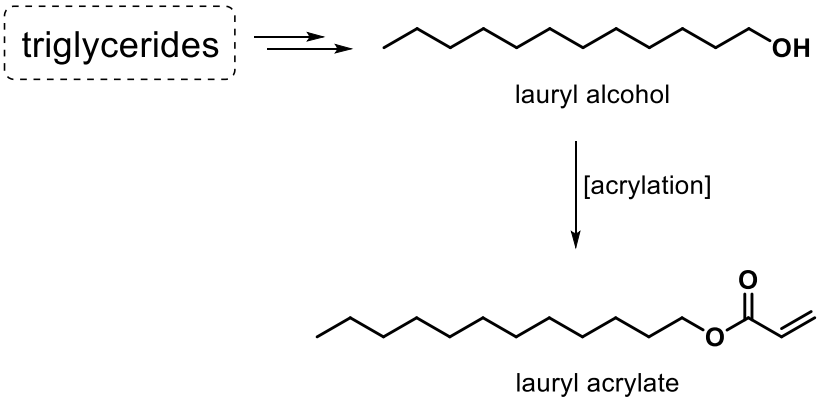

Figure 1. 6. Synthesis of lauryl acrylate from the triglycerides of vegetable oils.

The polymerization of lauryl acrylate yields a polymer with a low glass transition temperature, and the long alkyl side chains are highly hydrophobic, providing resistance towards hydrolytic degradation.[40–43] Previous work involving the copolymerization of lauryl acrylate and stearyl acrylate (another alkyl-acrylate derivative of fatty acids) yielded diblock copolymers which behaved as brittle, rigid materials. In another example, poly(lauryl acrylate) was synthesized via reversible addition-fragmentation chain transfer (RAFT) polymerization and Cu(0)- mediated radical polymerizations with the purpose of improving the compatibilization of carbon nanotubes (CNTs) with thermoplastic polymers, such as isotactic poly(propylene), for use in electronics, optics, and composite materials. Imaging through transmission electron microscopy (TEM) confirmed that poly(lauryl arylate) chains were successfully adsorbed on the surface of the CNTs (Figure 1.7).[44]

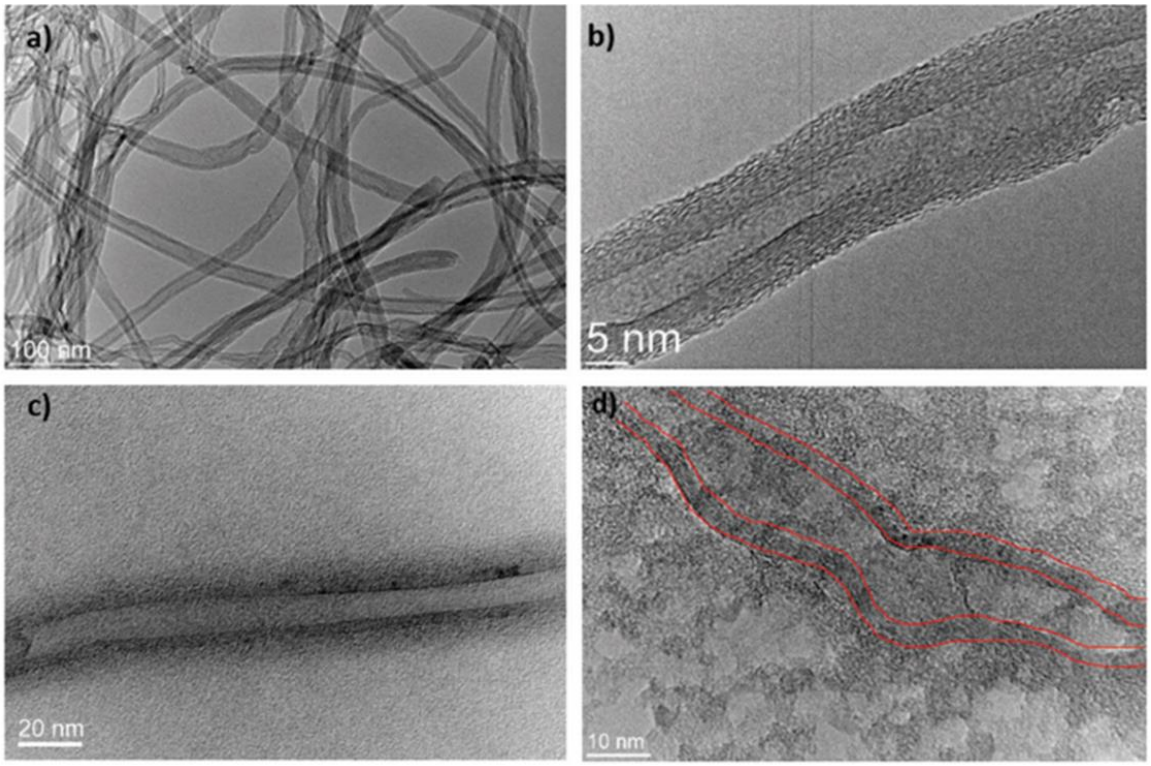

Figure 1. 7. TEM images of (a) unfunctionalized CNTs at 50,000x magnification, (b) unfunctionalized CNTs at 400,000x magnification, and (c) and (d) CNTs functionalized with poly(lauryl acrylate) with a red line indicating the inner and outer walls of the CNTs. Reproduced with permission from The Royal Society of Chemistry.[44]

The synthesis of triblock copolymers using poly(lauryl acrylate-co-stearyl acrylate) as the rubbery midblock and poly(styrene) as the glassy endblocks has also been reported.[45] Small-angle x-ray scattering and TEM experiments, in conjunction with thermal characterization with differential scanning calorimetry (DSC), supported microphase-separation of the immiscible blocks. Tensile testing revealed elastomeric behavior of the triblock copolymers, albeit with limited elongation and relatively low stress values at break (Figure 1.8). In the work described in this thesis, poly(lauryl acrylate) was synthesized via RAFT polymerization and copolymerized with an acrylic

derivative of TAL for the purpose of creating pressure-sensitive adhesives. The triblock copolymers were characterized and the adhesive capabilities of the material were tested, as detailed in Chapter 2.

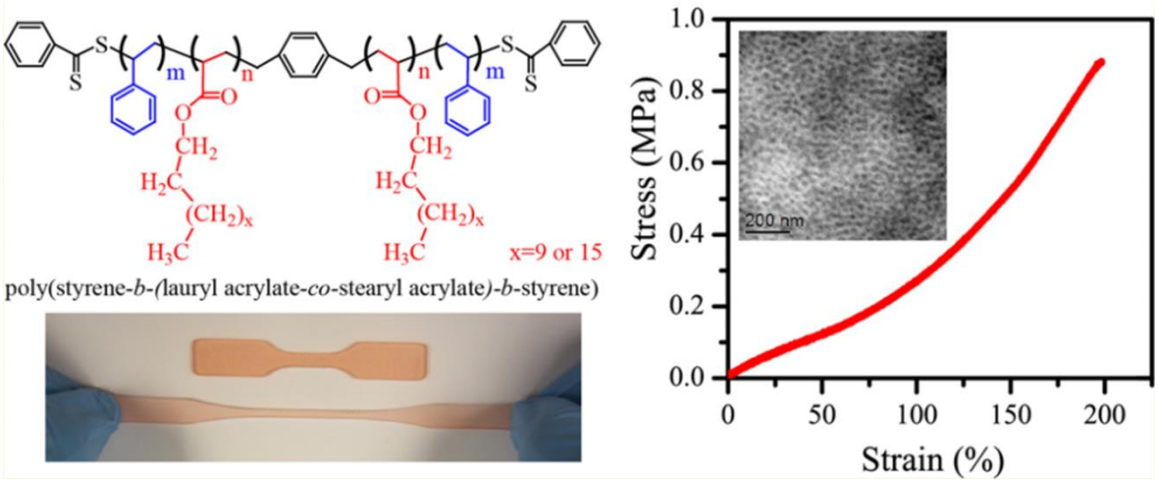

Figure 1. 8. Triblock copolymers comprised of poly(lauryl acrylate-co-stearyl acrylate) as the rubbery midblock and poly(styrene) as the glassy endblocks. The figure shows a drawing of the triblock copolymer (top left), a photograph of the elastomer in the shape of a dogbone (bottom left), and results from tensile analysis with a TEM image as the inset indicating microphase separation of the rubbery and glassy blocks (right). Reprinted with permission from Wang, S.; Vajjala Kesava, S.; Gomez, E. D.; Robertson, M. L. *Macromolecules* **2013**, *46*, 7202–7212. Copyright 2013 American Chemical Society.

1.2.3 Itaconic acid

Itaconic acid is a dicarboxylic acid with an acrylic-like, α,ß-unsaturated alkene bond. Similar to TAL, itaconic acid may be obtained via a synthetic route involving the thermal decomposition of citric acid, as initially reported in 1836,[46] or it may be bio-derived as a secondary metabolite of glucose fermentation in *Aspergillus terrus* (Figure

1.9).[47] Industrially, itaconic acid is currently produced on the kiloton-scale annually via the biosynthetic route shown in Figure 1.9, and is available in the dollar-per-kilogram price range.

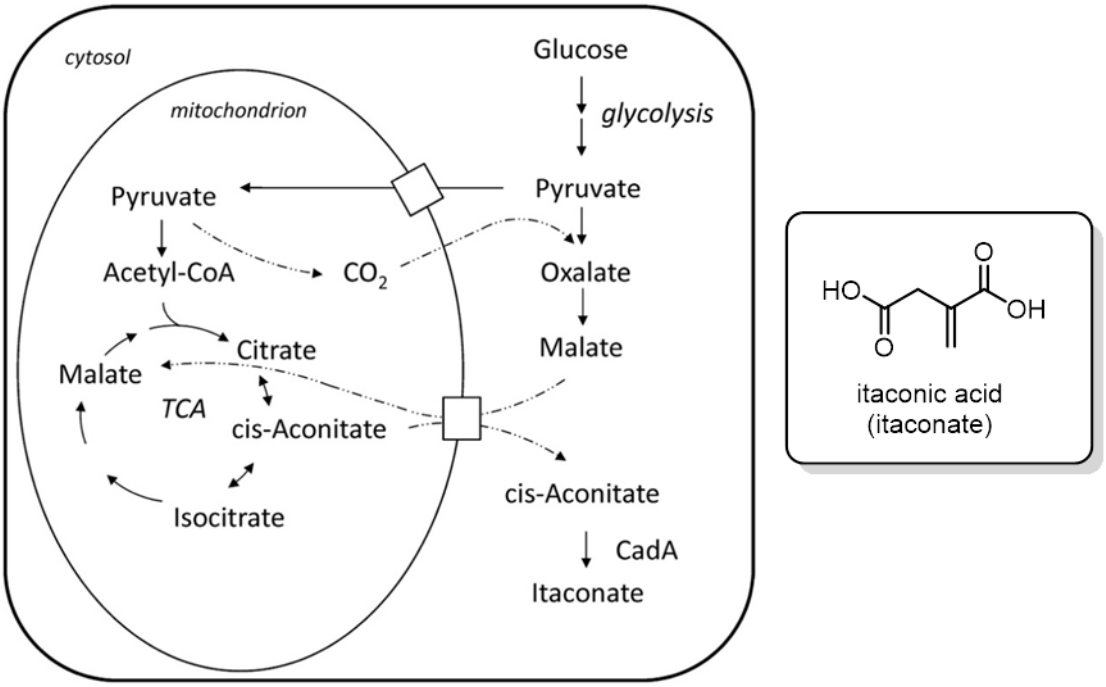

Figure 1. 9. Biosynthetic pathway depicting the citric acid cycle in *Aspergillus terreus* leading to the production of itaconic acid (itaconate). Figure adapted from Steiger et al. with permission.[47] Copyright 2013 Steiger, Blumhoff, Mattanovich and Sauer.

The free-radical polymerization of the acrylate-like moiety of itaconic acid has yielded polymers useful for applications like elastomers, vehicles for drug delivery, and resins for dental applications.[48,49] Commercially the free-radical polymerization of bio-derived itaconic acid is performed to produce poly(itaconic acid), and the resultant

material is marketed as a renewable alternative to poly(acrylic acid) for absorbents and dispersants (Figure 1.10).[50] Other examples demonstrating the incorporation of itaconic acid in polymeric materials include the production of epoxy resins,[51,52] polyamides,[53,54] and elastomers.[55]

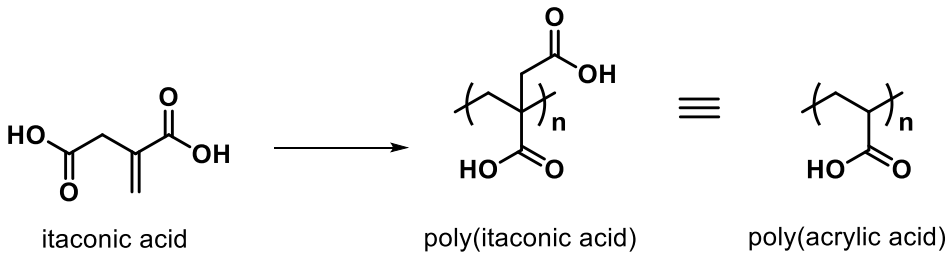

Figure 1. 10. The free radical polymerization of itaconic acid to poly(itaconic acid), a bio-derived alternative to poly(acrylic acid).

Since itaconic acid is a diacid, condensation-type polymerizations have also been performed with the intention to produce polyesters that can be modified post-polymerization by using the internal alkene bond (e.g. addition reactions or thiol-ene chemistry). However, to date, the condensation polymerization of itaconic acid has yielded only short oligomers because the rigorous conditions required for such polymerizations (i.e. high heat and strong vacuum) have caused undesirable branching or crosslinking due to the internal alkene bonds.[52,56–58] Itaconic acid has also been used as a precursor in the synthesis of a norbornene-functionalized monomer for ring opening metathesis polymerizations (ROMP) (Figure 1.11).[58] This report in particular served as

inspiration, in part, for the work described in Chapter 4, where norbornene-functionalized anhydride monomers derived from itaconic acid were used in photoinitiated, thiol-ene polymerizations to create water-degradable polyanhydride networks.

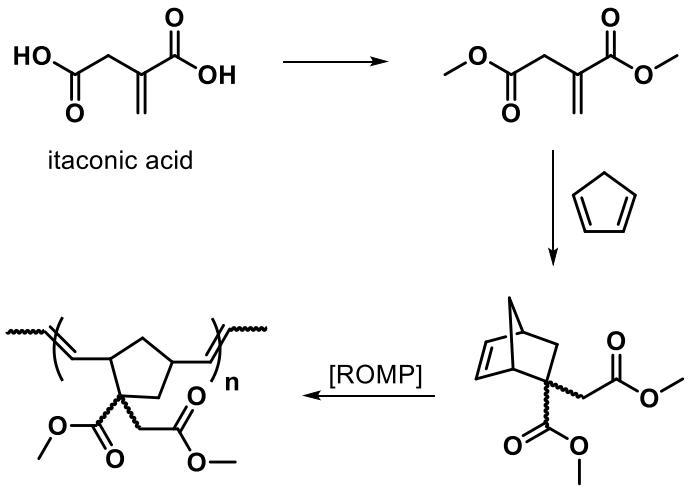

Figure 1. 11. Synthesis of norbornene-functionalized monomer from itaconic acid which can undergo ring opening methasis polymerizations (ROMP). Reprinted with permission from Winkler, M.; Lacerda, T. M.; Mack, F.; Meier, M. A. R. *Macromolecules* **2015**, *48*, 1398 – 1403. Copyright 2015 American Chemical Society.

1.3 Thesis Outline

The following three chapters of this text detail work focused on the use of the bio-derived feedstocks introduced above, triacetic acid lactone, lauryl acrylate, and itaconic acid, in the synthesis of novel polymeric materials. Chapter 2 describes the study of triblock copolymer pressure-sensitive adhesives created using high molecular weight poly(lauryl acrylate) as the functional midblock elastomer and a derivative of TAL as the glassy endblocks. Chapter 3 explores the synthesis of disubstituted six-membered lactones derived from TAL and their polymerizations to yield polyesters. The thermodynamics and kinetics of polymerization for the disubstituted lactones were explored to enhance our understanding of ring opening polymerizations. Chapter 4 focuses on the synthesis of water-degradable polyanhydride networks derived from itaconic acid via photo-initiated thiol-ene chemistry. Our efforts and outcomes with these emerging feedstocks demonstrate that new materials with useful properties can be created from renewable sources, and such discoveries represent important advances towards ultimately achieving a sustainable future for polymers.

Chapter 2.

Block Copolymer Pressure Sensitive Adhesives Derived From Fatty Acids and Triacetic Acid Lactone

Reproduced in part with permission from Sajjad, H.; Tolman, W. B.; Reineke, T. M.; Block Copolymer Pressure Sensitive Adhesives Derived From Fatty Acids and Triacetic Acid Lactone. *ACS Appl. Polym. Mater*. 2020, 2, 7, 2719–2728. DOI : 10.1021/acsapm.0c00317

2.1 Overview

A method for the development of ABA triblock copolymers for high performance pressure sensitive adhesives (PSAs) from the biorenewable chemicals lauryl acrylate and triacetic acid lactone (TAL) is presented. Lauryl acrylate, readily derived from vegetable oils, was polymerized via a reversible addition-fragmentation chain transfer (RAFT) process to yield high molecular weight telechelic polymers. The synthesis of triblock copolymers was accomplished by subsequent chain extension with TAL, which is available from carbohydrates via the action of genetically modified yeast. The resulting triblock copolymers were found to exhibit excellent adhesion, with tunable peel forces up to 8 N cm^{-1} when a rosin ester-based tackifier also was used. Tack forces up to 7 N cm^{-1} and no shear failure up to 100 h demonstrate the competitive performance of the potentially sustainable adhesives with commercial commodity products.

2.2 Introduction

Thermoplastic elastomers (TPEs) comprise an important class of reprocessable materials that have found use in a wide-range of applications including pressure sensitive adhesives, footwear, electronics, and medical devices.[59,60] Petroleum-based triblock copolymers with an ABA architecture, such as poly(styrene-butadiene-styrene) (SBS) or poly(styrene-isoprene-styrene) (SIS), traditionally have been used as TPEs. The ABA-type architecture, employing a "rubbery" midblock (B) and flanking "glassy" blocks (A), allows for molecular variation in composition, which influences the nanoscale structure of the material and ultimately dictates its application and use.[61,62] For example, immiscibility of the high T_g poly(styrene) domains with the low T_g poly(butadiene) domains in SBS triblock copolymers leads to phase-segregated nanostructures which enhance the mechanical properties of the material.[61]

The use of finite, petroleum-based platform chemicals for the manufacturing of TPEs, however, is concerning from a sustainability and environmental viewpoint. Consequently the development of soft materials from alternative, more sustainable sources is a major contemporary societal demand[13,63,64] and researchers have maintained a focused effort into replacing the outer (A) and/or inner (B) blocks with biorenewable feedstocks. For example, poly(lactide) (PLA) has been used as the glassy component in TPEs with various lactones, alkenes, glycols, menthide, or ricinoleic acid serving as the rubbery component.[8-22] Although PLA serves its purpose as the glassy component, its relatively low glass transition temperature (T_g) limits its utility in TPEs. Acrylics block copolymers, however, offer functional versatility (such as tunable T_g values) due to the

ability to vary the pendant ester group. Notable examples in recent years have employed renewable terpene derivatives as replacements for the rubbery and glassy blocks in triblock copolymers for pressure-sensitive adhesives and elastomers.[80,81] In a similar fashion, we previously reported on the production of TPEs employing acrylic derivatives of glucose and isosorbide as replacements for the glassy, styrene-based endblocks in traditional TPEs.[82–85] Using Reversible Addition-Fragmentation Chain Transfer (RAFT) polymerization as a controlled polymerization technique,[86,87] *n*-butyl acrylate (nBA) was copolymerized with the acrylate-functionalized sugar derivatives to create triblock copolymers with an ABA-type architecture. Poly *n*-butyl acrylate has a low glass transition temperature (-47 °C) and an entanglement molecular mass (M_e) of 28 kDa[88,89] and is often used as the rubbery midblock in ABA-type polymers for PSA applications. Because the elastic modulus of an elastomer is related to the average molecular weight between entanglements, polymers with larger M_e values are favorable for PSAs owing to their inherently lower elastic modulus compared to traditional butadiene- or isoprene-based elastomers.[90] The adhesive and mechanical properties of the resultant ABA-triblock materials were comprehensively evaluated and shown to exhibit promising properties that depended on block identity, molecular weight, and tackifier presence. Another notable example similarly used RAFT polymerization to copolymerize nBA with acrylic derivatives of phenolic compounds obtained from the depolymerization of lignocellulosic biomass to create PSAs.[91] While these studies substituted the glassy component of acrylic-based TPEs, sustainability is difficult to attain because of the use of p(nBA) as the rubbery midblock.

Although it is feasible to derive *n*-butyl acrylate from bio-sourced *n*-butanol,[92] an arguably more attractive choice for the midblock in the context of this work is lauryl acrylate (LauAc). Lauryl alcohol can be directly obtained from the fatty acids of vegetable oils and is a major component of coconut and palm kernel oils.[38,45] In illustrative applications, lauryl acrylate and stearyl acrylate were copolymerized with styrene via RAFT polymerization to create elastomers with an ABA-type architecture.[45,93] As a consequence of the high entanglement molecular weights of longer chain alkyl acrylates, the resultant elastomers were weaker than traditional SBS elastomers (i.e. exhibited lower stress and strain at break). PSAs of this architecture, however, benefit from the use of a base elastomer with a high entanglement molecular weight. We postulated that the higher M_e of p(LauAc) should yield an elastomer that exhibits a lower elastic modulus in comparison to p(nBa), a property that is desirable for instantaneous bonding of an adhesive to a substrate.

In addition to exploring alternatives for the midblock in ABA copolymers, we also sought to replace styrene with renewable feedstocks for use in synthesizing the glassy component in TPEs. We chose 4-hydroxy-6-methyl-2-pyrone (denoted triacetic acid lactone (TAL)), which can be obtained synthetically from acetic acid[19–21] or through biological pathways in select microbes, which synthesize the compound as a secondary metabolite of glucose and other sugars.[22–24] Notably, ongoing research into the genetic bioengineering of *Escherichia coli* and *Saccharomyces cerevisiae* suggests that biologically-synthesized TAL may be a viable feedstock.[25–29,94] Although TAL and its numerous derivatives have been studied for their efficacy as food preservatives,

antimicrobials, pharmaceuticals, etc., its use as a renewable feedstock for polymer synthesis has yet to be explored in detail.[21,29,30] In a recent study, partial substitution of p(epichlorohydrin) with TAL via post-polymerization modification resulted in an apparent increase in T_g of the material from -30 °C up to 70 °C depending on the degree of substitution.[29]

We hypothesized that TAL and its hydrogenated derivative could be readily substituted with acrylic groups and polymerized via controlled methods, resulting in a material with properties suitable for use as a glassy component in bio-sourced multiblock copolymer TPEs for PSA applications. In addition, we postulated that renewable rubbery blocks derived from vegetable oils can replace p(nBA) as the base elastomer. Herein, we report functionalization of TAL directly with acryloyl chloride, as well as the synthesis of a similarly substituted variant derived from hydrogenating TAL. Block-copolymerization with lauryl acrylate as the rubbery midblock was performed to create a series of well defined, high molar mass ABA acrylic triblock copolymers. Adhesion performance studies (peel adhesion, loop tack, and shear failure) revealed functional properties comparable to commercial PSAs. This work demonstrates a new strategy for the preparation of functional block copolymer PSAs from renewably sourced building blocks.

2.3 Results and Discussion

Initial efforts focused on targeting high molecular weight poly(lauryl acrylate) (p(LauAc) for testing as a suitable mid-block in an ABA triblock copolymer. Despite the advantage of using an elastomer with a high M_e as discussed above, appreciable peel adhesion values for triblock-based PSAs are only obtainable if the molecular weight of the rubbery midblock is at least 2 – 3 times the entanglement molecular weight of the polymer (i.e. the elastomer is "loosely" entangled).[95] RAFT polymerization of *n*-butyl acrylate using a bifunctional CTA was previously introduced by our group as a means to synthesize a living, chain-extendable rubbery midblock for an acrylic-based system.[83,84,85] Using a similar RAFT polymerization method with a commercially available difunctional CTA (3,5-Bis(2-dodecylthiocarbonothioylthio-1-oxopropoxy)benzoic acid, (BTCBA)), we synthesized high molecular weight (p(LauAc) with narrow dispersities (M_n = 300 kDa, $Đ$ = 1.19) while retaining the living nature of the polymer chain for chain extension with a glassy block (Scheme 2.1, Figure 2.1). TGA analysis of the p(LauAc) macro-CTA showed good thermal stability with 5% weight loss occurring at ~330 °C (Figure 2.2). The DSC thermogram displays T_m = 2 °C, T_c = -5 °C, and no discernible T_g feature (Figure 2.3). The thermal features seen in the thermogram of p(LauAc) correspond to the crystallization and melting events of the pendant alkyl chains.[96–98]

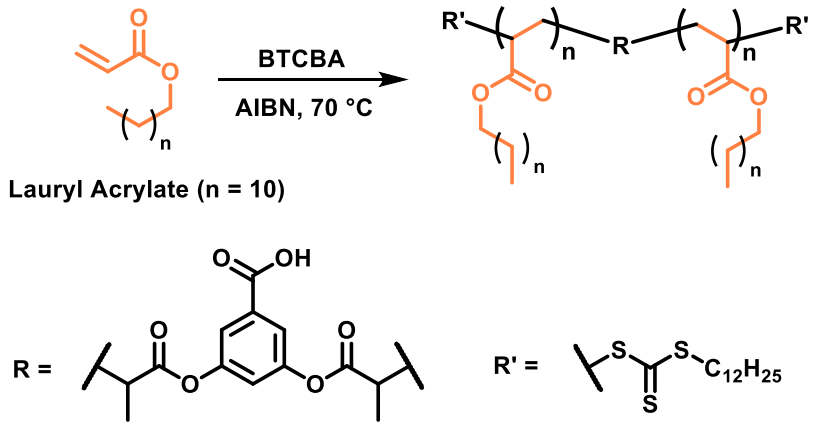

Scheme 2. 1. Synthesis of p(lauryl acrylate) via RAFT polymerization.

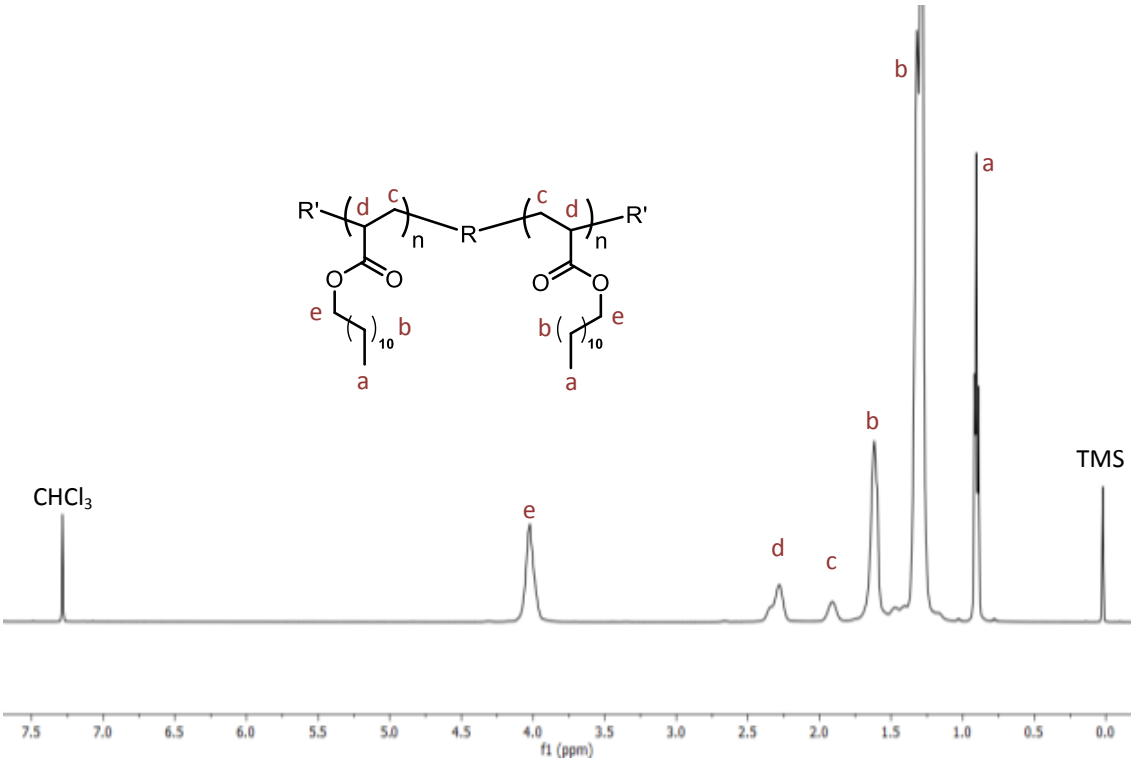

Figure 2. 1. ^{1}H NMR spectrum of the p(LauAc) macro-CTA ($CDCl_3$, 500 MHz).

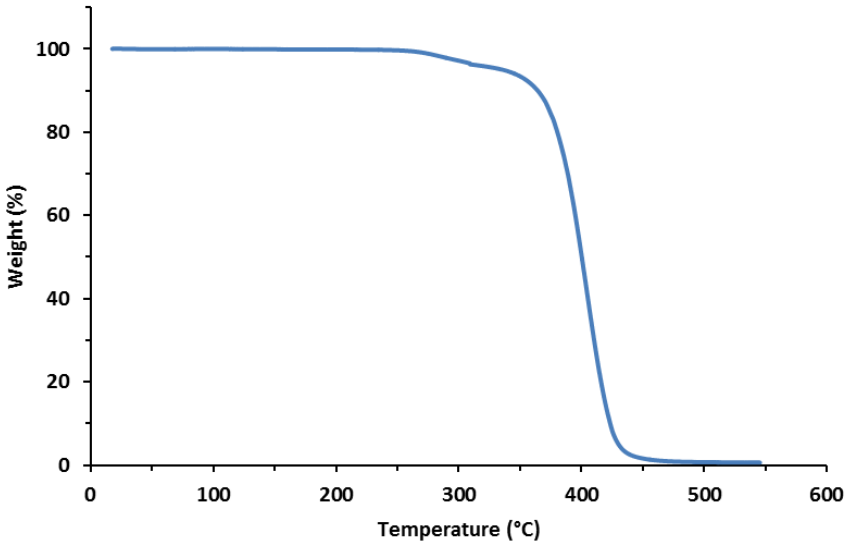

Figure 2. 2. TGA thermogram of p(LauAc) at a heating rate of 10 °C·min^{-1}.

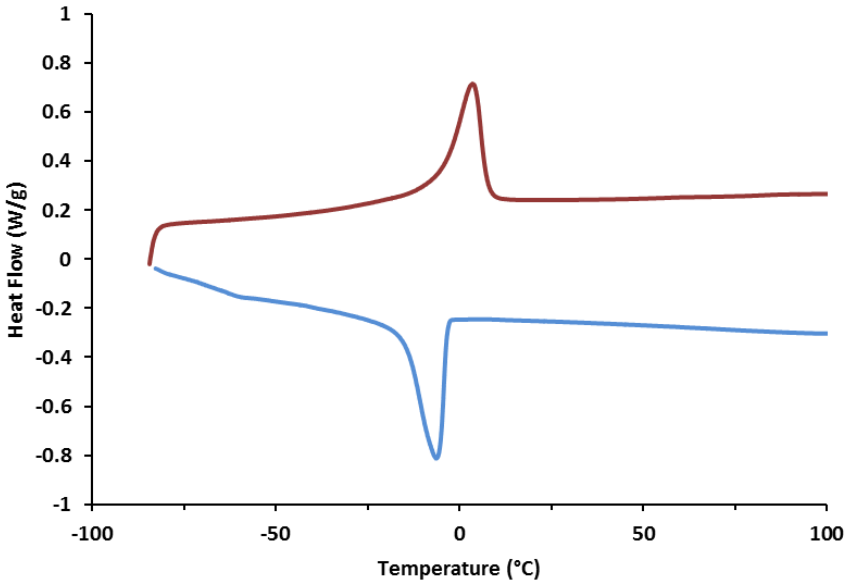

Figure 2. 3. DSC thermogram of p(LauAc) at a heating rate of 10 °C·min^{-1} taken on the second heating and cooling cycles. The thermogram shows a T_m = 2 °C and T_c = -5 °C and no discernible T_g feature.

To validate that p(LauAc) is minimally entangled at the synthesized molecular weights, dynamic mechanical analysis (DMA) was performed to calculate M_e, which had not been reported to date. The entanglement molecular weight was calculated using the moduli versus frequency plot shown in Figure 2.4 in conjunction with Equation 2.1,[99]

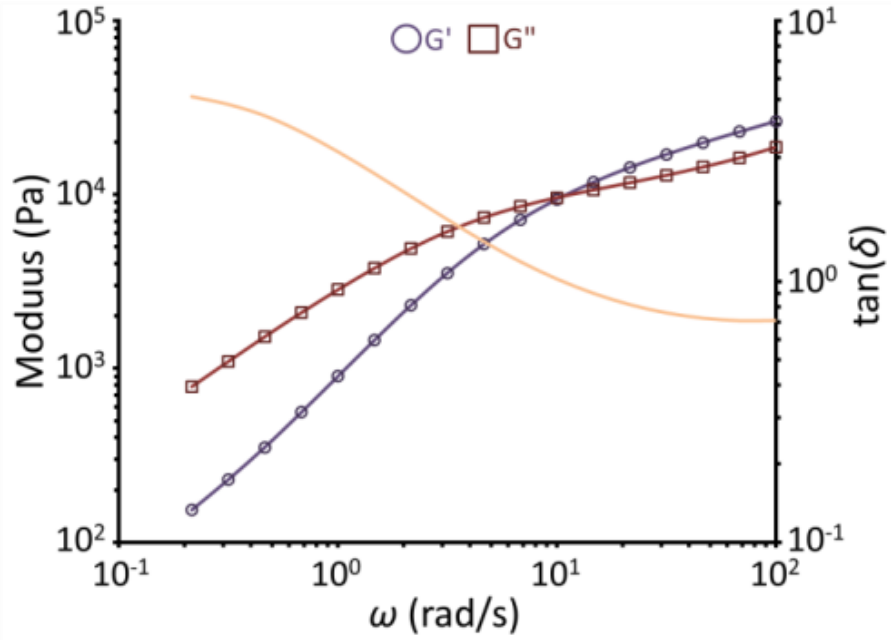

Figure 2. 4. Plot of elastic (G') and loss (G") moduli as a function of angular frequency at 5 °C of p(LauAc) with M_n = 300 kDa, $Đ$ = 1.19.

$$M_e = \frac{4}{5}\frac{\rho RT}{G_N^0} \tag{2.1}$$

where G^0_N is the plateau modulus determined from oscillatory shear experiments, ρ is the density of the polymer (taken as 0.94 g/mL at 21 °C from the literature),[45] R is the gas constant, and T is the temperature at which the rheological experiments were conducted (5 °C). We note that although the reference temperature differs from the temperature at which the density measurement was performed, the difference in density of p(LauAc) between the two temperatures is expected to be negligible. Using the minimum of tan δ, a ratio of the loss to elastic modulii, as a reference point, the plateau modulus was determined to be 26500 Pa and the M_e of p(LauAc) was calculated to be 70 kDa. Therefore, polymers above approximately 210 kDa (i.e. ~3 X M_e) are expected to be minimally entangled. A M_e value for poly(laurylmethacrylate) was reported to be 225 kDa based on rheological measurements on a sample of M_n= 82 kDa.[100] However, it is uncertain if the tested sample was suitably entangled in order to gather meaningful data for an accurate calculation.

We then sought to design efficient methods to create acrylic variants of TAL through two routes for polymerization into block polymer architectures (Scheme 2.2). Catalytic hydrogenation of TAL using Pd/C afforded the reduced lactone derivative (Figure 2.5).[30] The transformation approached near quantitative yields under the given conditions after 2-3 days, depending on the scale (see Experimental for synthetic details). The lengthy reaction time towards complete hydrogenation is attributed to an internal keto-enol tautomerism, largely in favor of the keto- form, which is established following partial reduction of the pyrone ring (Scheme 2.3, Figure 2.6). Esterification of the hydroxyl substituents on the both pyrone and lactone rings with acryloyl chloride yielded

4-acrylate-6-methyl-2-pyrone (AcPy, Figures 2.7 and 2.8) and 4-acrylate-6-methyl-2-lactone (AcLa, Figures 2.9 and 2.10), respectively.

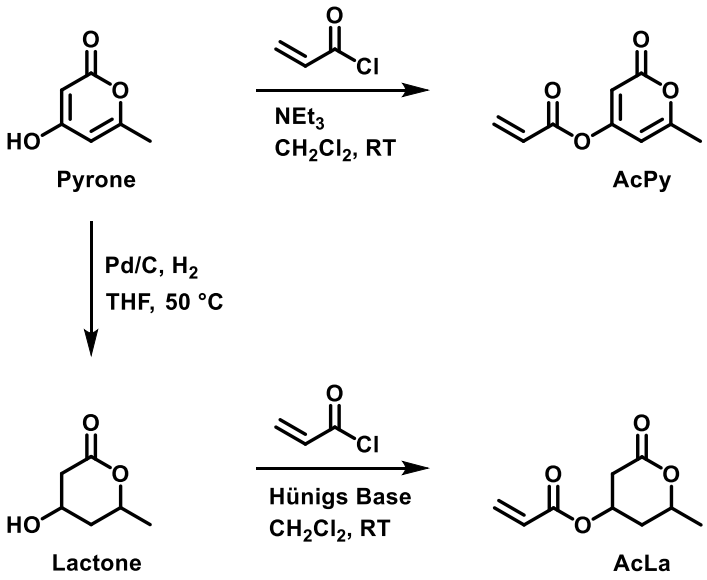

Scheme 2. 2. Syntheses of Acrylated-Pyrone (AcPy) and Acrylated-Lactone (AcLa).

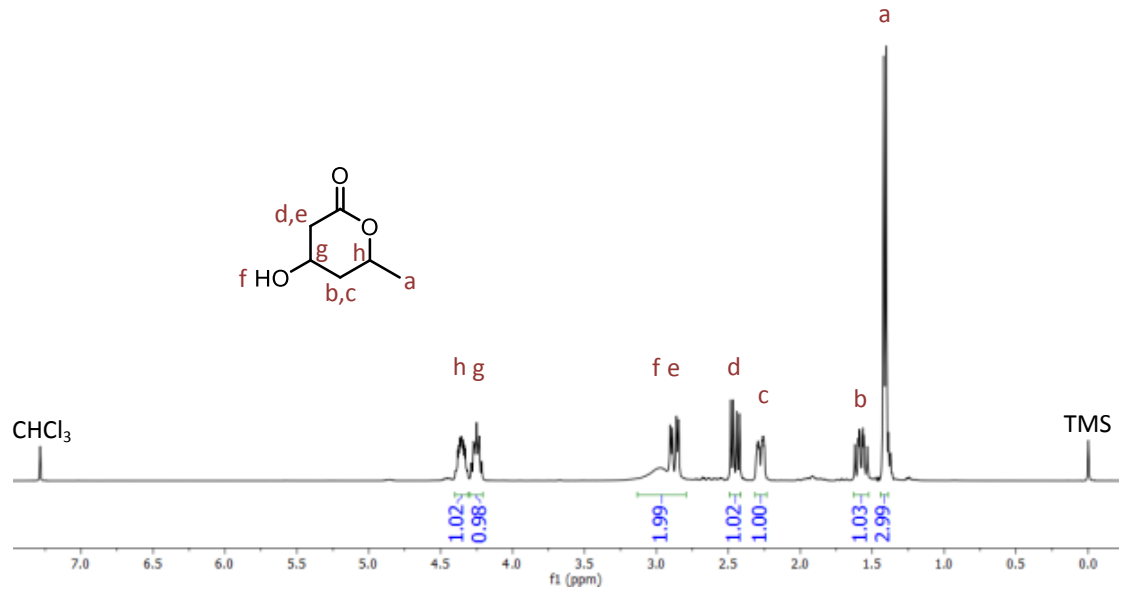

Figure 2. 5. ^{1}H NMR spectrum of the reduced lactone (La) ($CDCl_3$, 500 MHz).

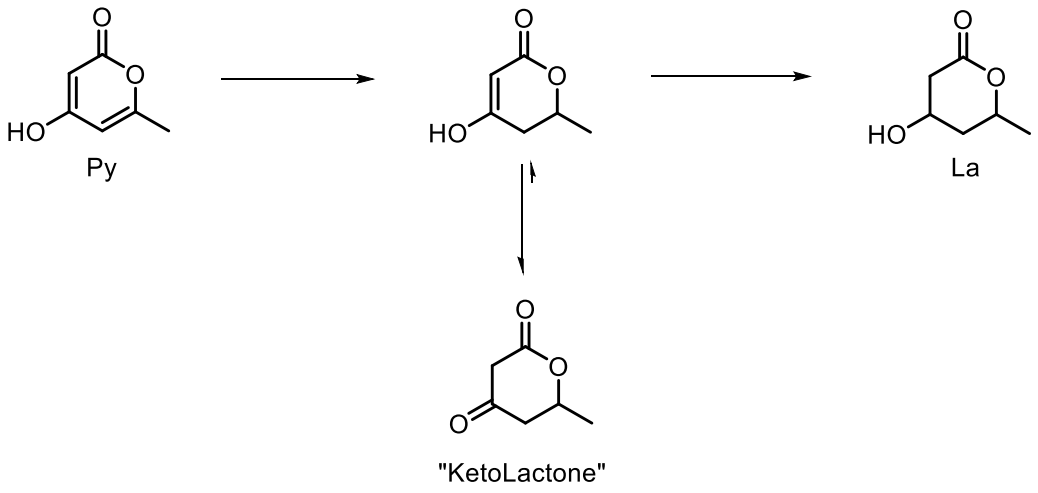

Scheme 2. 3. Hydrogenation of the pyrone (Py) to the lactone (La) involving a partially-reduced "enol" intermediate which undergoes tautomerization to the preferred "keto" form. See Figure 2.6 for ^{1}H NMR of "KetoLactone" isolated from the reaction mixture.

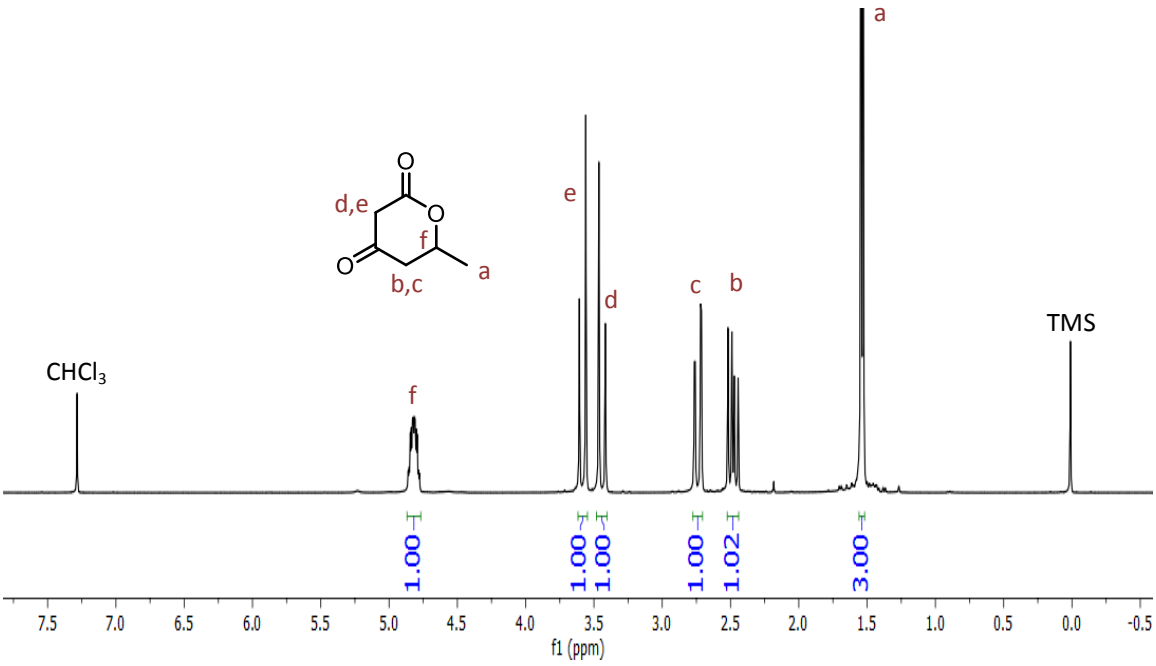

Figure 2. 6. ^{1}H NMR spectrum of "KetoLactone" ($CDCl_3$, 500 MHz).

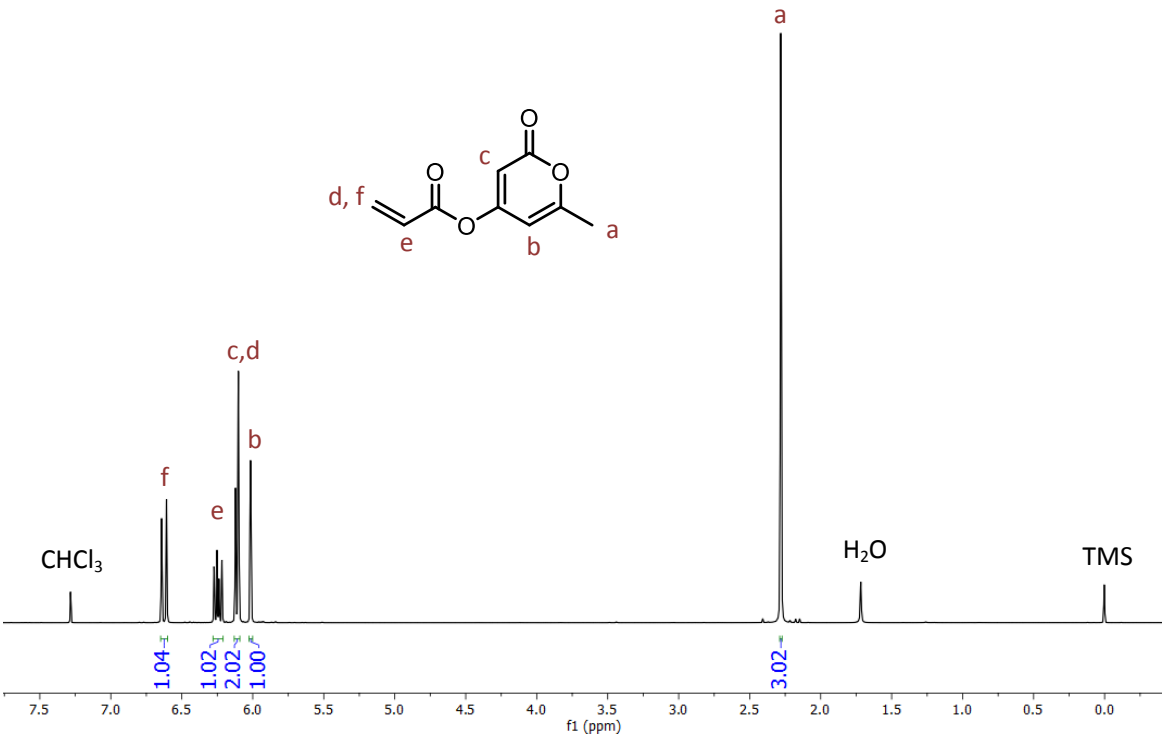

Figure 2. 7. ^{1}H NMR spectrum of acrylated-pyrone (AcPy) ($CDCl_3$, 500 MHz).

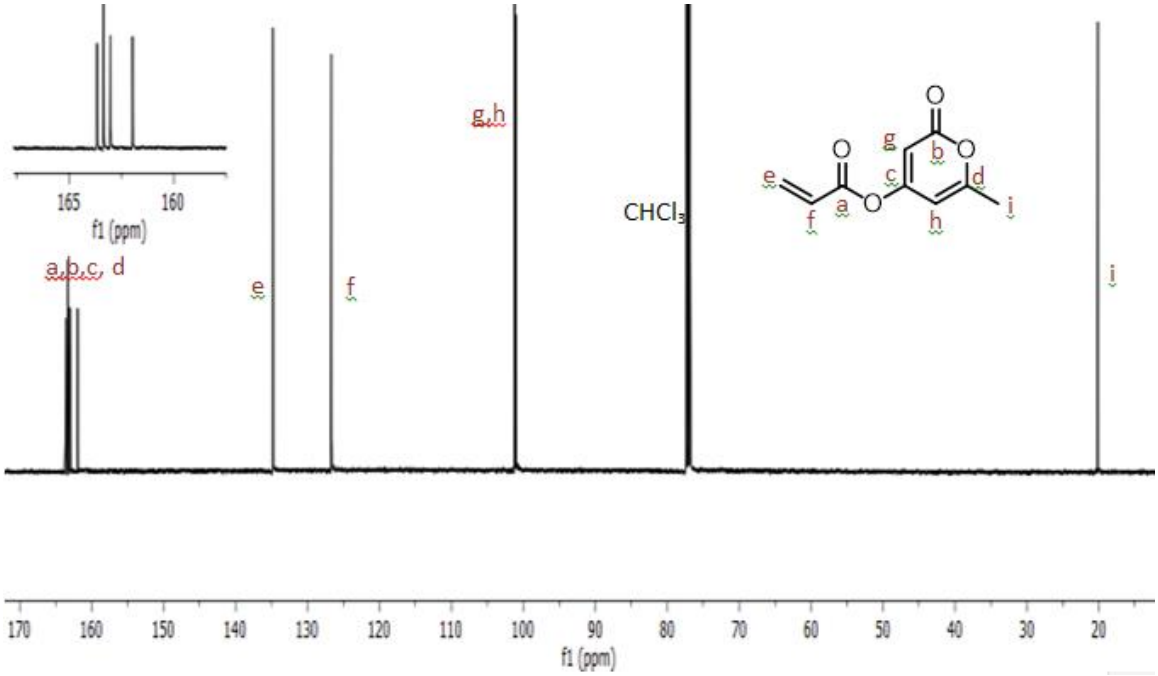

Figure 2. 8. $^{13}C\{^{1}H\}$ NMR spectrum of acrylated-pyrone (AcPy) ($CDCl_3$, 126 MHz).

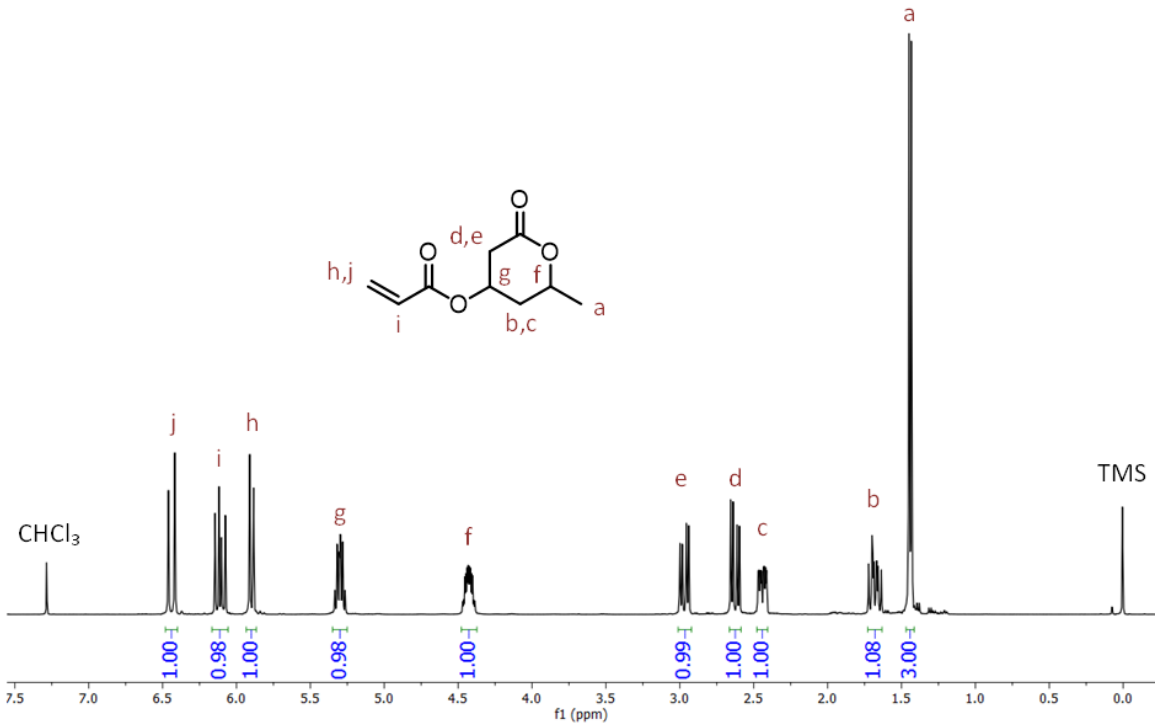

Figure 2. 9. ^{1}H NMR spectrum of acrylated-lactone (AcLa) ($CDCl_3$, 500 MHz).

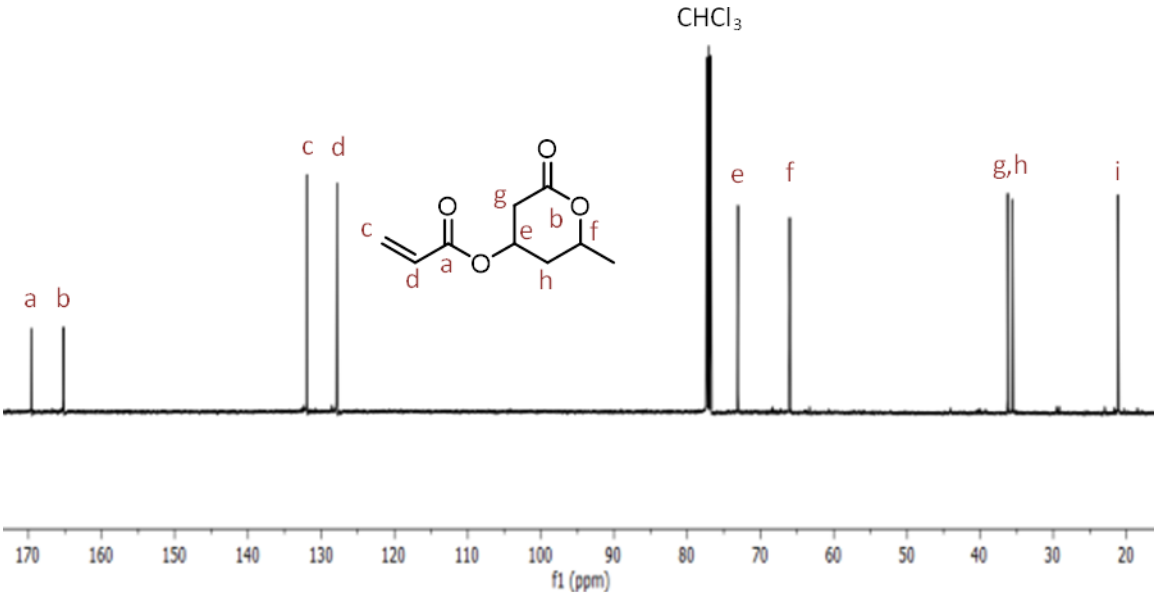

Figure 2. 10. $^{13}C\{^{1}H\}$ NMR spectrum of acrylated-lactone (AcLa) ($CDCl_3$, 126 MHz).

Prior to block-copolymerization with p(LauAc), attempts towards the free-radical and RAFT polymerizations of AcPy were carried out with azobis(isobutyronitrile) (AIBN) and various chain transfer agents (CTAs) at 70 °C in DMF to establish reactivity and kinetics. Aliquots taken from the reaction mixture over time were analyzed by ^{1}H NMR spectroscopy, and the results indicated that no appreciable polymerization had occurred. In contrast, the free radical polymerization of AcLa under similar reaction conditions yielded p(AcLa) (Figure 2.11), reaching equilibrium at 88% conversion (^{1}H NMR spectroscopy). We speculate that the observed difference in reactivity between AcPy and AcLa towards radical polymerizations may be attributed to the alkene bonds of the pyrone ring, which can react with propagating radicals and lead to chain-termination events.

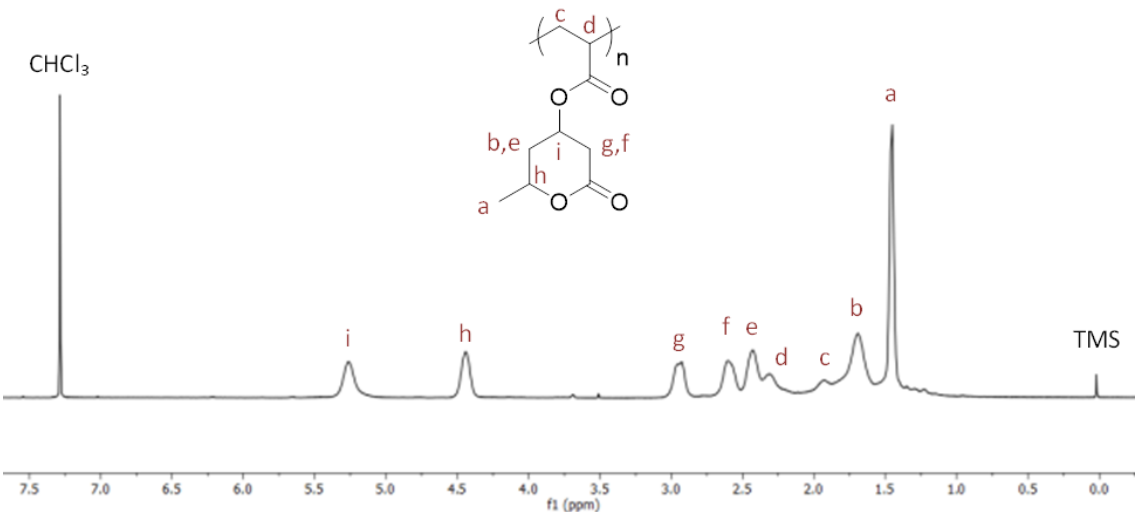

Figure 2. 11. ^{1}H NMR spectrum of p(AcLa) ($CDCl_3$, 500 MHz).

The purified p(AcLa) homopolymer was analyzed by size exclusion chromatography in DMF with multiangle laser light scattering (SEC-MALLS) to determine the number-average molar mass (M_n) = 30 kg mol^{-1} and dispersity ($Đ$) = 1.60 (Figure 2.12). Thermogravimetric analysis (TGA) showed a thermal degradation temperature (T_d, 5 wt% loss) of 197 °C (Figure 2.13). Since degradation of polyacrylic backbones typically occurs ~300 - 350 °C following a random chain scission mechanism, the relatively low observed T_d of p(AcLa) is likely due to the decomposition of the pendant lactone rings.[101,102] Differential scanning calorimetry (DSC) analysis of the homopolymer, scanning to a maximum temperature limit of 170 °C, initially indicated a T_g of 84 °C (Figure 2.14). This relatively high T_g of p(AcLa) suggests that it can be used as the 'glassy' component in a triblock copolymer system. Intriguingly, the DSC thermogram exhibited an exothermic feature beginning at 125 °C during the first temperature sweep; the second heating ramp in the experiment then showed a shift of the T_g value of the homopolymer to lower temperatures (~23 °C in Figure 2.14). Both the exothermic feature and the observed shift in T_g between consecutive heating ramps were not observed if the DSC experiment was conducted to a maximum temperature limit of 110 °C (Figure 2.15). The soluble fraction of a sample of p(AcLa) subjected to temperatures above 125 °C was analyzed via ^{1}H NMR spectroscopy. The results indicated the presence of parasorbic acid (Figure 2.16), which is presumably ejected from the polymer backbone at elevated temperatures.[30,103] A change in the polymer sequence (i.e. interspersed acrylic acid moieties along the backbone of the polymer) and the presence of a small molecule within the polymer matrix are likely responsible for the

observed shift in T_g seen in Figure 2.14. Nevertheless, since the formulated adhesives in this work are stable up to 125 °C, and only change chemically upon exposure to higher temperatures, processing temperatures of ~100 °C (i.e. above the T_g of both blocks) would be unlikely to interfere with treatment. Additionally, since most commodity PSAs are typically used at room temperature (tape, sticky notes, etc.), the chemical change observed at elevated temperatures will not limit user-end applicability.

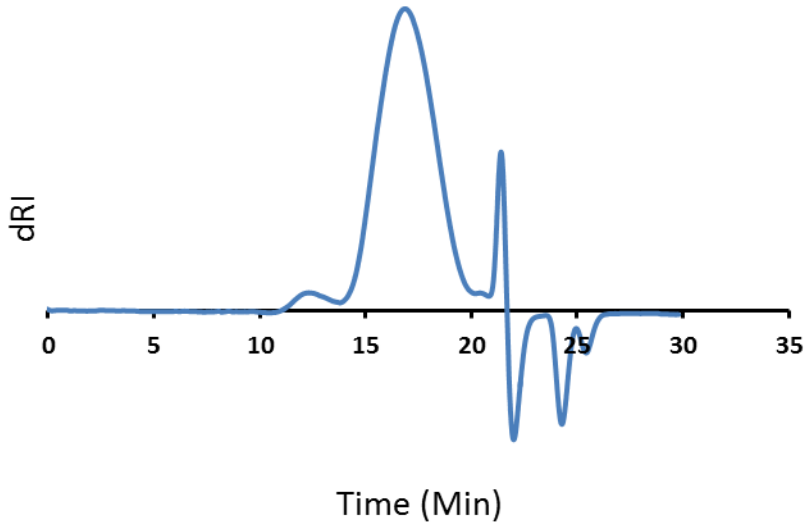

Figure 2. 12. DMF SEC trace of p(AcLa) with differential refractive index.

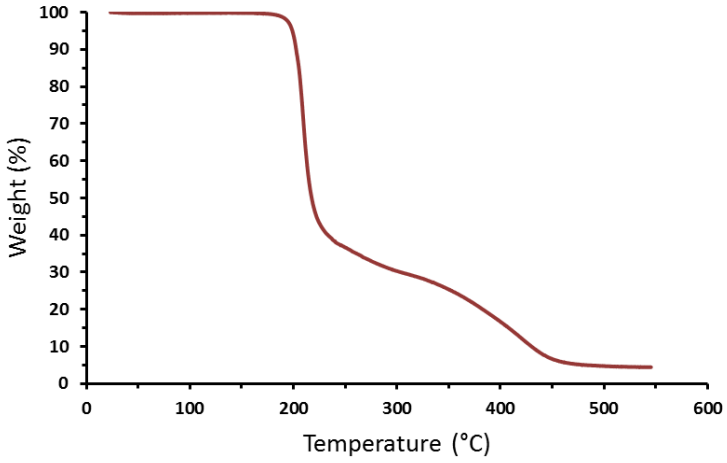

Figure 2. 13. TGA thermogram of p(AcLa) at a heating rate of 10 °C/min.

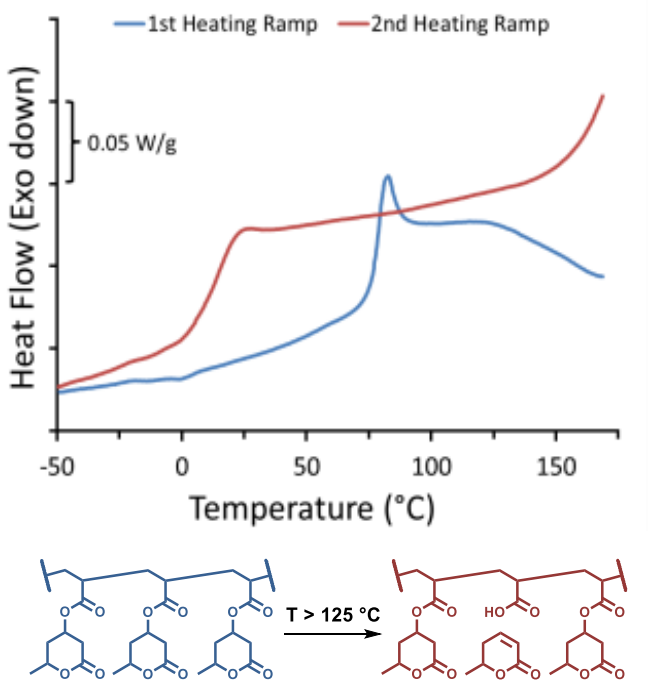

Figure 2. 14. DSC thermograms of p(AcLa) from -50 to 170 °C taken on the first and second ramps of heating at 10 °C/min. The synthetic scheme shown depicts the chemical change of the polymer at temperatures above 125 °C. ^{1}H-NMR spectrum of the ejected small molecule, parasorbic acid, can be found in Figure S9.

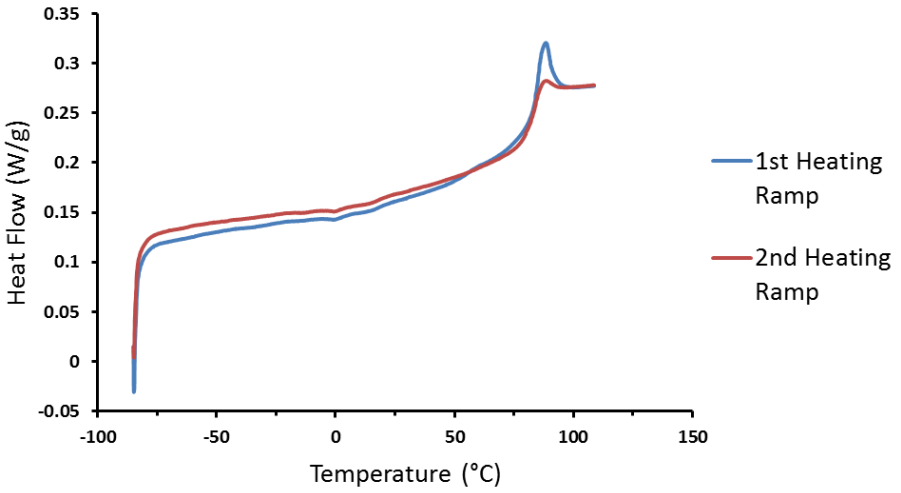

Figure 2. 15. DSC thermograms of p(AcLa) from -80 to 110 °C taken on the first and second ramps of heating at 10 °C/min.

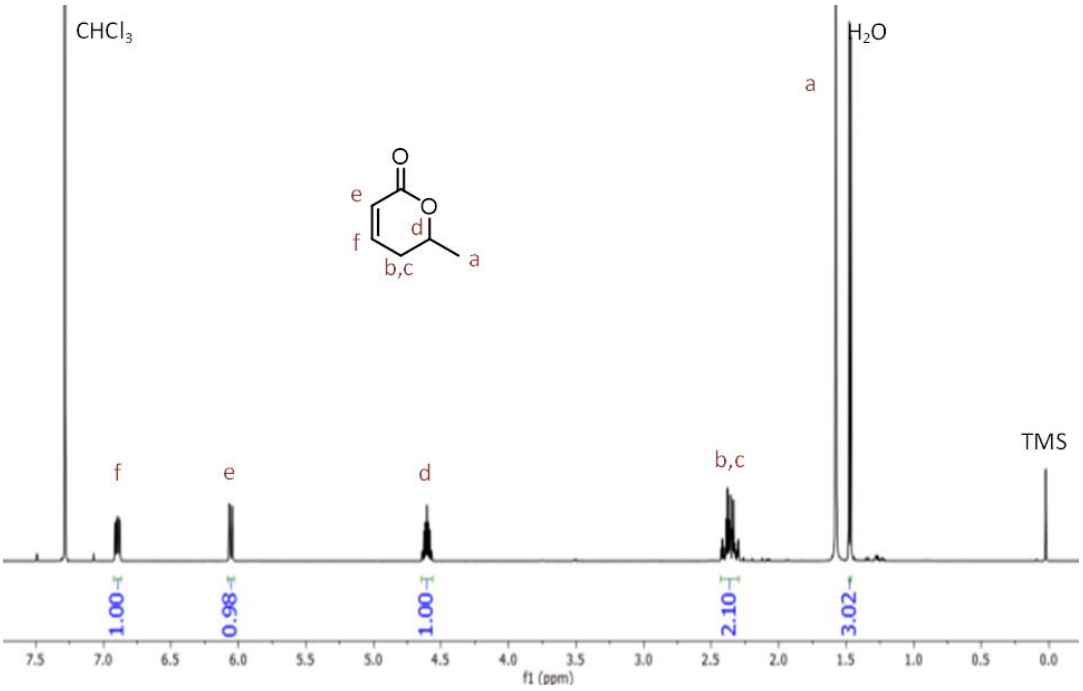

Figure 2. 16. ^{1}H NMR spectrum of parasorbic acid that is ejected from p(AcLa) upon exposure of the polymer to temperatures above 125 °C (CDCl3, 500 MHz).

We then used a controlled radical polymerization strategy to prepare a family of triblock copolymers (Scheme 2.4).[104–106] In addition to testing p(LauAc) as the base elastomer, nBA was also polymerized in accordance to previous methods.[83,84,91] A molecular weight of 55 kDa for the p(nBA) midblock was targeted to allow for direct comparisons among the various PSAs which have used p(nBA) of that molecular weight as the base elastomer and different acrylic derivatives as the glassy endblocks. RAFT polymerization of nBA was performed in the bulk with AIBN and BTCBA at 70 °C to afford the living macro-CTA (Figure 2.17). The number average molar mass, analyzed via THF SEC-MALLS, and the measured thermal data (T_d and T_g) of this rubbery midblock were in agreement with values previously reported for this synthetic procedure (Table 2.1, Figure 2.18, Figure 2.19).[83,84] Lauryl acrylate was polymerized to target molecular weights such that the elastomer is minimally entangled (~3 X M_e) and therefore has a low elastic modulus which is desirable for bonding of the adhesive to a given substrate. The molecular weights of the glassy p(AcLa) endblocks were varied to examine the effect of higher hard block weight percentages on the adhesive performance of the PSAs.

Scheme 2. 4. Synthesis of p(AcLa)-p(nBA)-p(AcLa) and p(AcLa)-p(LauAc)-p(AcLa) triblock copolymers via RAFT polymerization.

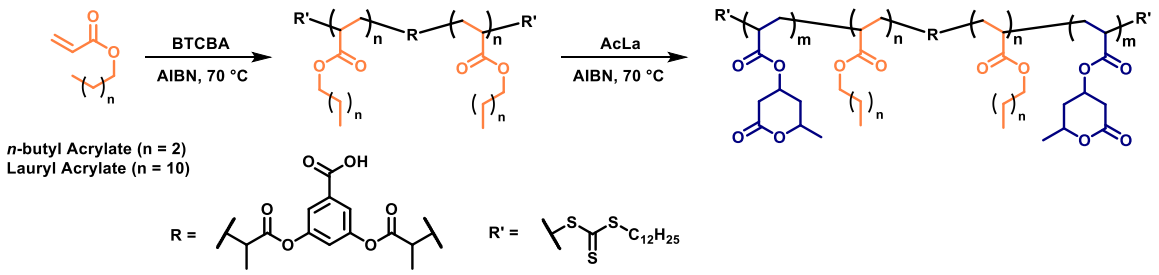

Table 2. 1. Data summary of the p(nBA) and p(LauAc) macro-CTAs and their corresponding chain-extended triblock copolymers.

Polymer	Sample Code[a]	M_n[b] (kDa)	$Đ$[c]	Hard block[d] (wt %)	T_d[e] (°C)	T_g[f] (°C)
p(nBA)	-	55	1.04	-	327	-47
p(AcLa)-p(nBA)-p(AcLa)	P1	2-55-2	1.13	5	286	-47
p(AcLa)-p(nBA)-p(AcLa)	P2	4-55-4	1.14	13	203	-47
p(AcLa)-p(nBA)-p(AcLa)	P3	7-55-7	1.16	20	200	-47, 84
p(AcLa)-p(nBA)-p(AcLa)	P4	10-55-10	1.14	27	198	-47, 84
p(LauAc)	-	230	1.16	-	336	-
p(AcLa)-p(LauAc)-p(AcLa)	P5	10-230-10	1.29	8	210	-
p(AcLa)-p(LauAc)-p(AcLa)	P6	15-230-15	1.25	12	203	84
p(LauAc)	-	300	1.19	-	336	-
p(AcLa)-p(LauAc)-p(AcLa)	P7	9-300-9	1.36	6	220	-

[a]p(nBA) was chain extended to synthesize **P1-P4** and p(LauAc) was chain extended to synthesize **P5-P7**. [b]Number-average molar mass as determined through size-exclusion chromatography (SEC). [c]Dispersity as determined through SEC. [d]AcLa content relative to total molecular weight. [e]Decomposition temperature corresponding to 5% weight loss as determined by thermal gravimetric analysis (TGA). [f]Observable glass transition temperature(s) determined by differential scanning calorimetry (DSC).

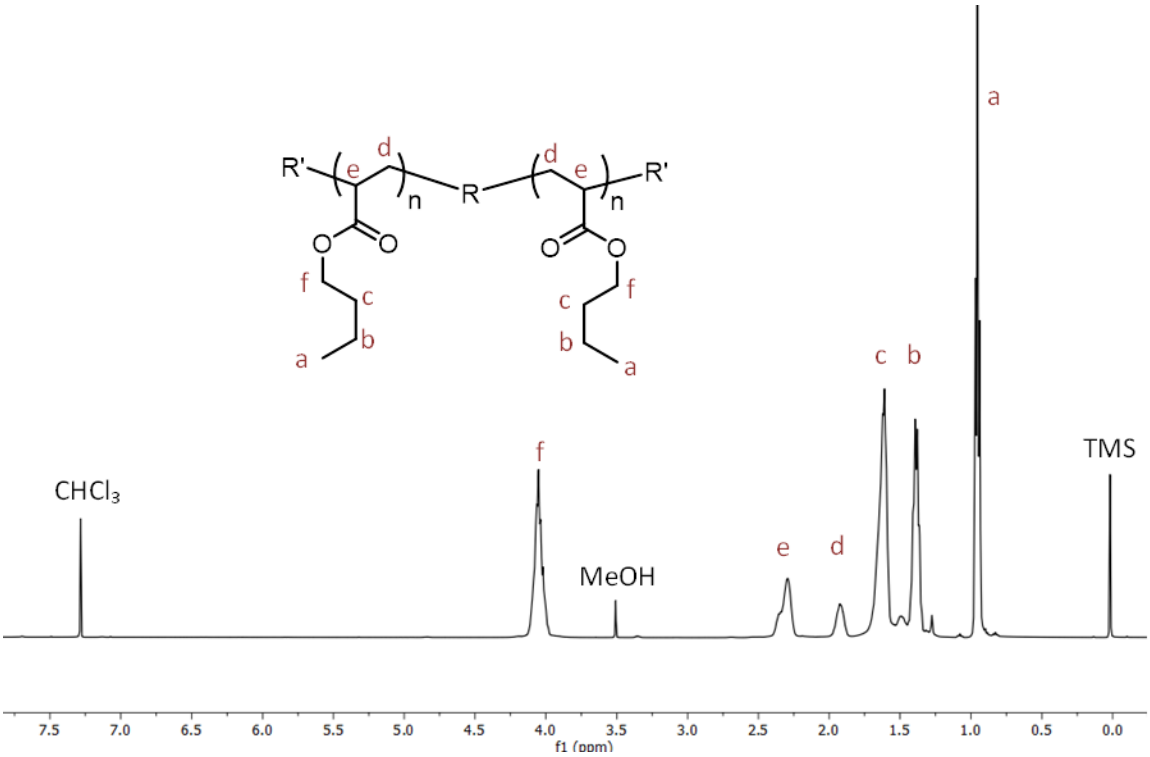

Figure 2. 17. ^{1}H NMR spectrum of the p(nBA) macro-CTA ($CDCl_3$, 500 MHz).

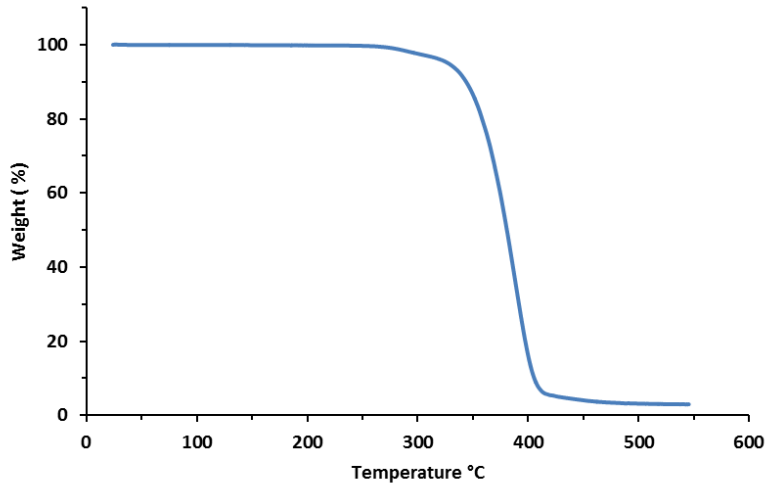

Figure 2. 18. TGA thermogram of p(nBA) macro-CTA at a heating rate of 10 °C·min^{-1}.

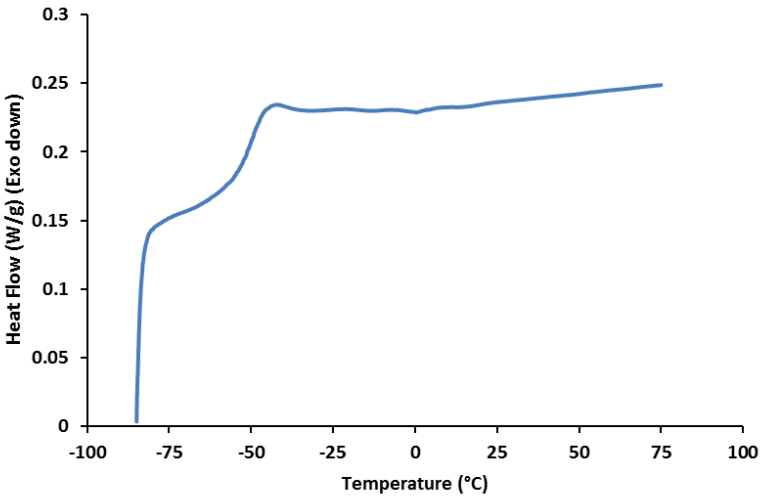

Figure 2. 19. DSC thermogram of p(nBA) macro-CTA at a heating rate of 10 °C·min^{-1} taken on the second heating cycle.

Subsequent chain extension of the p(nBA) and p(LauAc) macro-CTAs with AcLa afforded the desired triblock copolymers. Successful chain extension was validated by observation of peaks corresponding to p(AcLa) in the ^{1}H NMR spectra (Figures 2.20 and 2.21) accompanied by a clear shift of the SEC traces to lower retention times when compared to the macro-CTAs (Figures 2.22 – 2.24). The presence of a shoulder in the SEC traces at lower retention times is likely due to the formation of multiblock polymers stemming from termination-by-combination events. By adjusting the molar ratio of macro-CTA to AcLa in the reaction mixture, variable weight percentages of hard block content within the resultant triblock copolymers were attained (Table 2.1). TGA profiles of the triblock copolymers (**P1 – P7**) show two distinct features at 190 °C and 350 °C, corresponding to the decomposition of the pendant lactone rings and the acrylate backbone, respectively (Figures 2.25 – 2.31). While the glass transition temperature of

the p(nBA) midblock can be clearly seen in the DSC thermograms of **P1** – **P4** (Figure 2.32), the T_g feature of the p(AcLa) blocks is only well-defined in **P3** and **P4**, which have longer endblock lengths. The DSC thermograms of **P5 – P7** (Figures 2.33 – 2.35, respectively) show the T_m and T_c features of the dodecyl alkyl chains, but a discernable T_g peak for the p(AcLa) segments is only seen in **P6**, which also contains the highest weight fraction of the hard blocks. This observation has been reported for other triblock copolymers with relatively low hard block content and is likely a result of the shorter p(AcLa) segments,[83,84,91] which ultimately translates to imperceptible heat exchange in the calorimetry experiment. Furthermore, a match of both the p(nBA) and p(AcLa) T_g values in the triblock copolymers to those of their homopolymers suggests that the two blocks are immiscible.[107]

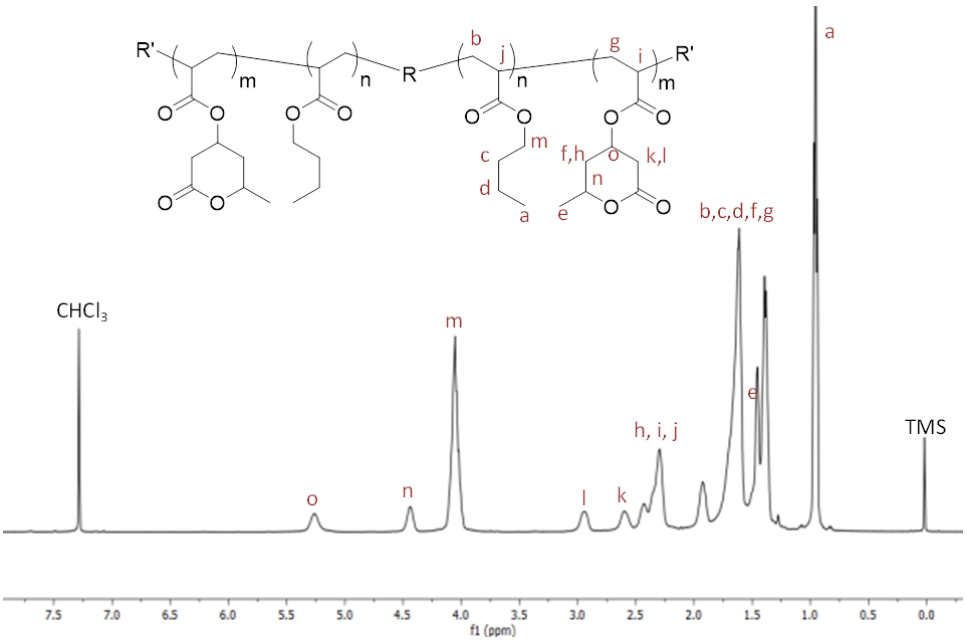

Figure 2. 20. Representative ^{1}H- NMR spectrum of p(AcLa)-p(nBA)-p(AcLa) triblock copolymers ($CDCl_3$, 500 MHz).

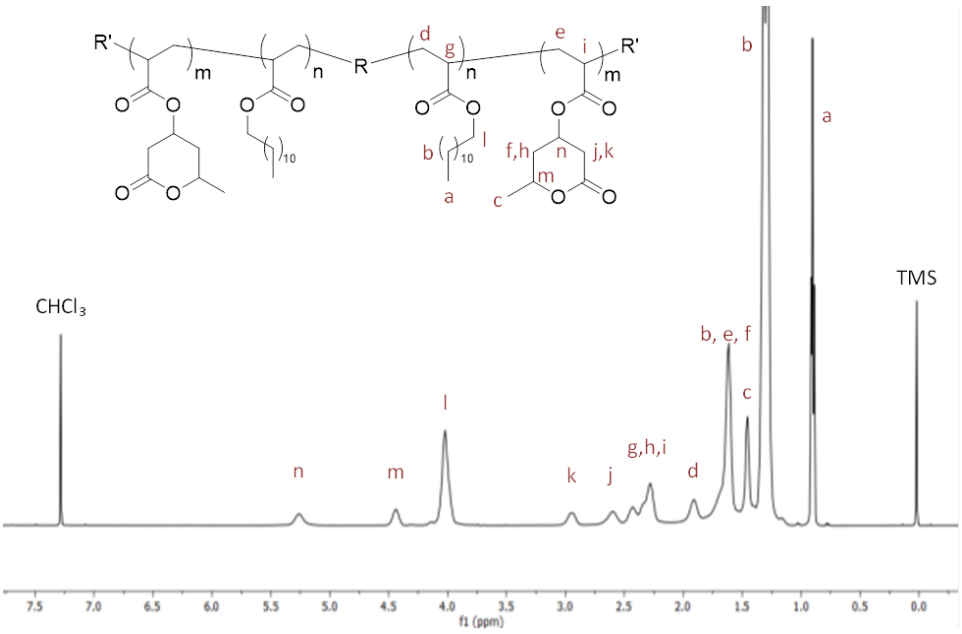

Figure 2. 21. Representative ^{1}H- NMR spectrum of p(AcLa)-p(LauAc)-p(AcLa) triblock copolymers ($CDCl_3$, 500 MHz).

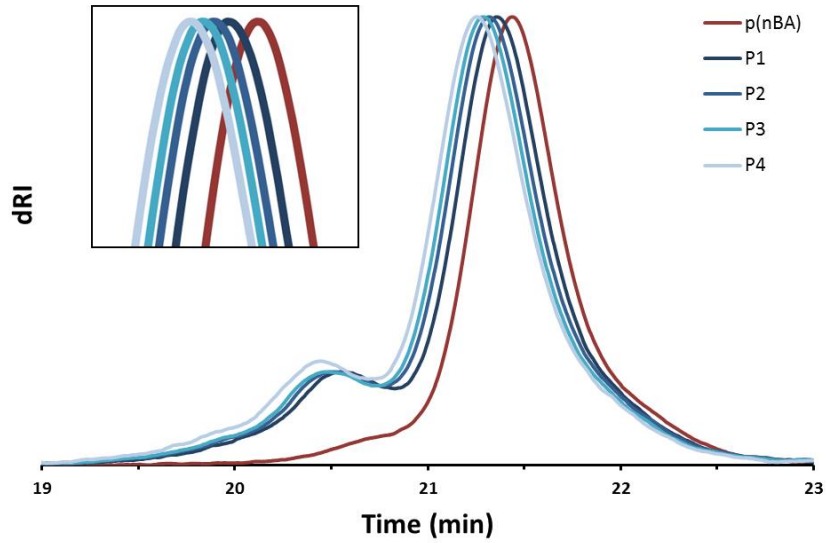

Figure 2. 22. Stacked SEC traces of the p(nBA) macro-CTA (red) and the chain-extended p(AcLa)-p(nBA)-p(AcLa) triblock polymers (blue) (eluent: THF).

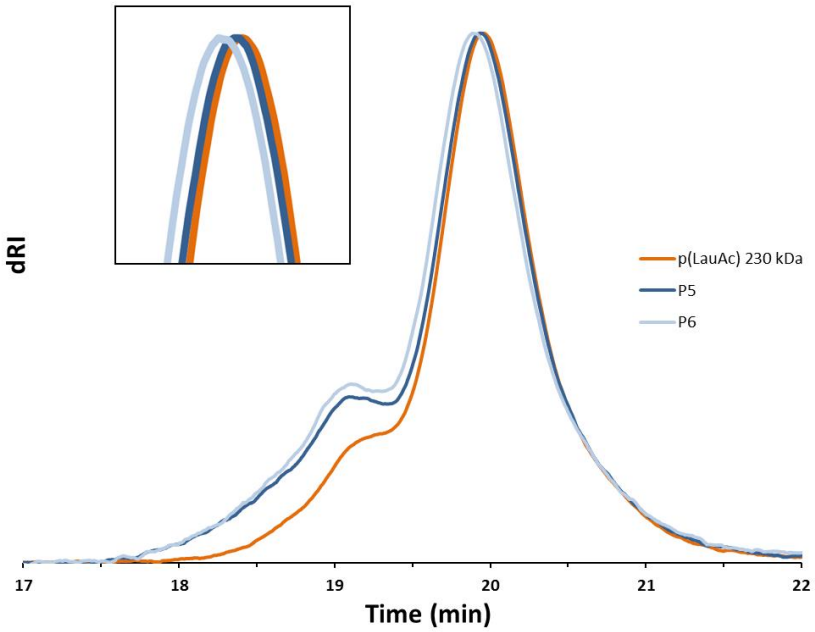

Figure 2. 23. Stacked SEC traces of the p(LauAc) macro-CTA (230 kDa) (orange) and the chain-extended p(AcLa)-p(LauAc)-p(AcLa) triblock polymers (blue) (eluent: THF).

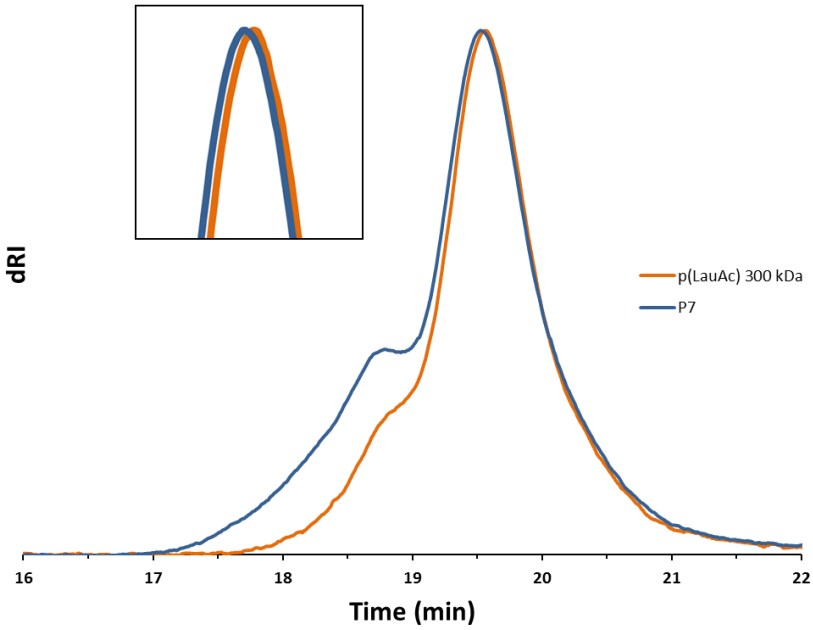

Figure 2. 24. Stacked SEC traces of the p(LauAc) macro-CTA (300 kDA) (orange) and the chain-extended p(AcLa)-p(LauAc)-p(AcLa) triblock polymer (blue) (eluent: THF).

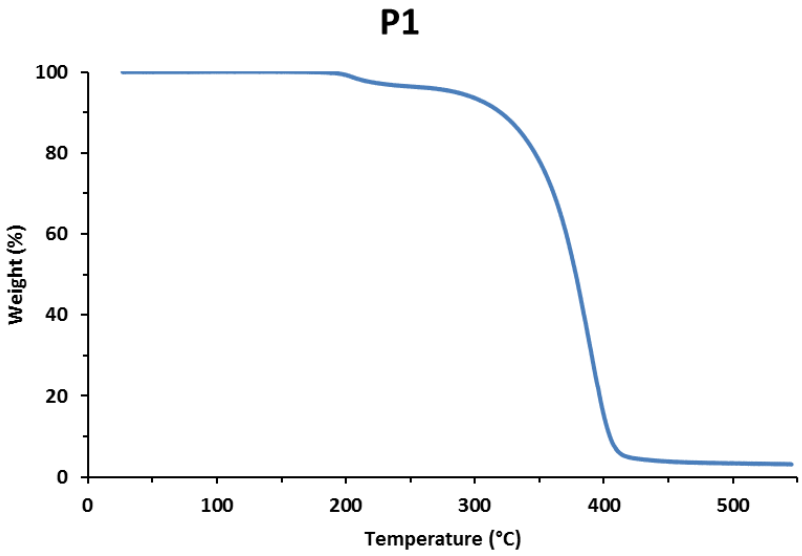

Figure 2. 25. TGA thermogram of P1 at a heating rate of 10 °C/min.

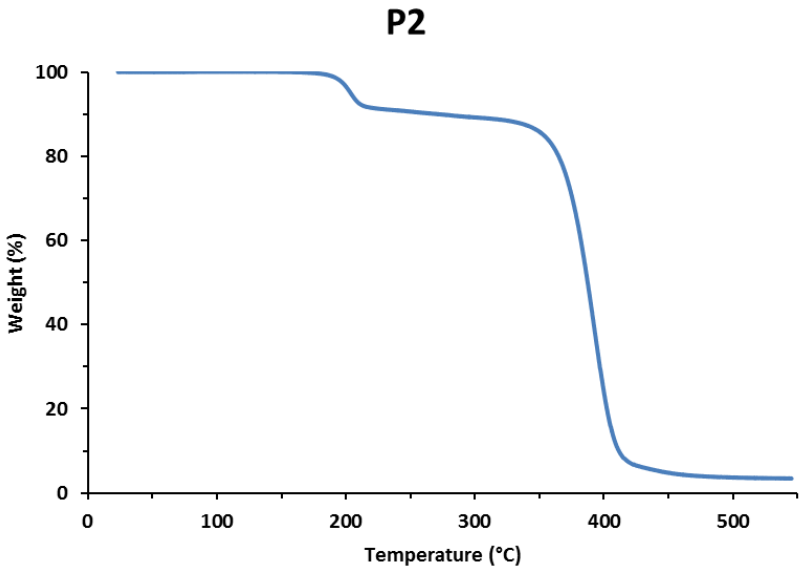

Figure 2. 26. TGA thermogram of P2 at a heating rate of 10 °C/min.

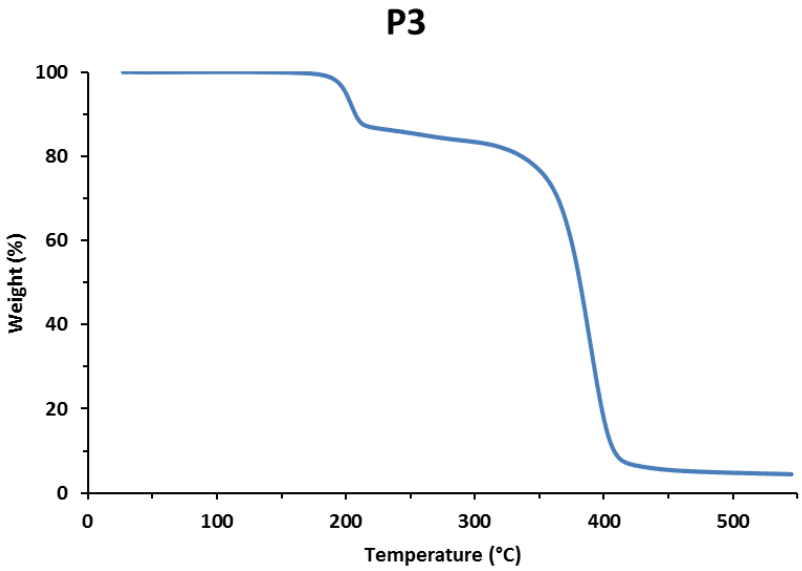

Figure 2. 27. TGA thermogram of P3 at a heating rate of 10 °C/min.

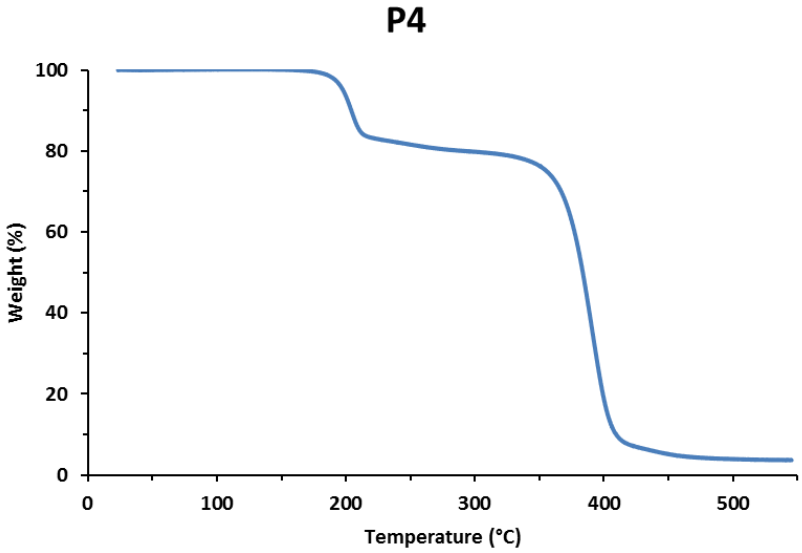

Figure 2. 28. TGA thermogram of P4 at a heating rate of 10 °C/min.

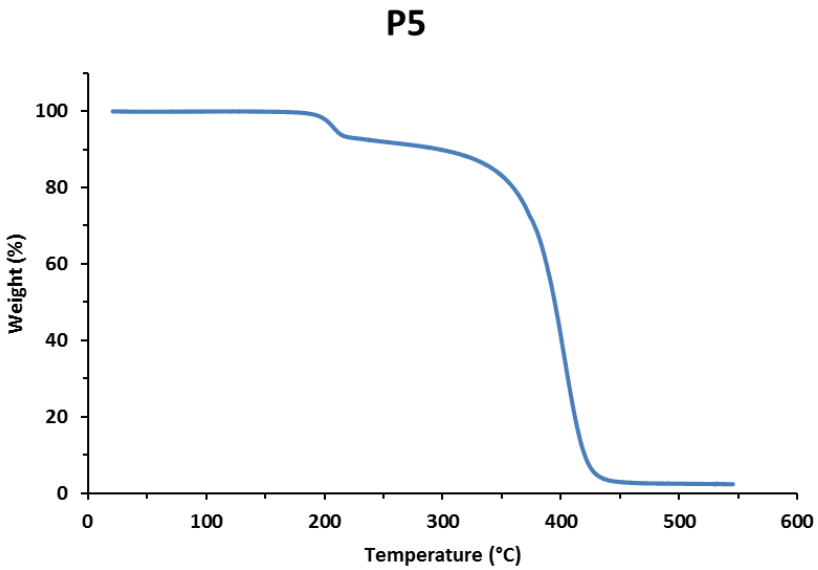

Figure 2. 29. TGA thermogram of P5 at a heating rate of 10 °C/min**.**

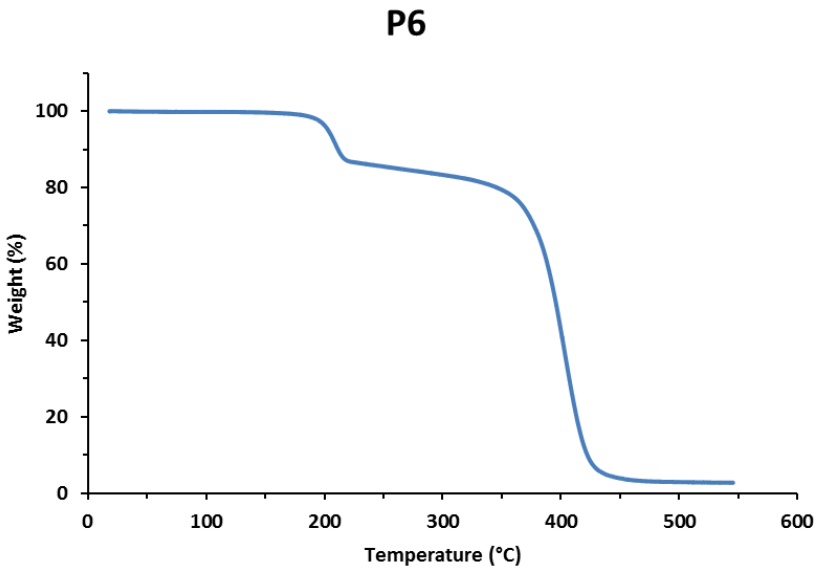

Figure 2. 30. TGA thermogram of P6 at a heating rate of 10 °C/min.

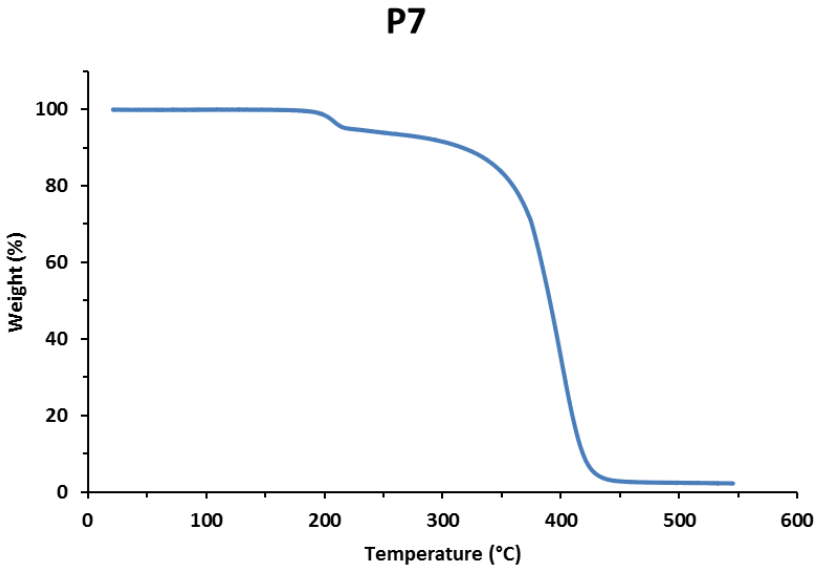

Figure 2. 31. TGA thermogram of P7 at a heating rate of 10 °C/min.

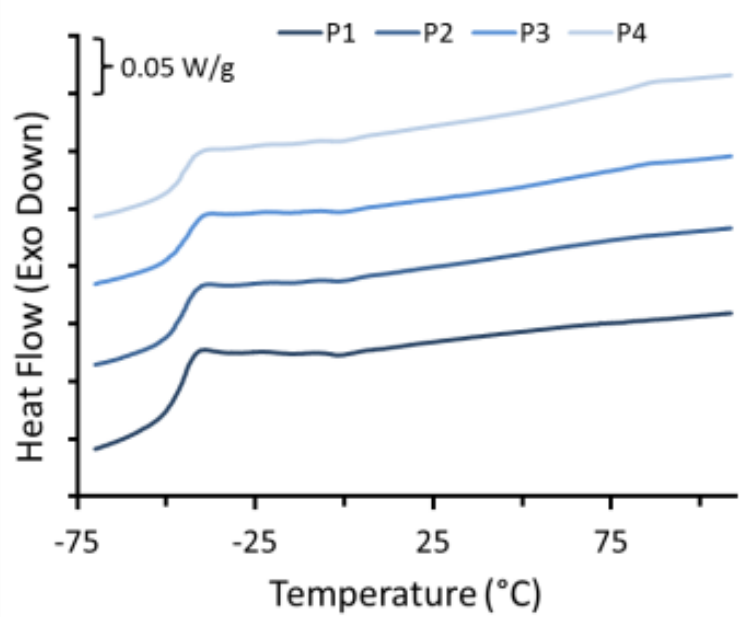

Figure 2. 32. DSC thermograms of the triblock copolymers P1-P4 at a heating rate of 10 °C·min^{-1} taken on the second heating cycle. The thermogram shows the T_g of the p(nBA) midblock to be -47 °C in all samples but a discernable feature corresponding to the T_g of the p(AcLa) endblocks at 84 °C only for P3 and P4.

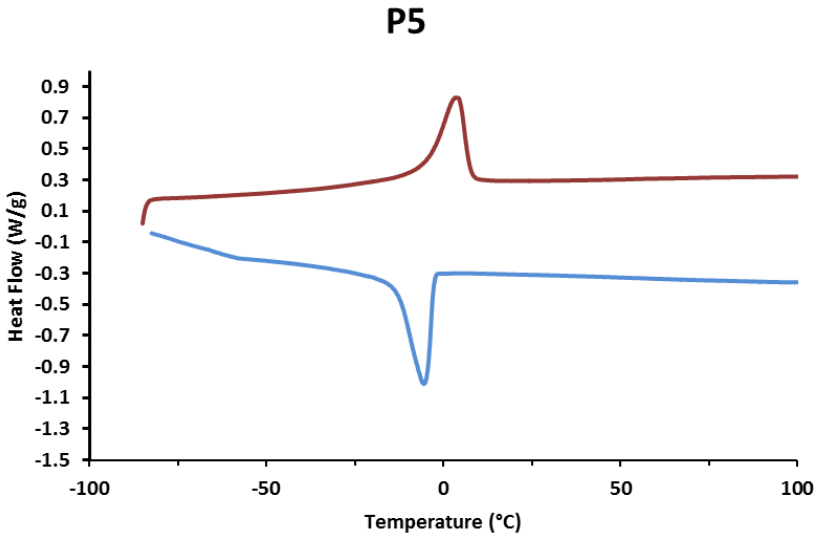

Figure 2. 33. DSC thermogram of the triblock copolymer P5 at a heating rate of 10 °C·min^{-1} taken on the second heating cycle.

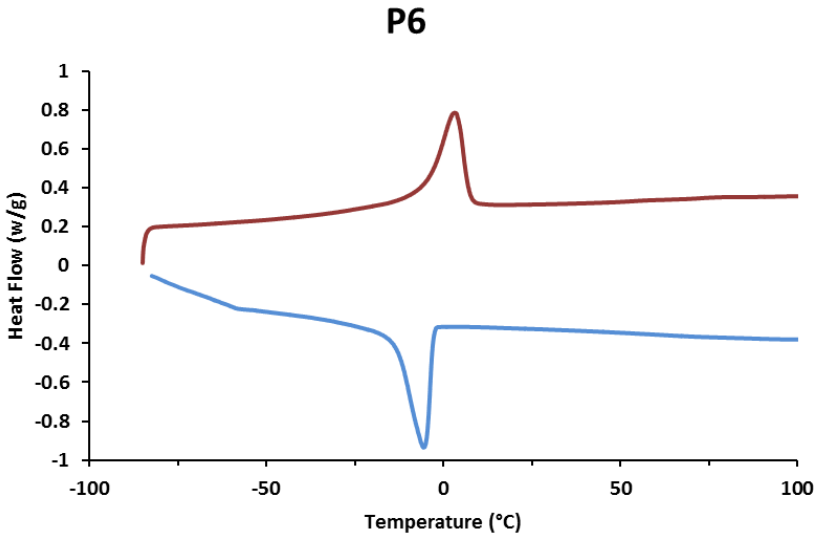

Figure 2. 34. DSC thermogram of the triblock copolymer P6 at a heating rate of 10 °C·min^{-1} taken on the second heating cycle.

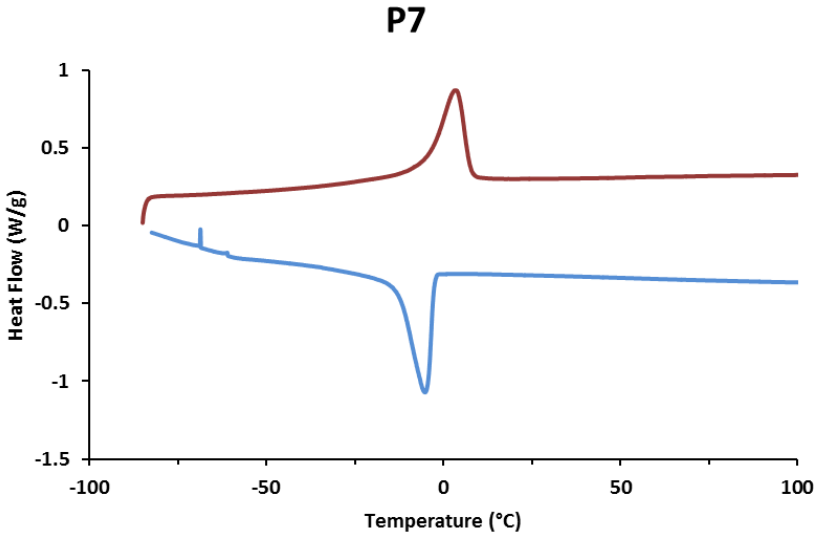

Figure 2. 35. DSC thermogram of the triblock copolymer P7 at a heating rate of 10 °C·min^{-1} taken on the second heating cycle.

To evaluate the materials as pressure sensitive adhesives and understand how the ratio of glassy block affects their properties, samples for adhesion testing were prepared by casting solutions of the polymers onto a sheet of PET film (see Experimental for details). The adhesive capabilities of thin films of the triblock copolymers with and without added ester-based tackifier were evaluated by Pressure Sensitive Tape Council (PSTC) standard methods. Samples of triblock copolymers were mixed with the appropriate amount of tackifier and the adhesive properties of the polymer and polymer/tackifier blends were evaluated and compared by a 180° peel test (PSTC-101) to assess adherence, a loop tack bonding test (PSTC-16) to measure tackiness (instantaneous bonding capability), and a static shear strength test (PSTC-107) to measure resistance to shear failure under an applied force. Another important factor in evaluating these PSAs is the mode of failure, which is qualitatively reported as "cohesive" or "adhesive". Cohesive failure is a result of failure within the adhesive layer which leaves behind residue on the surface, while adhesive failure occurs at the interfacial boundary. Either mode may be acceptable depending on the desired application of the adhesive, with cohesive failure being more favorable for permanent PSAs and adhesive failure sought for removable PSAs.[68,83,90,108,109] Blending of an appropriate tackifier was pursued in order to dilute entanglements of the midblock and effectively lower the elastic modulus of the material, allowing for tunable adhesive values under controlled test conditions.[90,110] DSC measurements of **P1** and **P2** with added Sylvalite 80HP rosin ester (a renewable resin manufactured by Arizona Chemicals) showed an increase in T_g of the p(nBA) midblock relative to the homopolymer (from -48 to -26 °C, Figures 2.36 and 2.37), suggesting

successful integration of the tackifier within the midblock.[111] A similar experiment with the p(LauAc) based triblock copolymers did not produce a discernable T_g feature in the DSC thermograms. Maximum values of peel adhesion were obtained with 30 wt% of tackifier added to the nBA based polymers and 40 wt% of tackifier added to the LauAc based polymers. Incorporation of greater amounts of tackifier (e.g. 60 wt%) led to a reduction in tack. This observation has similarly been seen with other block copolymers[74,111,112] and is explained by the apparent increase in T_g of the midblock with increasing tackifier content, ultimately diminishing tackiness. The results of the adhesion tests for the triblock copolymers are summarized in Figure 2.38 and Table 2.2. The raw data for the 180° peel tests and loop tack bonding tests is provided in Figures 2.39 – 2.58.

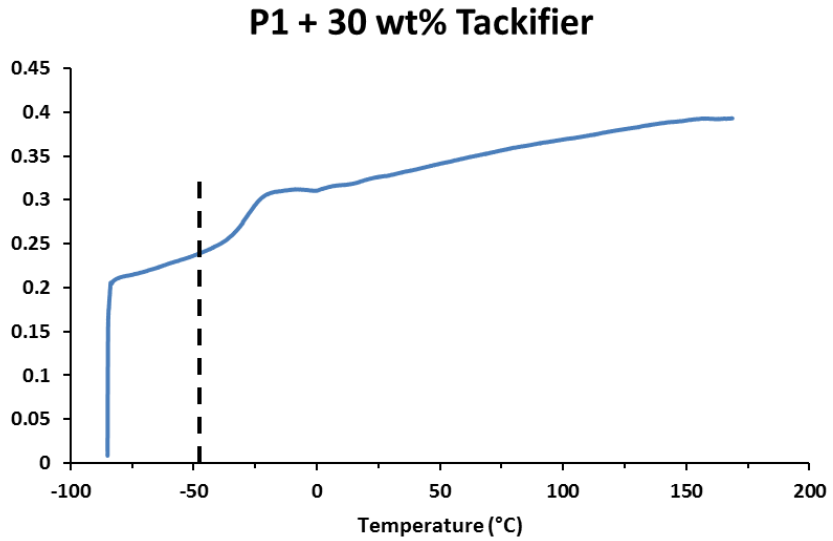

Figure 2. 36. DSC trace of P1 blended with 30 wt% of a rosin ester resin tackifier. The dashed line depicts the T_g of P1 without the addition of tackifier**.**

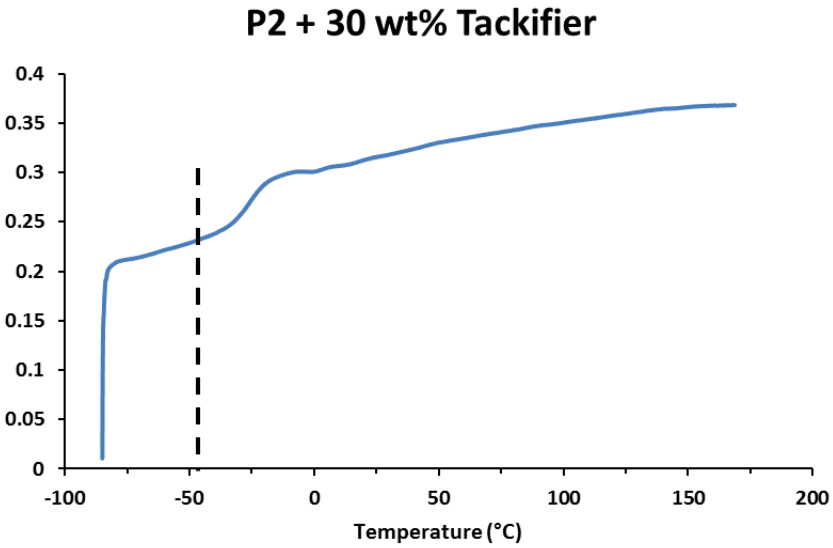

Figure 2. 37. DSC trace of P2 blended with 30 wt% of a rosin ester resin tackifier. The dashed line depicts the T_g of P2 without the addition of tackifier.

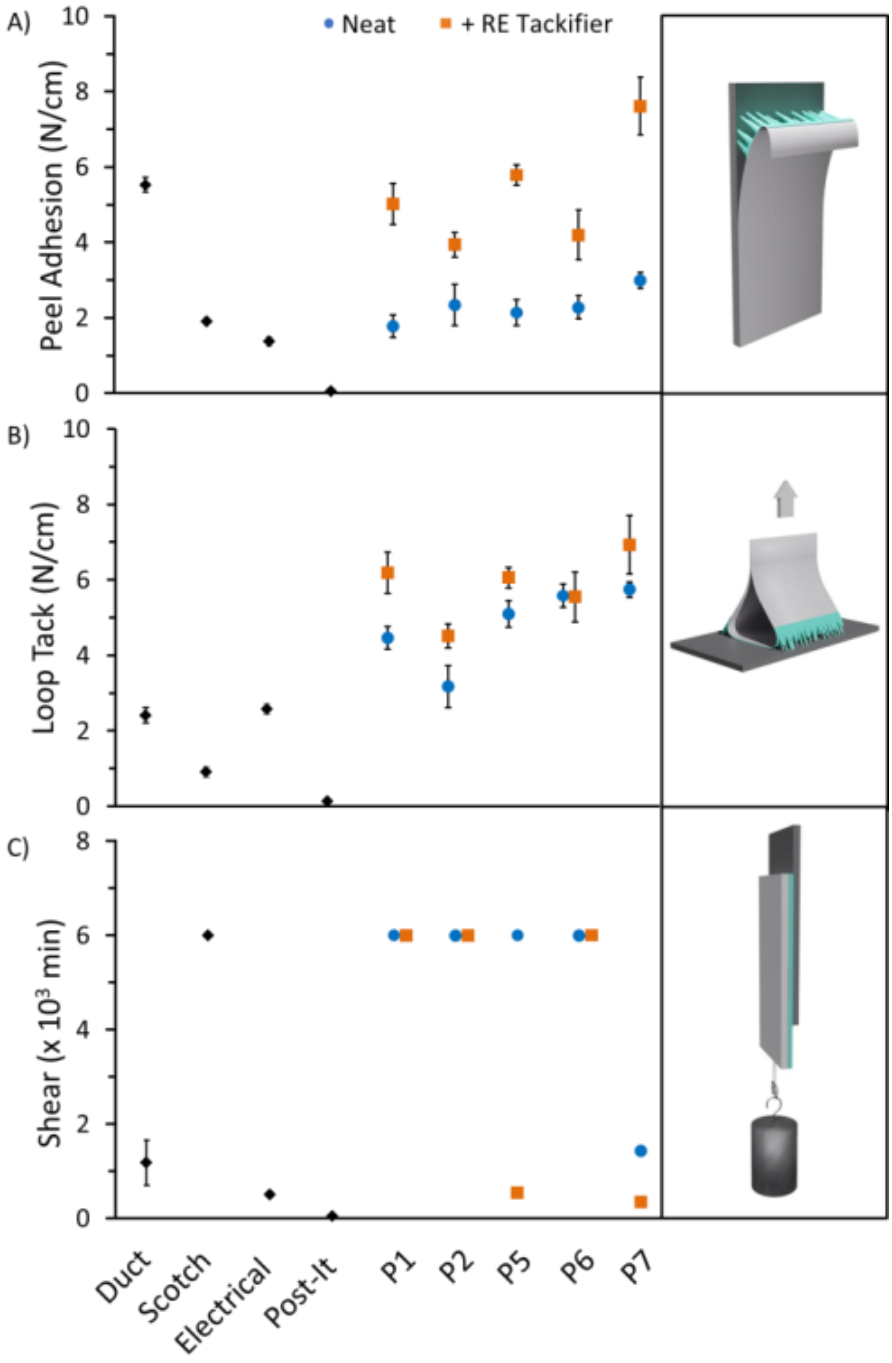

Figure 2. 38. Adhesive performance of p(AcLa)-p(nBA)-p(AcLa) (P1 and P2) and of p(AcLa)-p(LauAc)-p(AcLa) (P5 – P7) via a) 180° peel, b) loop tack, and c) static shear tests compared to commercial product values (black diamonds) reported in reference 51. The authors acknowledge John Beumer for creating the 3-D model images of the adhesion tests depicted in the figure.

Table 2. 2. Adhesion testing summary of the p(nBa) (P1 and P2) and p(LauAc) (P5 – P7) triblock copolymers.

Sample Code	M_n (kDa) (Hard block wt %)	Peel adhesion[b] (N/cm)	Loop tack[c] (N/cm)	Shear[d] (min)
P1	2-55-2 (7)	1.78 ± 0.30 5.02 ± 0.55[a]	4.46 ± 0.64 6.19 ± 0.95[a]	>6000 >6000[a]
P2	4-55-4 (13)	2.34 ± 0.55 3.94 ± 0.32[a]	3.17 ± 0.85 4.52 ± 0.82[a]	>6000 >6000[a]
P5	10-230-10 (8)	2.14 ± 0.35 5.79 ± 0.27[a]	5.10 ± 0.64 6.06 ± 0.33[a]	>6000 548 ± 19[a]
P6	15-230-15 (12)	2.28 ± 0.31 4.20 ± 0.66[a]	5.58 ± 0.59 5.55 ± 0.15[a]	>6000 >6000[a]
P7	9-300-9 (6)	2.99 ± 0.20 7.62 ± 0.77[a]	5.74 ± 0.37 6.93 ± 1.59[a]	1430 ± 26 343 ± 71[a]

[a]Adhesion values for the polymer blended with a rosin ester resin as a tackifier. [b]180° peel test using a stainless steel plate as the adherand, test method: PSTC-101. Loop tack test to a stainless steel plate, test method: PSTC-16. [d]Static shear adhesion to a stainless steel plate using 2.54 cm x 2.54 cm films and a 1 kg load, test method: PSTC-107.

By varying the tackifier content, peel adhesion values of the p(nBA)-based polymers can be tuned in the range of 2 – 6 N cm^{-1}, which are comparable to commercial commodity products such as Duct tape, Scotch tape, etc.[85,91] Cohesive failure was observed during the peel adhesion test of **P1**, while adhesive failure was observed for **P2**. The difference in the failure modes between **P1** and **P2** likely stems from the degree of endblock length, whereby longer lengths of the hardblocks translate to stronger intermolecular interactions within the glassy domains. These interactions result in stronger cohesive forces within the adhesive layer which leads to adhesive failure. Measured loop tack forces were in the range of 3 – 6 N cm^{-1}, also comparable to commercial products. Notably, the adhesives demonstrated excellent shear resistance under an applied static load. All formulations examined for adhesion, regardless of

hardblock weight percentage or tackifier content, did not fail for the duration of the testing period (100 h at room temperature). A comparison of these results to previous studies which have also used p(nBA) as the rubbery component for triblock-based PSAs[83,84,91] shows that peel adhesion forces are within the same 2 - 4 N cm^{-1} range (when tackifier is disregarded), despite the fact that different acrylic derivatives were used as the glassy component in each study. These results suggest that the adhesive forces in triblock PSA systems are predominately influenced by the base elastomer. That is, if p(nBA) is "loosely" entangled and contributes 80 - 90% of the copolymer by weight, the measured adhesion forces will be similar regardless of which glassy component is used. The materials obtained from **P3** and **P4**, which incorporated greater amounts of the glassy component in the polymers, exhibited negligible tack and thus could not be tested for adhesion.

Samples of **P5 - P7** were also blended with the rosin ester tackifier and the polymers and polymer/tackifier blends were evaluated as previously described. The results of the adhesion tests are summarized in Figure 2.38. Peel adhesion values are tunable in the range of 2 – 8 N cm^{-1} depending on tackifier content. Adhesive failure mode was observed only for **P6** which has the greatest hardblock content in this series. The measured peel adhesion forces of the neat p(LauAc)-based polymers were in the same range as the neat p(nBA)-based polymers (2 - 4 N cm^{-1}), proving that longer alkyl acrylates can effectively be used as the base elastomer for PSAs as long as the higher M_e can be overcome. The measured loop tack forces were in the range of 5 – 8 N cm^{-1}, consistently greater than those measured for the PSAs which use p(nBA) as the rubbery

midblock with similar hardblock lengths. This observation is likely a consequence of the lower elastic modulus of p(LauAc) than that of p(nBA), resulting in a "tackier" material which adheres to the substrate more quickly. The shear test results indicated that the p(LauAc) series of polymers performed worse than the p(nBA) series. Only **P6**, which has the greatest hard block weight fraction, demonstrated resistance to shear failure on par with the p(nBA) series. Addition of tackifier to **P5** and **P7**, which theoretically lowers the elastic modulus of the elastomer, resulted in greater peel adhesion and loop tack forces but led to a reduction in shear resistance. The spread of adhesion/tack forces and shear failure shows that the formulations of these sustainably sourced acrylic adhesives can be modified in a systematic manner to target a specific application (i.e. permanent vs removable PSAs) and are competitive in performance to commodity products on the market today. Additionally, in contrast to other biorenewable PSAs which use a polyester-based rubbery midblock,[68,74,76,77] this acrylic-based system is shown to exhibit good adhesion both with and without tackifier additives because of the lower elastic modulus; however, polyester-based PSAs still maintain the distinct advantage of better degradability over their acrylic counterparts.

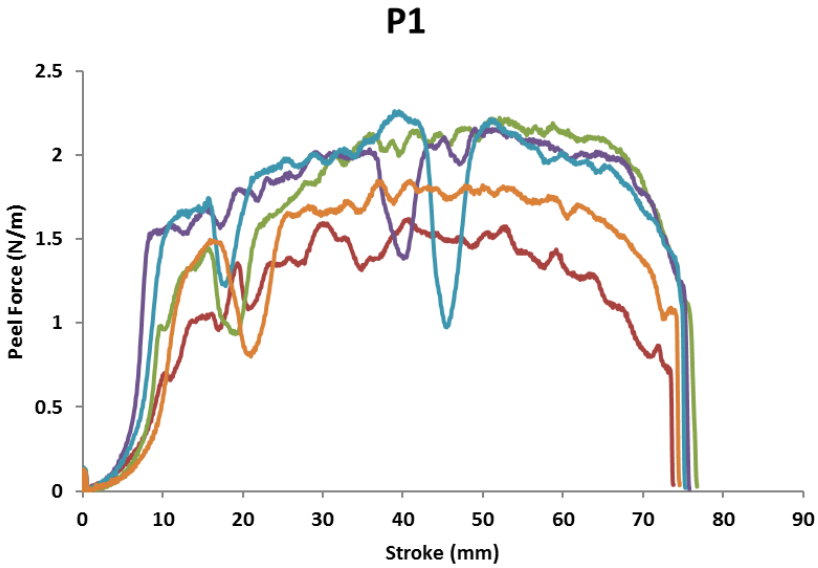

Figure 2. 39. 180° peel test of P1.

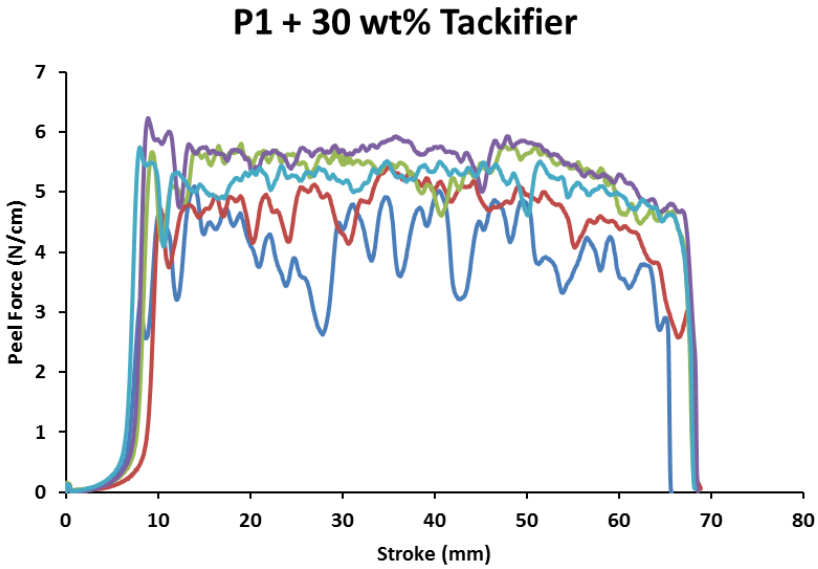

Figure 2. 40. 180° peel test of P1 blended with 30 wt% of a rosin ester resin tackifier.

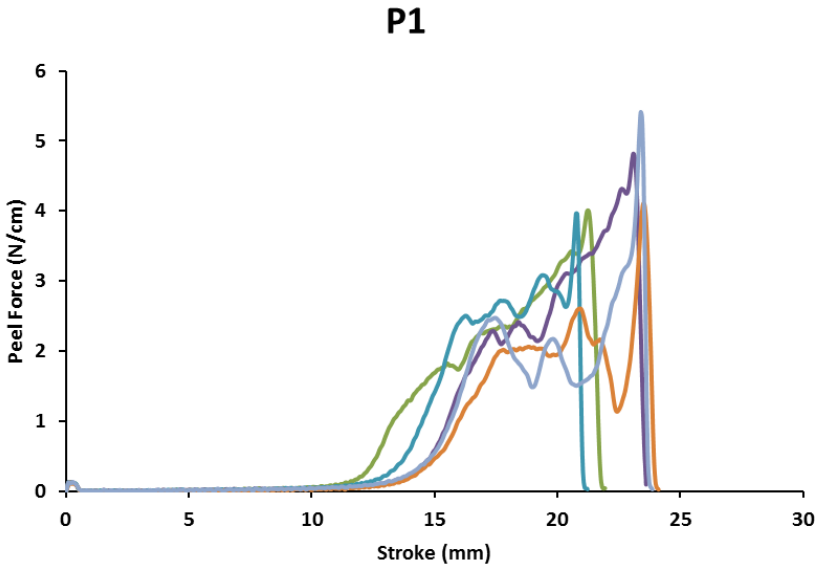

Figure 2. 41. Loop tack test of P1.

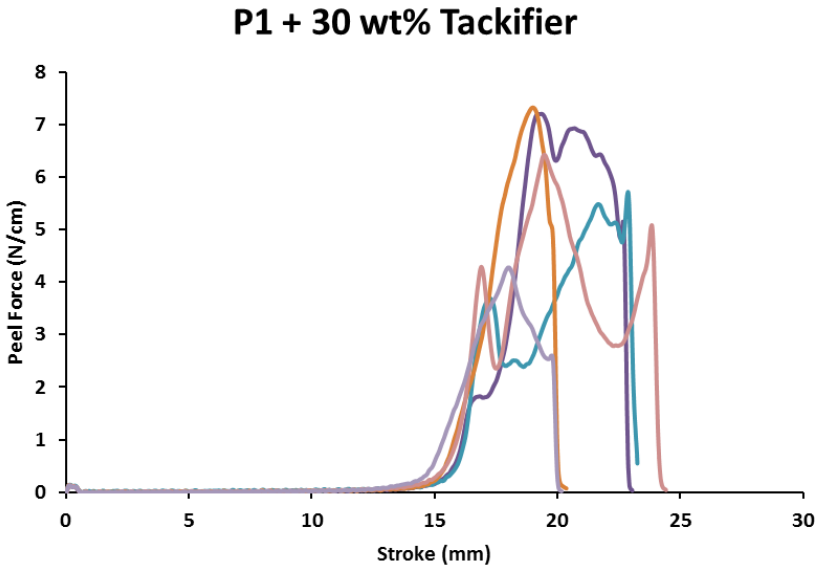

Figure 2. 42. Loop tack test of P1 blended with 30 wt% of a rosin ester resin tackifier.

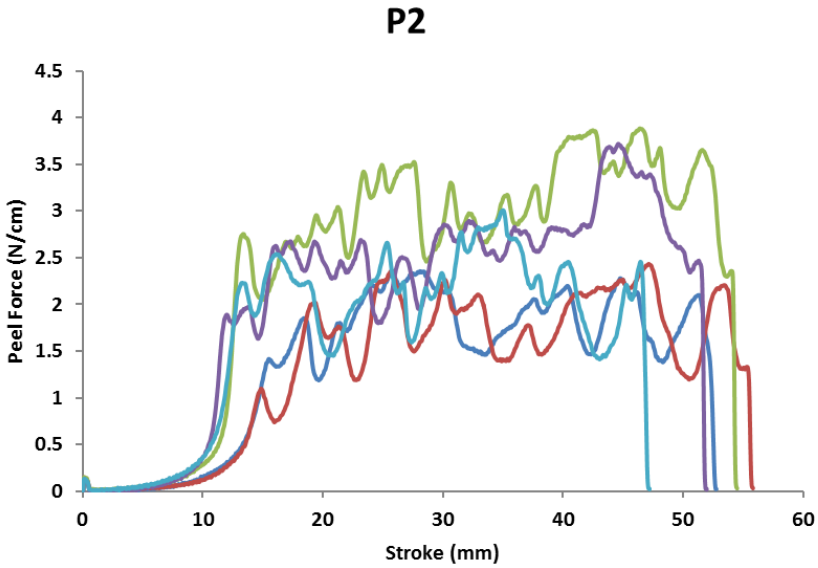

Figure 2. 43. 180° peel test of P2.

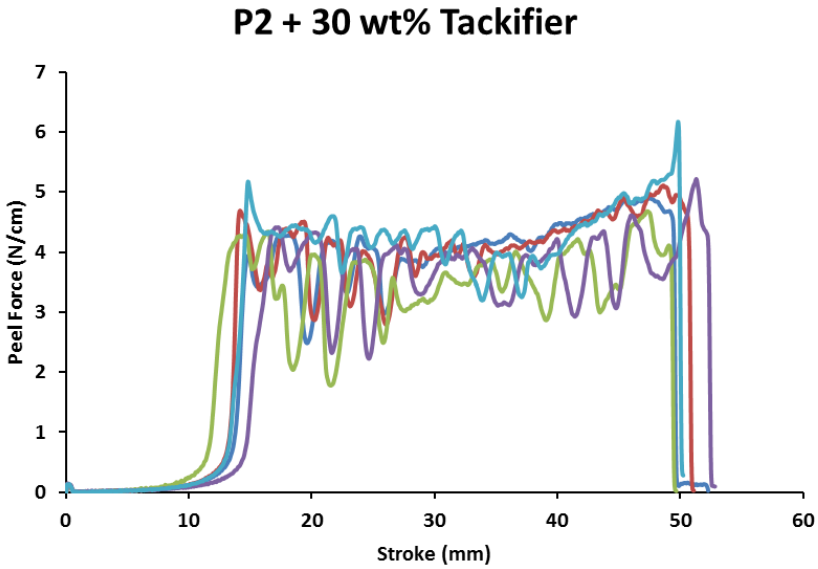

Figure 2. 44. 180° peel test of P2 blended with 30 wt% of a rosin ester resin tackifier.

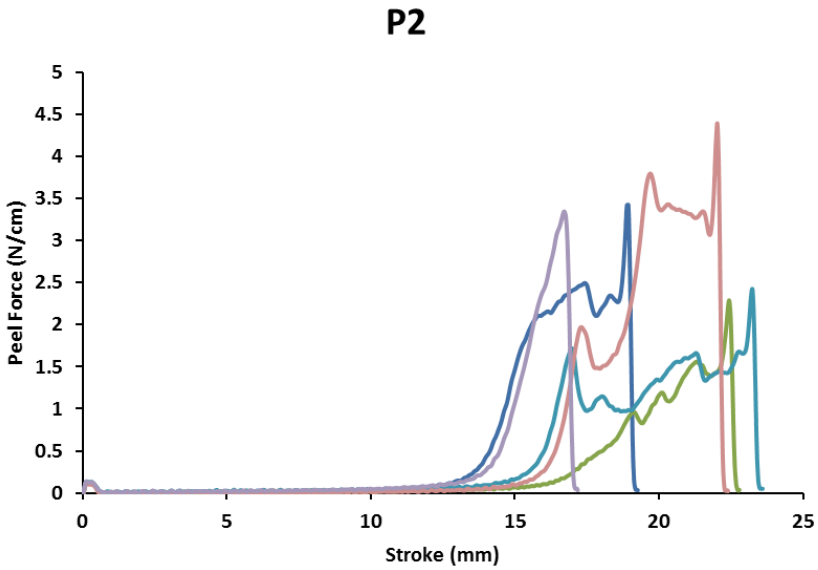

Figure 2. 45. Loop tack test of P2.

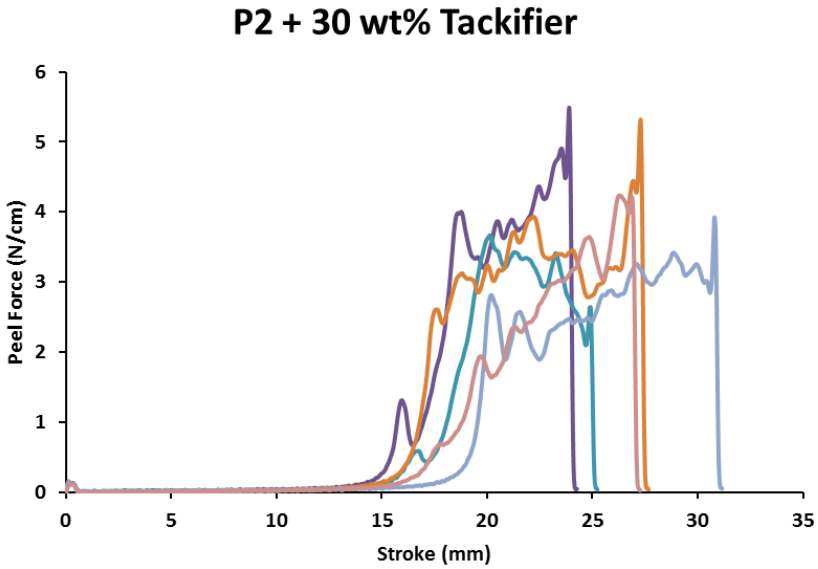

Figure 2. 46. Loop tack test of P2 blended with 30 wt% of a rosin ester resin tackifier.

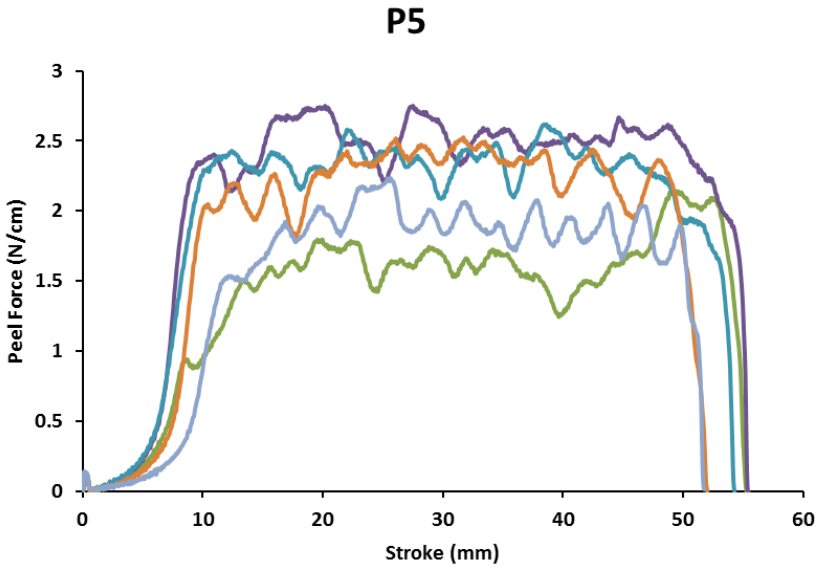

Figure 2. 47. 180° peel test of P5.

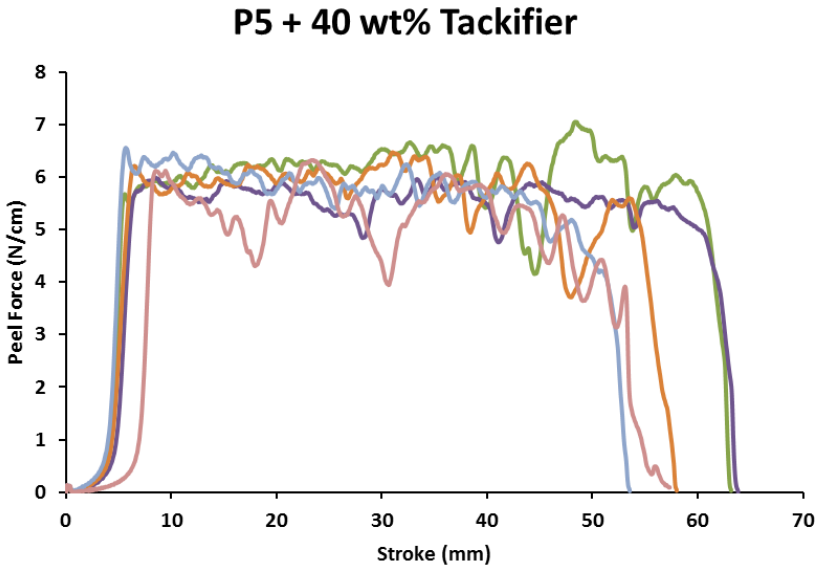

Figure 2. 48. 180° peel test of P5 blended with 40 wt% of a rosin ester resin tackifier.

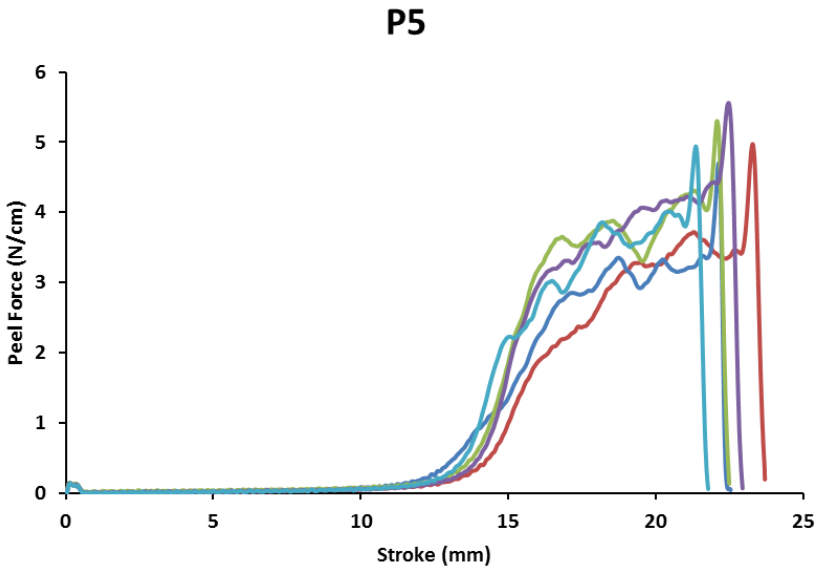

Figure 2. 49. Loop tack test of P5.

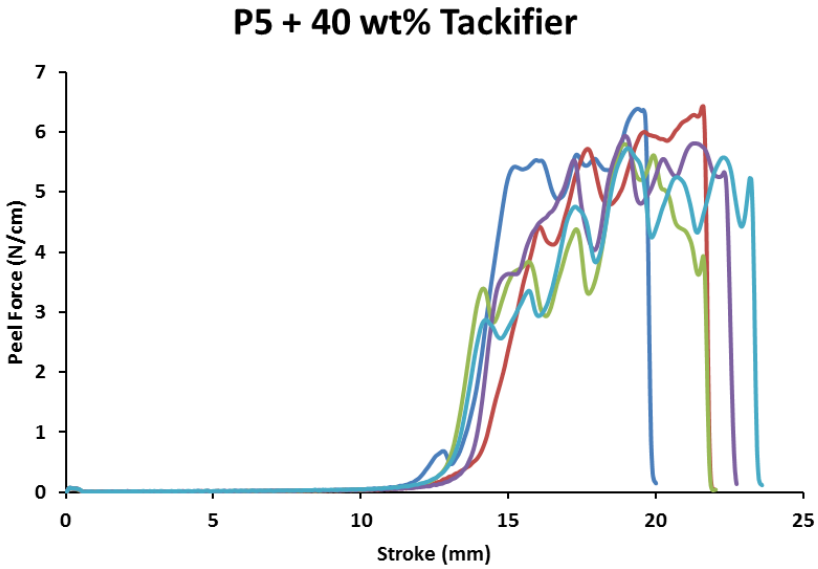

Figure 2. 50. Loop tack test of P5 blended with 40 wt% of a rosin ester resin tackifier.

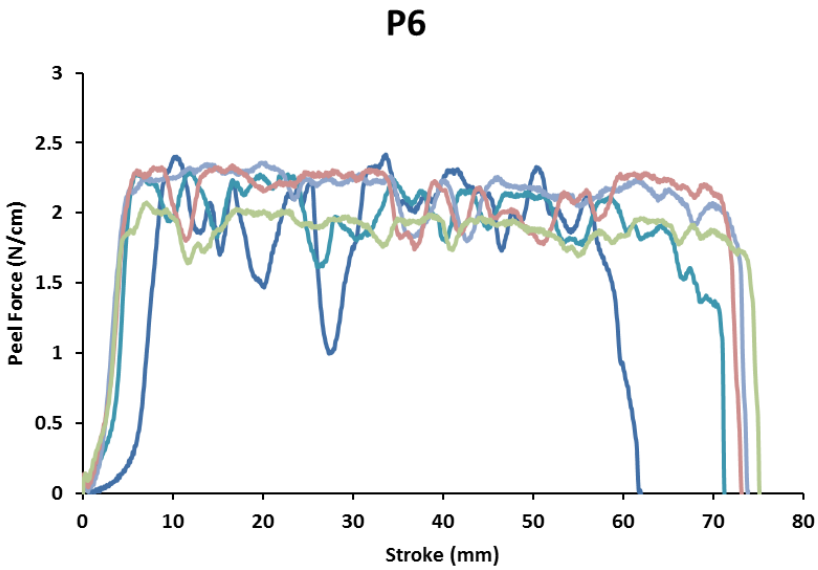

Figure 2. 51. 180° peel test of P6.

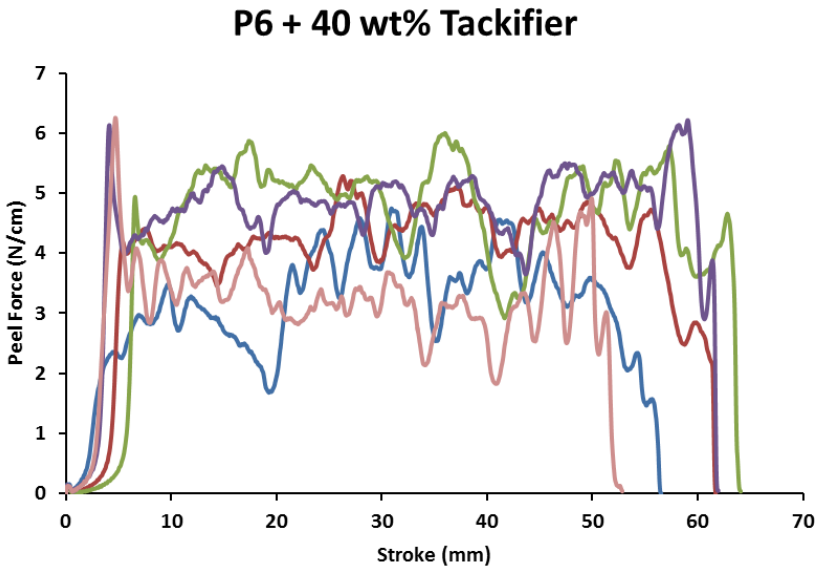

Figure 2. 52. 180° peel test of P6 blended with 40 wt% of a rosin ester resin tackifier.

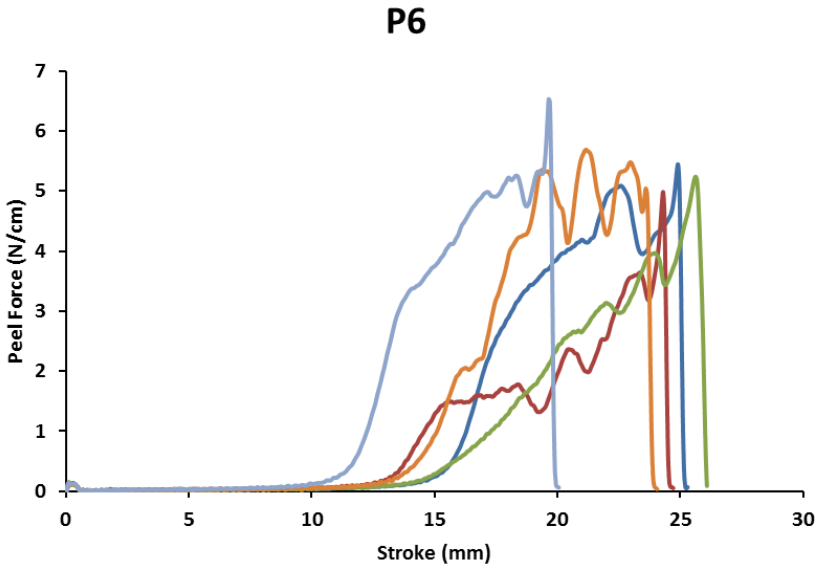

Figure 2. 53. Loop tack test of P6.

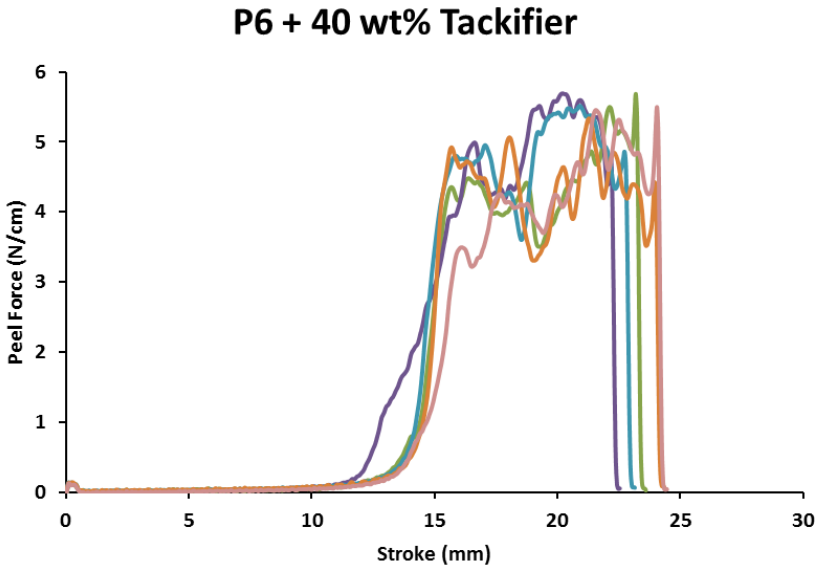

Figure 2. 54. Loop tack test of P6 blended with 40 wt% of a rosin ester resin tackifier.

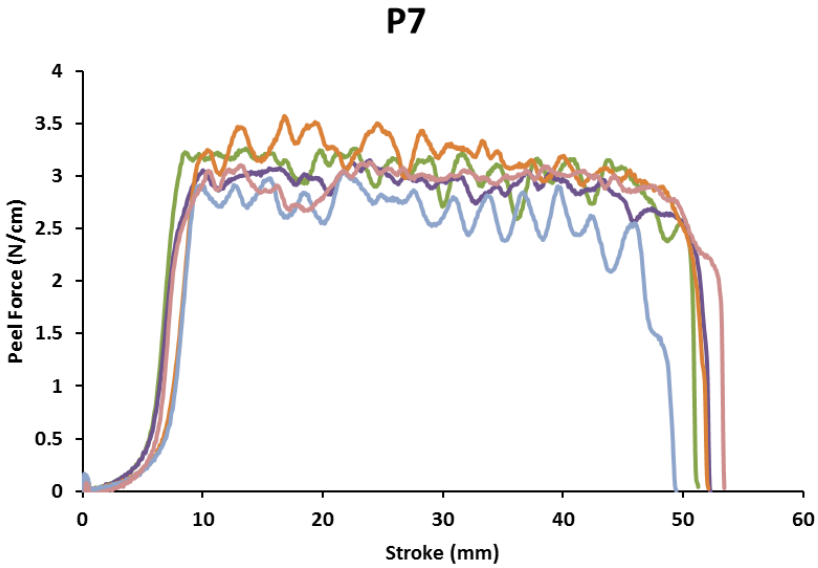

Figure 2. 55. 180° peel test of P7.

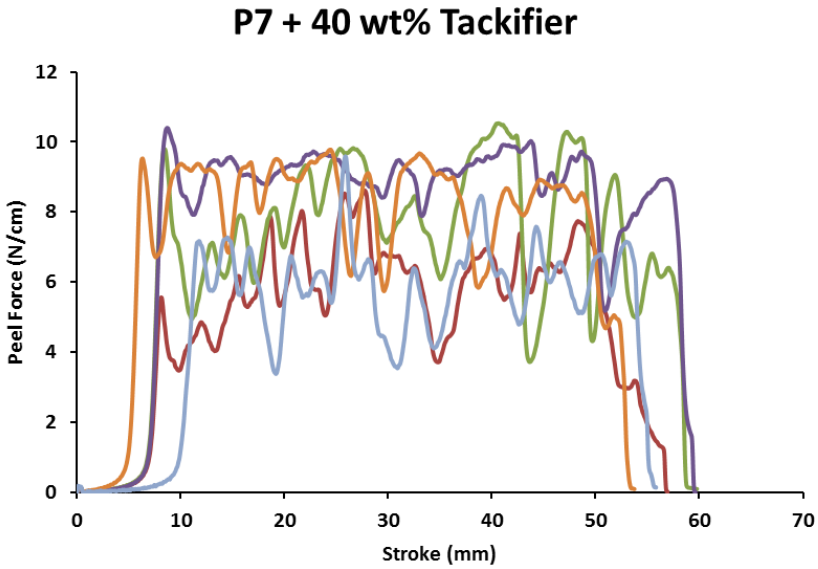

Figure 2. 56. 180° peel test of P7 blended with 40 wt% of a rosin ester resin tackifier.

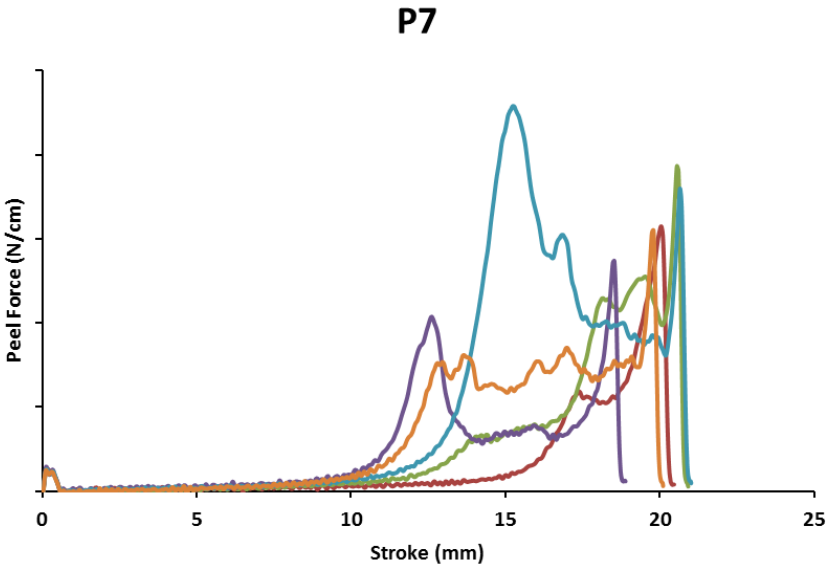

Figure 2. 57. Loop tack test of P7.

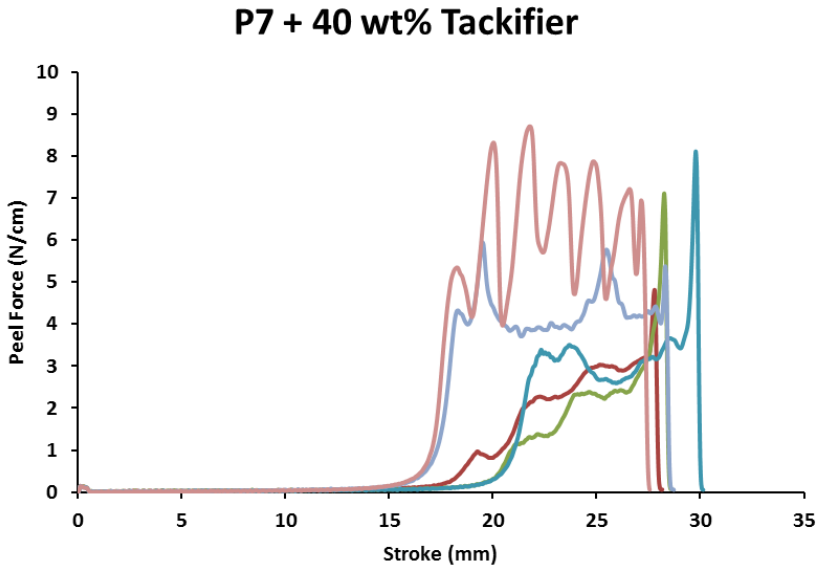

Figure 2. 58. Loop tack test of P7 blended with 40 wt% of a rosin ester resin tackifier.

2.4 Conclusions

In summary, we have reported the synthesis and study of new sustainable acrylic triblock copolymers for pressure sensitive adhesives. Lauryl acrylate was employed as the rubbery midblock in place of commonly used *n*-butyl acrylate in an effort to improve upon the renewability aspect of the adhesives. Furthermore, TAL, an emerging platform chemical, was modified and subsequently co-polymerized via RAFT polymerization to develop an acrylate-based system suitable for PSAs. The synthesized polymers were of high molecular weights and narrow dispersities, specific component ratios were targeted, and the adhesives demonstrated similar performance to commercial products. The intrinsically lower elastic modulus of p(LauAc) promoted excellent adhesion and tack capabilities of the resultant triblock copolymers. Use of the high T_g p(AcLa) as the glassy component in the triblock copolymers enhanced the physical properties of the adhesives (e.g. high shear forces and adhesive failure mode), albeit with limited thermal stability at temperatures above 125 °C, which could be explored to trigger thermally-responsive release properties. We demonstrate through this robust strategy that it is indeed possible to utilize renewable, long-chained alkyl-acrylates with high M_e in conjunction with biologically accessible TAL to realize a fully sustainable system for high-performance PSA applications.

2.5 Experimental

Materials. 4-Hydroxy-6-methyl-2-pyrone ("Triacetic Acid Lactone (TAL)" "pyrone") was purchased from Oakwood Chemical and used without further purification. Pd/C (10 wt% loading) was purchased from Sigma-Aldrich and dried under vacuum prior to use. Acryloyl chloride, *n*-butyl acrylate, and lauryl acrylate were purchased from Sigma-Aldrich, passed through basic alumina to remove inhibitors, and stored at -30 °C until further use. The RAFT chain-transfer agent (BTCBA) and 2,2'-Azobis(2-methylpropionitrile) (AIBN) were purchased from Sigma-Aldrich and used as-received. The rosin ester tackifier (Sylvalite RE-80HP) was used, as-received, from Arizona Chemical.

Characterization. All reported ^{1}H-NMR spectra were collected on a Bruker Avance III HD 500 MHz spectrometer in deuterated chloroform ($CDCl_3$) and chemical shifts are referenced to tetramethylsilane (TMS) at 0.00 ppm. Spectra of all small molecules were collected at 22 °C with a D1 = 1s (16 scans) and spectra of all polymers were collected at 22 °C with a D1= 10s (64 scans). High resolution mass spectrometry (HRMS) was performed using a Bruker Bio-TOF II in positive mode. THF size-exclusion chromatography (SEC) was performed in uninhibited THF utilizing a Waters Styragel guard column and three consecutive Waters Styragel columns at a flow rate of 1 mL min^{-1} at 22 °C. The instrument was equipped with an Agilent 1260 Infinity liquid chromatography coupled with a Wyatt Dawn Heleos II multiangle light scattering detector (18 angles from 10° to 160° and a 662.6 nm laser) and a Wyatt Optilab T-rEX

refractive index detector. DMF SEC was performed in DMF with 0.05 M LiBr at a flow rate of 1.0 mL min^{-1} at 50 °C. The instrument was equipped with a Wyatt Dawn Heleos II multiangle light scattering detector (18 angles from 10° to 160° and a 662.6 nm laser) and a Wyatt Optilab T-rEx refractive index detector. Reported dn/dc values were calculated from the RI signal using a known sample concentration and assuming 100% mass recovery from the column and used for molar mass determination. Thermal gravimetric analysis (TGA) was performed on a TA Instruments Q500 series at a heating rate of 10 °C min^{-1} under 60/40 nitrogen/oxygen flow. Differential scanning calorimetry (DSC) experiments were conducted with a TA Instruments Discovery DSC, using samples hermetically sealed in aluminum pans, at a heating/cooling rate of 10 °C min^{-1}. Reported T_g/ T_c/ T_m values are from the second heating/cooling ramps. Adhesion and tensile testing was performed on a Shimadzu AGS-X tensile tester.

Hydrogenation of 4-hydroxy-6-methyl-2-pyrone (Triacetic Acid Lactone (TAL)). Uninhibited THF was stirred over activated 3Å molecular sieves for 24 hours and filtered through a bed of Celite prior to use. A 300 mL high-pressure reactor vessel was charged with TAL (12.0 g, 95.1 mmol), Pd/C (1.2 g, 10% by mass), and 200 mL of THF. The reactor was sealed, and first pressurized and de-pressurized with Argon (3X) to remove O_2, then pressurized with gaseous H_2 to 100 PSI, heated to 50 °C, then pressurized to 500 PSI. Over the next 48 h, the reactor vessel was periodically re-pressurized to 500 PSI, after which time the vessel was cooled to room temperature and purged with Argon to remove H_2. The reaction mixture was then filtered through a bed of Celite to remove the

Pd/C. The THF was removed under vacuum to afford 4-hydroxy-6-methyl-2-lactone ("Lactone") (11.7 g, 95% isolated yield). 1H NMR (400 MHz, Chloroform-d) δ 4.44 – 4.29 (m, 1H), 4.25 (ddt, J = 9.3, 7.8, 5.7 Hz, 1H), 2.97 (s, 1H), 2.91 – 2.83 (m, 1H), 2.45 (ddd, J = 17.1, 7.8, 1.9 Hz, 1H), 2.28 (dddd, J = 13.8, 5.8, 3.1, 1.4 Hz, 1H), 1.63 – 1.52 (m, 1H), 1.41 (dd, J = 6.1, 1.8 Hz, 3H). ^{1}H NMR shifts reported here match the spectrum previously reported in ref. 49.

Synthesis of 4-acrylate-6-methyl-2-pyrone (Acrylated-Pyrone, AcPy). Triacetic Acid Lactone (4-hydroxy-6-methyl-2-pyrone) (10.0 g, 79.3 mmol), acryloyl chloride (7.18 g, 79.3 mmol), and 100 mL of anhydrous CH_2Cl_2 were sequentially added to a dry 200 mL round-bottom flask. The flask was sealed with a rubber septum and submerged in an ice-bath, then NEt_3 (10.1 ml, 7.29 g, 72.1 mmol) was added drop-wise to the stirring solution. After 4 h, the precipitated NEt_3HCl salt was removed by filtration, and the filtrate was washed with 100 mL of a saturated sodium bicarbonate solution (x3) and once with 100 mL of brine. The organic layer was dried over magnesium sulfate, filtered, and concentrated under vacuum to yield a yellow liquid. The yellow liquid was loaded on to a silica column (2" diameter x 1.5' length) and a mixture of diethyl ether/hexanes (4:1) was used as the eluent. The desired compound elutes first from the column. The solvents were then removed under vacuum to afford AcPy (6.2 g, 43.6% isolated yield). 1H NMR (500 MHz, Chloroform-d) δ 6.62 (d, J = 17.2 Hz, 1H), 6.24 (dd, J = 17.2, 10.5 Hz, 1H), 6.11 (d, J = 10.1 Hz, 2H), 6.02 (d, J = 1.8 Hz, 1H), 2.28 (s, 3H). ^{13}C{^{1}H} NMR (126 MHz,

Chloroform-d) δ 163.67, 163.35, 163.03, 134.83, 126.68, 101.23, 101.07, 20.12. HRMS (ESI-TOF, *m/z*) calculated for $C_9H_8O_4Na^+$: 203.0315; Observed: 203.0305.

Synthesis of 4-acrylate-6-methyl-2-lactone (Acrylated-Lactone, AcLa). Lactone (11.7 g, 89.9 mmol), acryloyl chloride (8.97 g, 99.1 mmol), and 100 mL of anhydrous CH_2Cl_2 were sequentially added to a dry 200 mL round-bottom flask. The flask was sealed with a rubber septum and submerged in an ice-bath, then N,N-Diisopropylethylamine (17.3 mL, 12.8 g, 99.1 mmol) was added drop-wise to the stirring solution. After 2 h, the $CH_2Cl_2$was removed under vacuum to yield a dark-orange oil. The oil was diluted with 5 mL of CH_2Cl_2 and loaded onto a silica column (5" diameter x 1' length) and neat diethyl ether was used as the eluent (note: excess acryloyl chloride elutes first, then the desired product R_f = 0.35). The solvent was removed under vacuum to afford AcLa (11.0 g, 66.4% isolated yield). 1H NMR (400 MHz, Chloroform-d) δ 6.43 (dd, J = 17.3, 1.3 Hz, 1H), 6.10 (dd, J = 17.3, 10.5 Hz, 1H), 5.89 (dd, J = 10.4, 1.3 Hz, 1H), 5.29 (m, 1H), 4.47 – 4.37 (m, 1H), 2.96 (ddd, J = 17.2, 6.4, 1.0 Hz, 1H), 2.62 (dd, J = 17.3, 6.6 Hz, 1H), 2.43 (dddd, J = 14.0, 6.2, 2.9, 1.0 Hz, 1H), 1.67 (ddd, J = 14.1, 11.6, 8.6 Hz, 1H), 1.43 (d, J = 6.3 Hz, 3H). $^{13}C\{^1H\}$ NMR (126 MHz, Chloroform-d) δ 169.53, 165.18, 131.93, 127.81, 73.08, 66.01, 36.23, 35.56, 21.17. HRMS (ESI-TOF, *m/z*) calculated for $C_9H_{12}O_4Na^+$: 207.0628; Observed: 207.0621.

Synthesis of poly(acrylated-lactone) (p(AcLa)) via Free Radical Polymerization. Acrylated-Lactone (0.200 g, 1.09 mmol), AIBN (1.78 mg, 10.8 µmol) (from dilute stock solution), and 5 mL acetonitrile added to a vacuum flask. The flask was sealed and degassed by 4 consecutive freeze-pump-thaw cycles, then submerged in a pre-heated oil bath at 70 °C. After stirring vigorously for 18 h, the flask was immediately submerged in liquid nitrogen until frozen and opened to the atmosphere. After thawing the solution at room temperature, the polymer was precipitated in cold H_2O and washed repeatedly with methanol until pure (monitored via ^{1}H-NMR). The polymer was then dried in a vacuum oven at 60 °C for 24 h (50% conversion via ^{1}H-NMR spectroscopy, 0.100 g, 50% isolated yield). 1H NMR (400 MHz, Chloroform-d) δ 5.26 (s, 1H), 4.45 (s, 1H), 2.28 (s, 1H), 2.61 (s, 1H), 2.42 (s, 1H), 2.30 (s, 1H), 1.86 (s, 2H), 1.69 (s, 1H), 1.45 (s, 3H). M_n(p(AcLa)) = 30 kg mol^{-1}, $Đ$ = 1.60.

Synthesis of poly(n-butyl acrylate) via RAFT (CTA-p(nBA)-CTA). The synthesis of the macro-CTA was performed following literature procedures.[24-26] AIBN (5.12 mg, 0.031 mmol), 3,5-bis(2-dodecylthiocarbonothioylthio-1-oxopropoxy)benzoic acid (BTCBA) (128 mg, 0.156 mmol), and n-butyl acrylate (10.0 g, 78.0 mmol) were added to a dry 50 mL vacuum flask. The flask was sealed and degassed by four freeze-pump-thaw cycles, then submerged in a pre-heated oil bath at 70 °C. After stirring vigorously for 2 h, the flask was immediately submerged in liquid nitrogen and opened to the atmosphere. 10 mL of CH_2Cl_2 was added to the flask and the polymer was precipitated in 200 mL of cold methanol. After allowing the contents to settle for 1 h, the methanol was decanted and

200 mL of additional cold methanol was added. The process was repeated twice more and then the purified CTA-p(nBA)-CTA polymer was dried in a vacuum oven at 60 °C for 18 h (84% conversion via ^{1}H-NMR spectroscopy, 8.14 g, 81.0% isolated yield). 1H NMR (500 MHz, Chloroform-d) δ 4.04 (dq, J = 18.6, 10.1 Hz, 2H), 2.40 – 2.22 (m, 1H), 1.93 (m, 2H), 1.63 (m, 2H), 1.39 (m, 2H), 0.95 (t, J = 7.5 Hz, 3H). M_n(CTA-p(nBA)-CTA) = 55 kg mol^{-1}, $Đ$ = 1.05, dn/dc = 0.066.

Synthesis of CTA-p(AcLa)-p(nBA)-p(AcLa)-CTA. An illustrative example is provided. CTA-p(nBA)-CTA (1.0 g, 0.018 mmol), acrylated-lactone (AcLa) (0.335 g, 1.81 mmol), AIBN (0.299 mg, 1.82 μmol) (from a dilute stock solution), and 10 mL of DMF added to a vacuum flask. The flask was sealed and degassed by 4 consecutive freeze-pump-thaw cycles, then submerged in a pre-heated oil bath at 70 °C. After stirring vigorously for 24 h, the flask was immediately submerged in liquid nitrogen and opened to the atmosphere. The polymer was precipitated in cold H_2O and washed repeatedly with methanol until DMF and unreacted monomer was removed (monitored via ^{1}H-NMR). The precipitates were then dried in a vacuum oven at 60 °C for 24 h. 1H NMR (500 MHz, Chloroform-d) δ 5.26 (s, 1H), 4.44 (s, 1H), 4.05 (m, 2H), 2.94 (s, 1H), 2.59 (s, 1H), 2.50 – 2.22 (m, 4H), 1.92 (s, 2H), 1.79 – 1.54 (m, 4H), 1.50 – 1.33 (m, 5H), 0.95 (t, J = 7.6 Hz, 3H).

Synthesis of poly(lauryl acrylate) via RAFT (CTA-p(LauAc)-CTA). The synthesis of the macro-CTA was performed following modified literature procedures.[24-26] AIBN (0.27

mg, 1.64 µmol from stock solution), 3,5-bis(2-dodecylthiocarbonothioylthio-1-oxopropoxy)benzoic acid (BTCBA) (6.8 mg, 8.36 µmol), and lauryl acrylate (2.0 g, 8.32 mmol) were added to a dry 50 mL vacuum flask. The flask was sealed and degassed by four freeze-pump-thaw cycles, then submerged in a pre-heated oil bath at 70 °C. After stirring vigorously for 3 h, the flask was immediately submerged in liquid nitrogen and opened to the atmosphere. 10 mL of $CHCl_3$ was added to the flask and the polymer was precipitated in 200 mL of cold methanol. After allowing the contents to settle for 1 h, the methanol was decanted and 200 mL of additional cold methanol was added. The process was repeated twice more and then the purified CTA-p(LauAc)-CTA polymer was dried in a vacuum oven at 60 °C for 18 h (88% conversion via ^{1}H-NMR spectroscopy, 1.60 g, 80.0% isolated yield). 1H NMR (500 MHz, Chloroform-d) δ 4.01 (s, 2H), 2.31 (m, 1H), 1.91 (s, 2H), 1.70 – 1.54 (m, 8H), 1.31 (m, J = 19.0 Hz, 16H), 0.90 (t, J = 6.8 Hz, 3H). M_n(CTA-p(LaulAc)-CTA) = 230 kg mol^{-1}, $Đ$ = 1.16, dn/dc = 0.067.

Synthesis of CTA-p(AcLa)-p(LauAc)-p(AcLa)-CTA. An illustrative example is provided. CTA-p(LauAc)-CTA (0.5 g, 2.17 µmol), acrylated-lactone (AcLa) (0.12 g, 0.65 mmol), AIBN (71.4 µg, 0.43 µmol) (from a dilute stock solution), and 5 mL of $CHCl_3$ was added to a vacuum flask. The flask was sealed and degassed by 4 consecutive freeze-pump-thaw cycles, then submerged in a pre-heated oil bath at 70 °C. After stirring vigorously for 24 h, the flask was immediately submerged in liquid nitrogen and opened to the atmosphere. The polymer was precipitated in cold methanol and washed repeatedly with methanol until unreacted monomer was removed (monitored via ^{1}H-NMR). The

precipitates were then dried in a vacuum oven at 60 °C for 24 h. 1H NMR (500 MHz, Chloroform-d) δ 5.24 (s, 1H), 4.44 (s, 1H), 4.07 (s, 2H), 2.95 (s, 1H), 2.60 (s, 1H), 2.52 – 2.19 (m, 3H), 1.94 (s, 2H), 1.62 (s, 11H), 1.46 (s, 3H), 1.30 (m, 16H), 0.90 (t, J = 6.8 Hz, 3H).

Dynamic Mechanical Analysis. Dynamic mechanical analysis of poly(LauAc) (M_n = 300 kDa) was performed at 5 °C within the linear viscoeleastic regime. An oscillatory stress was applied to sample between two 25 mm steel plates and the sinusoidal stress response was measured. The resultant complex modulus was decoupled into the in-phase/elastic (G') and out-of-phase/viscous (G") moduli. The loss tangent (tan δ), which is the ratio of the viscous modulus G" to the elastic modulus G', was also calculated. The plateau in the storage modulus vs. angular frequency curve (26460 Pa), corresponding to a minimum in tan δ, was used to calculate the entanglement molecular weight (M_e) of poly(LauAc) as 66 kDa.

Adhesion Testing. Samples for pressure-sensitive adhesive evaluations were prepared by dissolving the polymer or polymer/tackifier blend in THF or $CHCl_3$ to produce 30% solids content solution (example: 100 mg polymer or 70 mg polymer/30 mg tackifier in 265 µL THF). The solution was then solvent-casted onto a 50 µm thick sheet of PET film using a standard laboratory drawdown rod to target a coat weight of 25 gsm. The films were allowed to dry under ambient conditions for 24 h and then cut into 1 cm wide strips for adhesion testing.

180° Peel Adhesion (PSTC-101 Adhesion Test Method). A 1 cm wide strip of the polymer-coated PET film was adhered, using a 500 g roller, to a dry stainless steel plate that was cleaned with acetone prior to the test. The PET-film was then peeled from the stainless steel plate using a Shimadzu AGX-X tensile tester at a peel rate of 305 mm min^{-1}. The peel force was recorded as the maximum force measured during the test and the reported average and standard deviation values were acquired from five replicates.

Loop Tack (PSTC-16 Adhesion Test Method). A 1 cm wide strip was of the polymer-coated PET film was formed into a tear-drop shaped loop and mounted onto the upper grip of the tensile tester. The loop was then lowered onto a dry stainless steel plate that was cleaned with acetone prior to the test to give a contact area of 1 cm x 1 cm. The tack force was recorded as the maximum force measured while raising the upper grip at a rate of 305 mm min^{-1} and the reported average and standard deviation values were acquired from five replicates.

Shear Adhesion (PSTC-107 Adhesion Test Method). A 2.54 cm x 2.54 cm strip of the polymer-coated PET film was adhered, using a 500 g roller, to a dry stainless steel plate that was cleaned with acetone prior to the test. The steel plate was held at a 2° angle relative to a vertical plane and a 1 kg weight was suspended from the test strip. The time to adhesive failure was recorded for three samples.

Acknowledgements

This work was supported by the National Science Foundation under the Center for Sustainable Polymers (CHE-1413862). The authors acknowledge John Beumer for creating the 3-D model images of the adhesion tests in Figure 2.38.

Chapter 3.

Disubstituted δ-Valerolactones from Triacetic Acid Lactone: Insights into the Thermodynamics and Kinetics of Ring Opening Polymerization

3.1 Introduction

The success and advancement of modern society is dependent, in part, on materials created from polymers. Use in commodity products such as clothing and household goods, resources for infrastructure, and implementation in medical devices and other sophisticated technologies are but a few examples of how polymers have improved and continue to improve our daily lives. The vast majority of such polymeric materials, however, are derived from unsustainable petrochemical processes.[6,113] Thus, the impetus to supplement or entirely replace petroleum-based polymers with those created from renewable feedstocks has become increasingly urgent.[13,14,63,114] The use of biomass as a platform for generating renewable chemicals is an attractive approach towards ultimately achieving a sustainable and energy efficient paradigm within the multi-billion dollar polymer industry.

Triacetic acid lactone (TAL, (**1**)) (Scheme 3.1) can be obtained synthetically from acetic acid[19–21] or via the biological actions of genetically modified microorganisms which synthesize the compound as a secondary metabolite of sugars.[22–29,94] We propose the use of TAL as a potentially renewable feedstock for the generation of new polymeric materials. To date, only two reports have demonstrated the use of TAL in polymers. In the first, post-polymerization modification of p(epichlorohydrin) with TAL resulted in an increase in the glass transition temperature of the material from -30 °C up to 70 °C, depending on the degree of substitution.[29] In the second, TAL was modified with an acrylic moiety and polymerized via a controlled radical polymerization technique to

develop acrylic triblock copolymers suitable for pressure-sensitive adhesive applications.[115]

Drawing inspiration from the well-established ring opening polymerization (ROP) chemistry of various lactones such δ-valerolactone, ε-caprolactone, lactide and their derivatives,[116,117] we envisioned using TAL as a feedstock for the synthesis of new, disubstituted δ-valerolactones that can yield useful aliphatic polyesters via ROP. The polymerization behavior of lactone monomers is highly dependent on ring size and degree of substitution.[118–120] While the polymerizations of δ-valerolactone and numerous monosubstituted δ-valerolactone monomers have been studied,[70,121–123] that of disubstituted δ-valerolactone monomers have not been reported to date.

In this report, we synthesized a small library of disubstituted δ-valerolactones derived from TAL and examined their polymerization behavior. Thermodynamic parameters associated with the ring-opening process of substituted δ-valerolactones, Gibbs free energy (ΔG_{rxn}), enthalpy of reaction (ΔH_{rxn}), and entropy of reaction (ΔS_{rxn}), were computationally modeled by Dr. Mukunda Mandal in order to identify promising candidates for the ROP of TAL derivatives (Table 3.1). Because the ROP of lactones is an isodesmic reaction (i.e. an ester bond is cleaved and a new, similar ester bond is then formed), the ΔH_{rxn} is directly correlated with ring strain energy. The theoretical calculations presented in Table 3.1 suggest that, on average, the ring strain energy of δ-valerolactones decreases with increasing degree of substitution. Additionally, the calculations indicate that ΔG_{rxn} differs between the two possible diastereomers of

disubstituted δ-valerolactones, in which the two substituents may *cis* or *trans* (i.e. 'RS' or 'SS').

Species	R/S	N_{conf}		G_{diff} (kcal/mol)		ΔG_{rxn} (kcal/mol)	ΔH_{rxn} (kcal/mol)	ΔS_{rxn} (cal/mol-K)
		Ring	Chain	Ring	Chain			
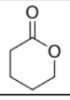		1	9	-0.2	-0.6	-5.2	-11.9	-22.6
	R	2	7	-0.3	-0.8	-4.9	-11.7	-22.9
	S	1	6	-0.3	-0.7	-4.7	-11.7	-23.2
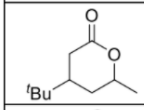	RS	1	0	-0.3	-0.1	0.4	-8.7	-30.5
	SS	1	3	-0.2	-0.5	-1.2	-9.5	-27.8
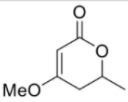	R	0	3	-0.1	-0.7	0.6	-7.1	-25.9
	S	0	3	-0.1	-0.7	0.6	-7.0	-25.7
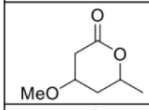	RS	3	5	-0.6	-0.8	-2.3	-10.6	-27.8
	SS	1	2	-0.3	-0.6	-2.6	-10.8	-27.4
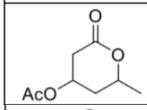	RS	4	2	-0.7	-0.4	-3.0	-12.6	-32.3
	SS	2	3	-0.5	-0.6	-1.9	-10.5	-28.9
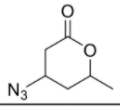	RS	2	4	-0.5	-0.8	-4.1	-12.6	-28.6
	SS	2	11	-0.2	-1.0	-4.7	-12.8	-27.2
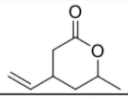	RS	0	3	0	-0.5	-3.7	-11.4	-25.7
	SS	0	3	0	-0.7	-5.1	-11.9	-23.0
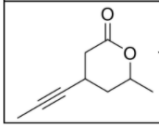	RS	0	2	0	-0.6	-4.2	-11.4	-24.4
	SS	1	7	-0.1	-0.9	-4.2	-11.3	-23.7

** N_{conf} = Number of additional conformers within 1 kcal/mol of global minima

** G_{diff} = Difference between the average free energy of all conformers, and the global minima

Table 3. 1. Ring strain parameters computed at SMD(ethylethanoate)//M06-2X/6-311+G(d,p)//M06-L/6-31+G(d,p) level of theory. Different conformers of ring-closed monomer and ring-opened product were explored using MacroModel program, and all reported values are calculated over the population of all conformers within 1 kcal/mol of the global minima conformer. The calculations given here were performed by Dr. Mukunda Mandal.

From the disubstituted δ-valerolactones listed in Table 3.1, β-acetoxy-δ-methylvalerolactone, β-methoxy-δ-methylvalerolactone, and β-vinyl-δ-methylvalerolactone were the potential monomers selected for ROP studies. The decision to synthesize and study these lactones over others was supported by the theoretically favorable thermodynamic parameters for polymerization and feasibility/ease of synthesis using TAL as the initial feedstock. Through our studies, we identified a successful candidate, β-acetoxy-δ-methylvalerolactone (**4**) (Scheme 3.2) that can undergo ROP with typical organocatalysts to produce a new polyester. The thermal properties of the polymer were studied, and the polymerization behavior of (**4**) was investigated and compared to that of other δ-valerolactone monomers, which provided valuable insights into the kinetics and thermodynamics of ROP of substituted δ-valerolactones.

3.2 Results and Discussion

The catalytic hydrogenation of triacetic acid lactone (TAL, (**1**)) using Pd/C was accomplished following previously established procedures (Scheme 3.1).[30,103,115] A brief discussion of the hydrogenation process and the observed intermediate (**2**) is provided in the Results and Discussion section of Chapter 2; ^{1}H NMR spectra of (**2**) and (**3**) are provided in Figures 2.6 and 2.5, respectively. The J-coupling constants for each proton pair of (**3**) were determined from the ^{1}H NMR spectrum of using methods described in the literature (Figure 3.1).[124,125] In a previous literature report, (**3**) was synthesized via hydrogenation of the partially-reduced keto/enol intermediate (**2**) shown in Scheme 3.1 using Pd/C.[126] The hydrogenations led to very high (>99%) stereoselectivity for the *cis* isomer of (**3**), and the authors postulated that the high selectivity is due to syn addition of hydrogen atoms to the C(3) and C(4) carbons on the side of the ring that is trans to the 6-methyl substituent.[126] The ^{1}H NMR chemical shifts and J-coupling constants we observed for (**3**) in our work match exactly with the values previously reported for the *cis* isomer, indicating that the hydrogenation of TAL using Pd/C is likewise >99% diastereoselective. The relative configuration of the hydroxyl and methyl substituents on the reduced δ-valerolactone ring is *cis* and (**3**) is obtained as a racemic mixture of the two enantiomers (4R,6S and 4S,6R). The *trans* isomer of (**3**) (4S,6S and 4R,6R) is also reported in the literature, and is distinguished from the *cis* isomer by different ^{1}H NMR chemical shifts and the associated J-coupling constants.[127,128]

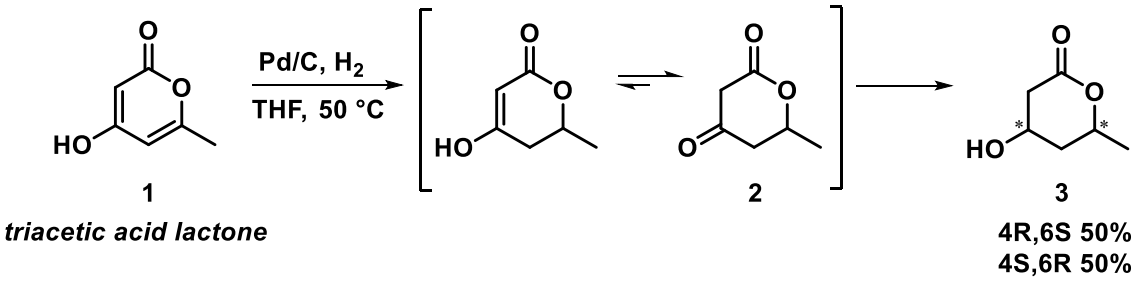

Scheme 3. 1. Catalytic hydrogenation of TAL using Pd/C to yield (3) as a racemic mixture of two enantiomers. The absolute configuration is highlighted for the two chiral centers at the 4- and 6-positions of the lactone ring.

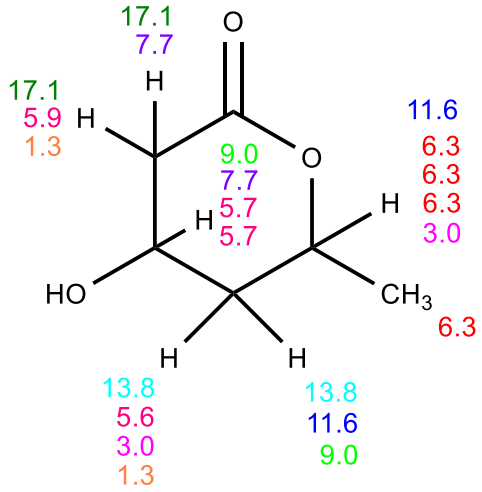

Figure 3. 1. J-coupling constants for each proton pair (color-coded) as determined from the ^{1}H NMR spectrum of (3).

Acetylation of the free hydroxyl group in (**3**) was easily accomplished using acetic anhydride and a catalytic amount of 4-(dimethylamino)pyridine (DMAP) as the base to yield β-acetoxy-δ-methylvalerolactone (**4**) (Scheme 3.2, Figures 3.2 – 3.3). Since the acetylation reaction does not involve an inversion of configuration, we hypothesized that (**4**) would be obtained as a racemic mixture of one diastereomer, with the acetoxy and methyl substituents on the lactone ring also in the *cis* arrangement. Indeed, the ^{1}H NMR chemical shifts and J-coupling constants we observed for (**4**) (Figure 3.4) match exactly with those previously reported for the *cis* isomer of the compound,[126] supporting our hypothesis.

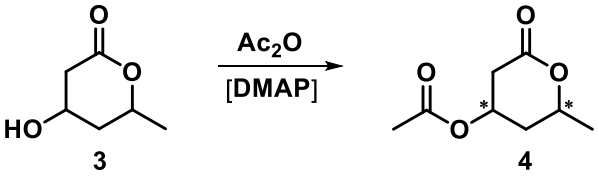

Scheme 3. 2. Synthesis of β-acetoxy-δ-methylvalerolactone (4) via acetylation of (3) using acetic anhydride (Ac_2O). The absolute configuration is highlighted for the two chiral centers at the 4- and 6-positions of the lactone ring.

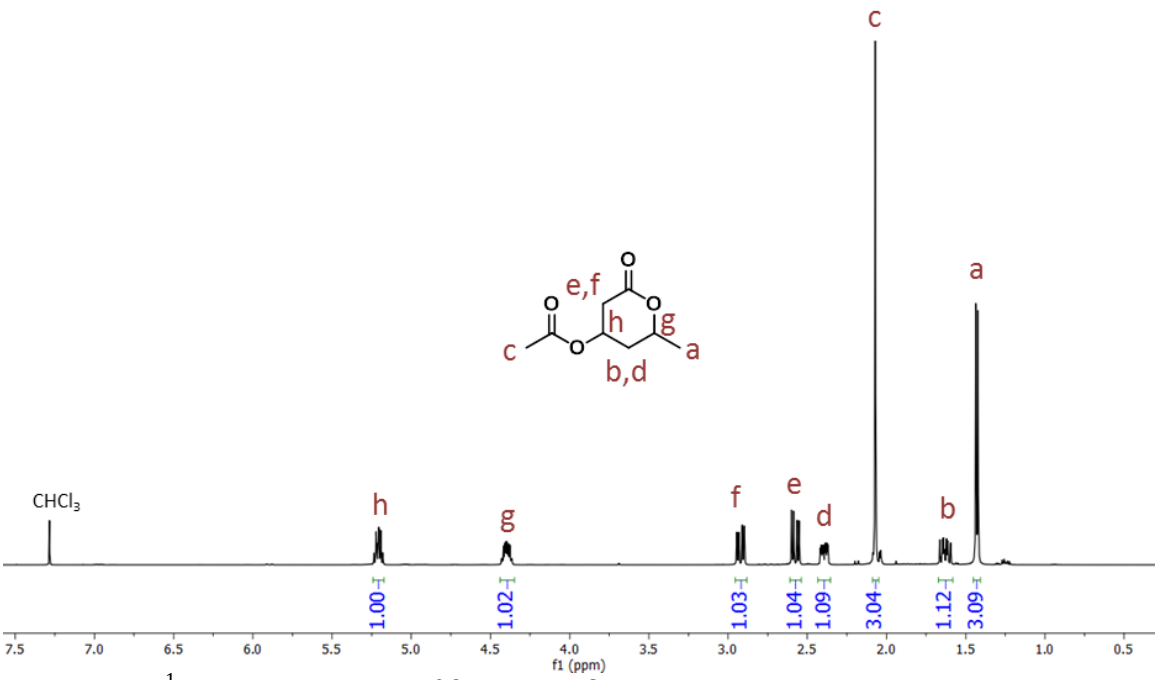

Figure 3. 2. ^{1}H NMR spectrum of β-acetoxy-δ-methylvalerolactone (4) ($CDCl_3$, 500 MHz).

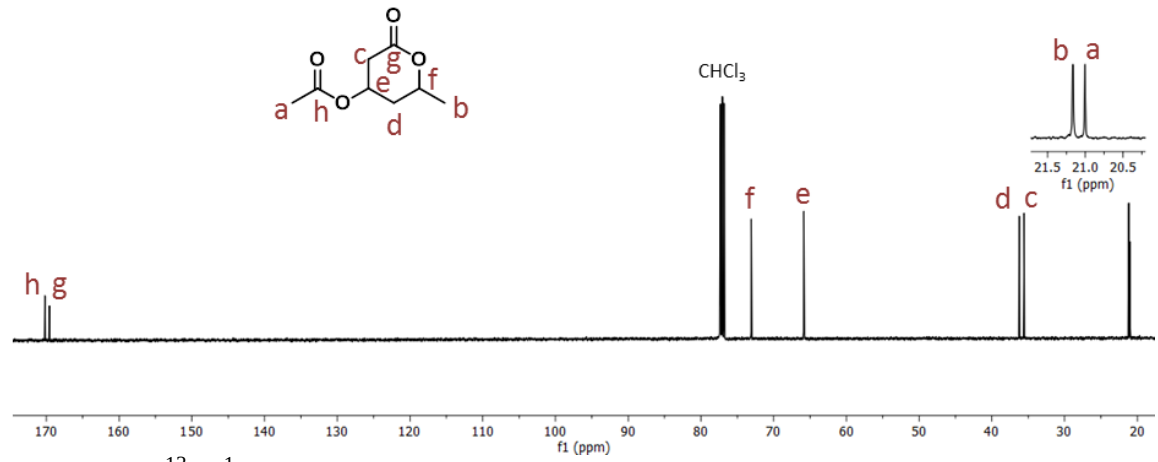

Figure 3. 3. ^{13}C{^{1}H} NMR spectrum of β-acetoxy-δ-methylvalerolactone (4) ($CDCl_3$, 126 MHz).

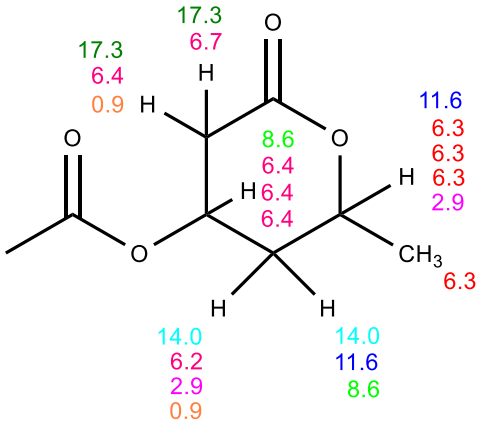

Figure 3. 4. J-coupling constants for each proton pair (color-coded) as determined from the ^{1}H NMR spectrum of β-acetoxy-δ-methylvalerolactone (4).

Synthesis of β-methoxy-δ-methylvalerolactone (**6**) was accomplished by initially methylating the free hydroxyl group of TAL (**1**) using trimethylphosphate ($(CH_3)_3PO_4$) following a previously published literature protocol[129] to obtain (**5**) (Scheme 3.3, Figure 3.5). Subsequent catalytic hydrogenation of (**5**) using Pd/C yielded (**6**) in high conversions and purity. Similar to the hydrogenation of TAL (**1**), the hydrogenation of (**5**) is highly stereoselective, presumably due to syn addition of hydrogen atoms to the C(3) and C(4) carbons on the side of the ring that is trans to the 6-methyl substituent. The ^{1}H NMR chemical shifts and J-coupling constants we observed for (**6**) in this work (Figures 3.6 – 3.7) are in agreement with those previously published for the *cis* isomer.[126]

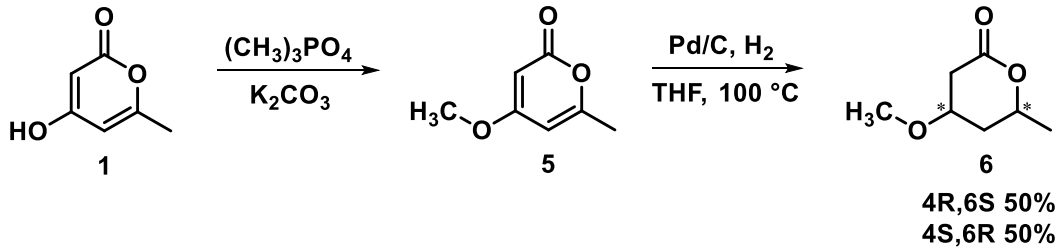

Scheme 3. 3. Two-step synthesis of β-methoxy-δ-methylvalerolactone (6) from TAL (1). The absolute configuration is highlighted for the two chiral centers at the 4- and 6-positions of the lactone ring.

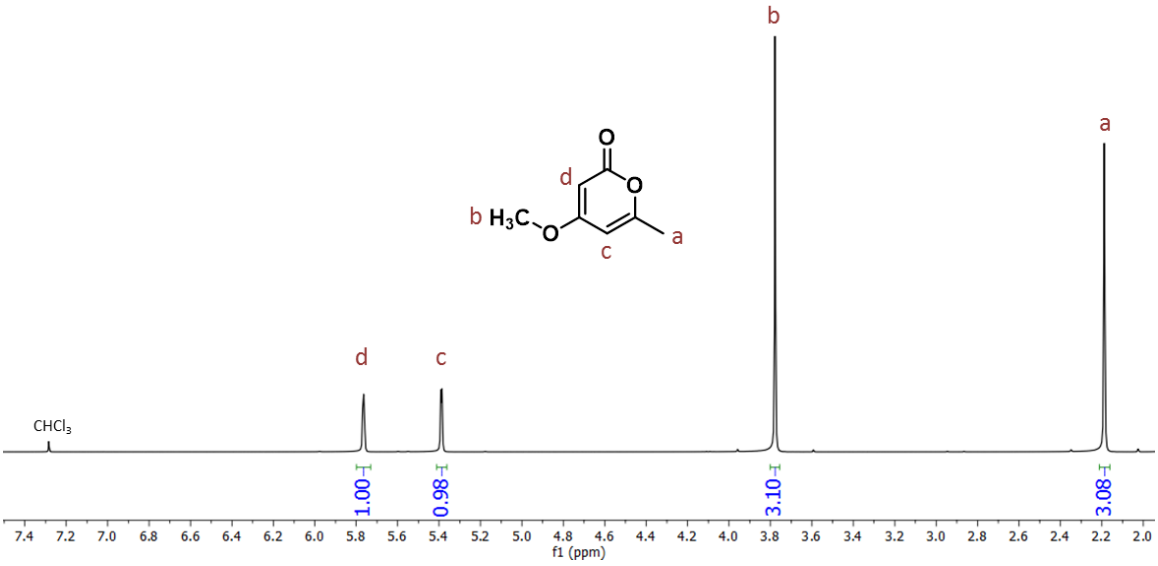

Figure 3. 5. ^{1}H NMR spectrum of (5) ($CDCl_3$, 500 MHz).

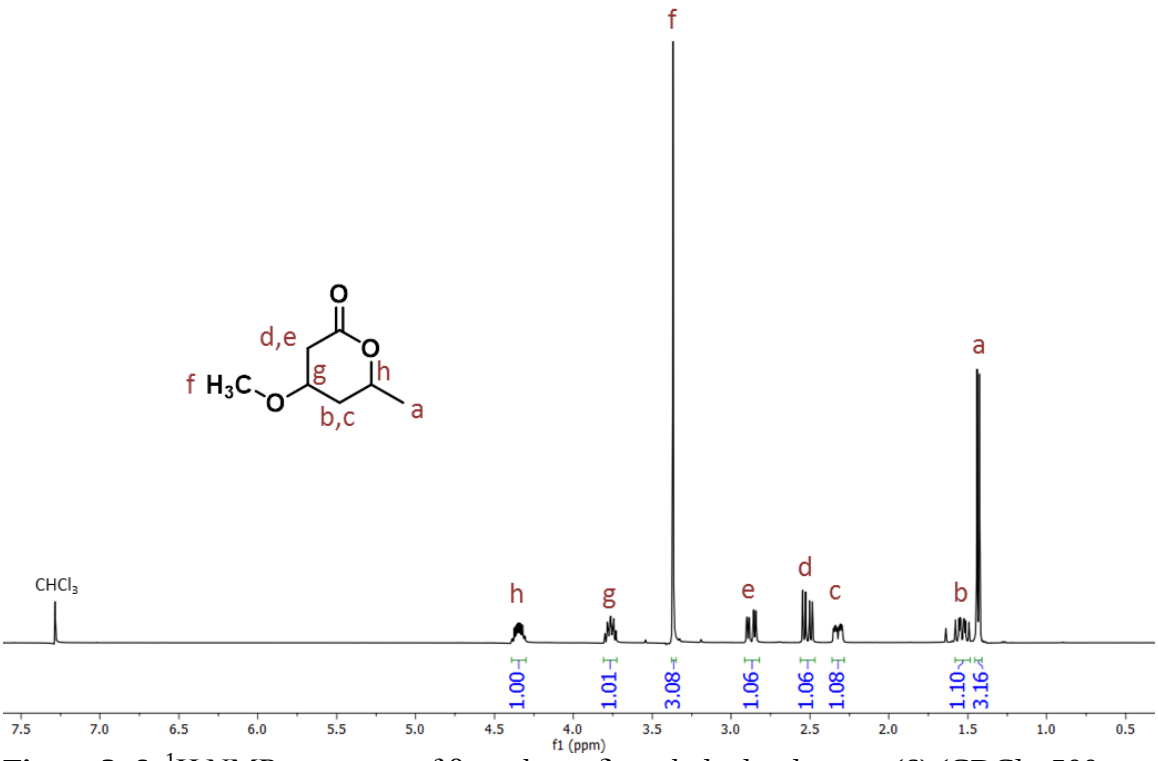

Figure 3. 6. ^{1}H NMR spectrum of β-methoxy-δ-methylvalerolactone (6) ($CDCl_3$, 500 MHz).

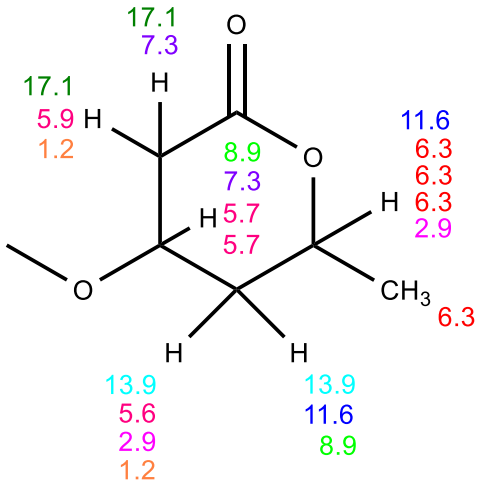

Figure 3. 7. J-coupling constants for each proton pair (color-coded) as determined from the ^{1}H NMR spectrum of β-methoxy-δ-methylvalerolactone (6).

The synthesis of β-vinyl-δ-methylvalerolactone (**8**) was accomplished using a two-step synthetic procedure (Scheme 3.4). The acid-catalyzed elimination of H_2O from (**3**) to yield parasorbic acid (**7**) is well documented.[30,103] By simply using the trace amount of acid that exists in chloroform as the catalyst, we quantitatively transformed (**3**) to parasorbic acid (**7**) at 150 °C (Figures 3.8 – 3.9). Next, the copper (I) salt-catalyzed conjugate addition of vinylmagnesium bromide to (**7**) yielded β-vinyl-δ-methylvalerolactone (**8**) in the documented *trans* stereoselective manner (Figures 3.10 – 3.11).[130,131] The ^{1}H NMR chemical shifts we observed for (**8**) are in agreement with those previously reported for the *trans* isomer of the compound.[130,131]

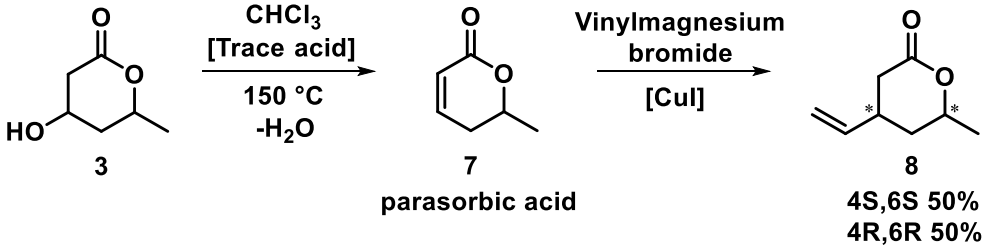

Scheme 3. 4. Two-step synthesis of β-vinyl-δ-methylvalerolactone (8) from (3). The absolute configuration is highlighted for the two chiral centers at the 4- and 6-positions of the lactone ring.

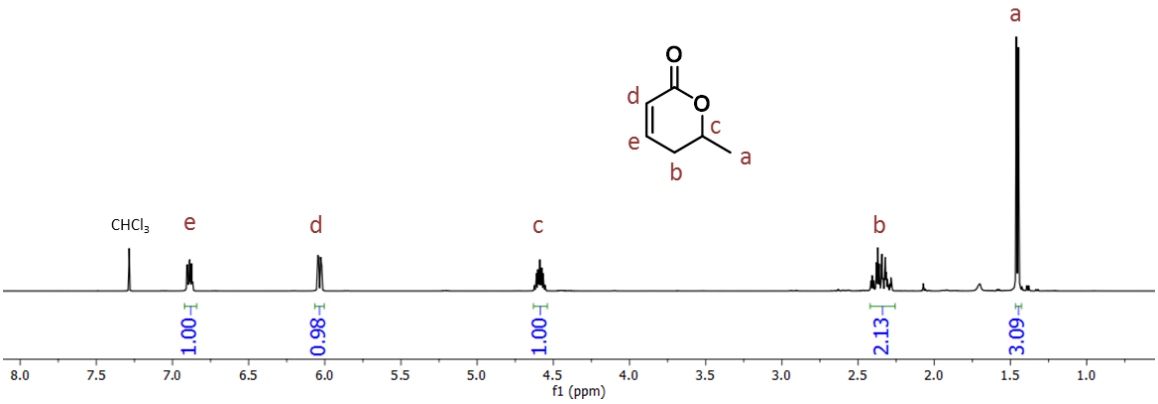

Figure 3. 8. ^{1}H NMR spectrum of parsorbic acid (7) ($CDCl_3$, 500 MHz).

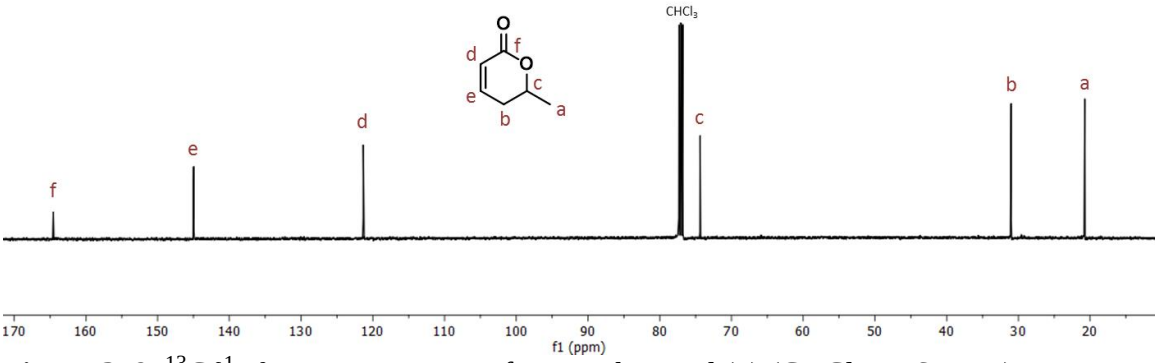

Figure 3. 9. $^{13}C\{^{1}H\}$ NMR spectrum of parasorbic acid (7) ($CDCl_3$, 126 MHz).

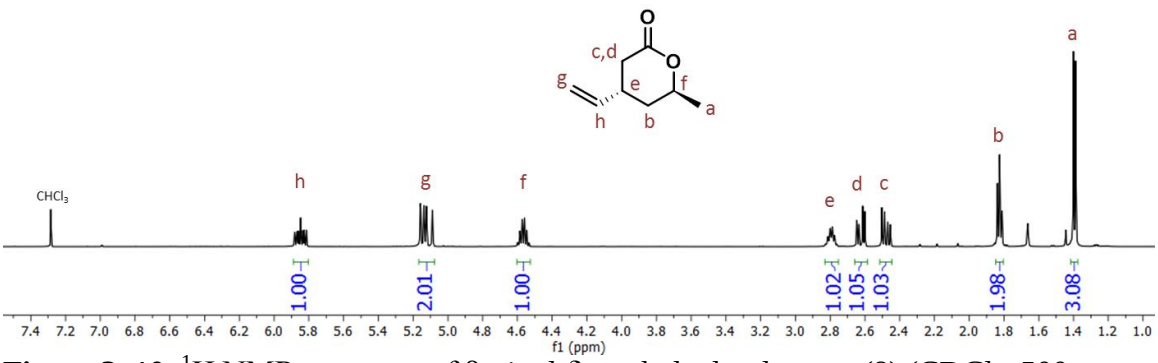

Figure 3. 10. ^{1}H NMR spectrum of β-vinyl-δ-methylvalerolactone (8) ($CDCl_3$, 500 MHz).

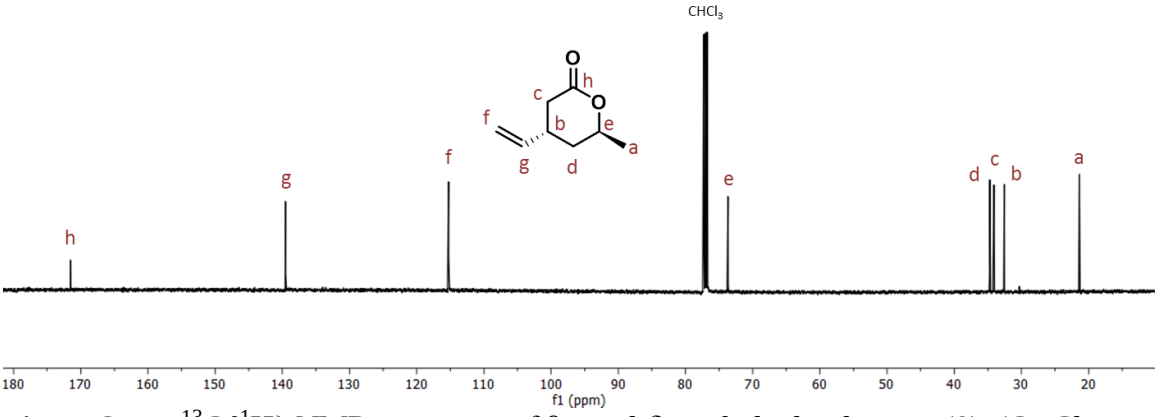

Figure 3. 11. $^{13}C\{^{1}H\}$ NMR spectrum of β-vinyl-δ-methylvalerolactone (8) ($CDCl_3$, 126 MHz).

The disubstituted δ-valerolactones (**2**), (**3**), (**4**), (**6**), and (**8**) were tested for ring opening polymerizations with a variety of catalysts, including typical organo- and organometallic catalysts[116,132] such as diphenyl phosphate (DPP), triazabicyclodecene (TBD), 1,8-diazabicyclo[5.4.0]undec-7-ene (DBU), phosphazene base P_4-*t*-Bu, $BF_3{\cdot}OEt_2$, Bi subsalycilate, $Sn(Oct)_2$, $Al(iOPr)_3$, and $Ti(iOPr)_4$, as well as highly active Zn- and Al-based[133–135] catalysts. Although theoretical calculations suggested similar thermodynamics of polymerization for the disubstituted δ-valerolactones (**4**), (**6**), and (**8**) as discussed above, (**4**) was the only monomer in the tested series to undergo successful polymerization. The source of such a drastic difference in polymerization behavior among the tested disubstituted δ-valerolactones is not well understood at this time. One possible explanation may be that each lactone does indeed possess favorable thermodynamic parameters for polymerization, but kinetically, are polymerized too slowly with the tested catalysts to be monitored over the duration of the experiments (typically weeks to a month). In any case, through our screenings, we identified DPP as a catalyst that can facilitate the conversion of (**4**) to **poly(4)** to an appreciable degree at relatively slow rates (discussed in further detail below).

Bulk polymerization of a sample of (**4**) using DPP as the catalyst and benzyl alcohol (BnOH) as the initiator produced **poly(4)** as an amorphous material, reaching an equilibrium monomer conversion of 45% at ambient temperature (Scheme 3.5, Figure 3.12). During the ROP of (**4**) with DPP, we observed the formation parasorbic acid (**7**) as a byproduct within the reaction mixture (2-5% by ^{1}H NMR over the course of the reaction time), which is formed via the acid-catalyzed elimination of acetic acid from the

ring. At this time, any effect(s) arising from the presence of acetic acid within the reaction mixture on the polymerization behavior of (**4**) is unknown.

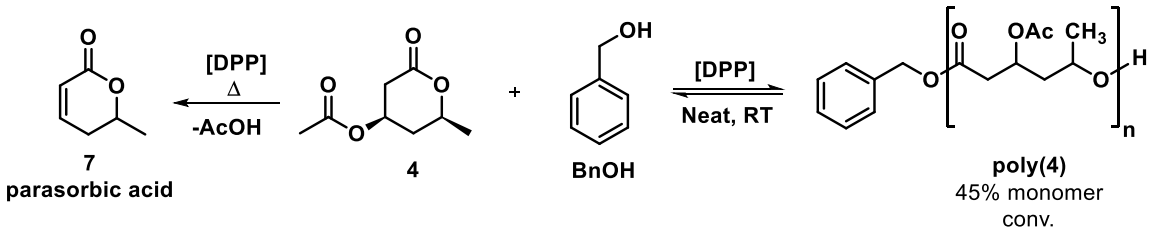

Scheme 3. 5. Polymerization of (4) using DPP as the catalyst and the elimination of acetic acid from (4) to produce parasorbic acid (5).

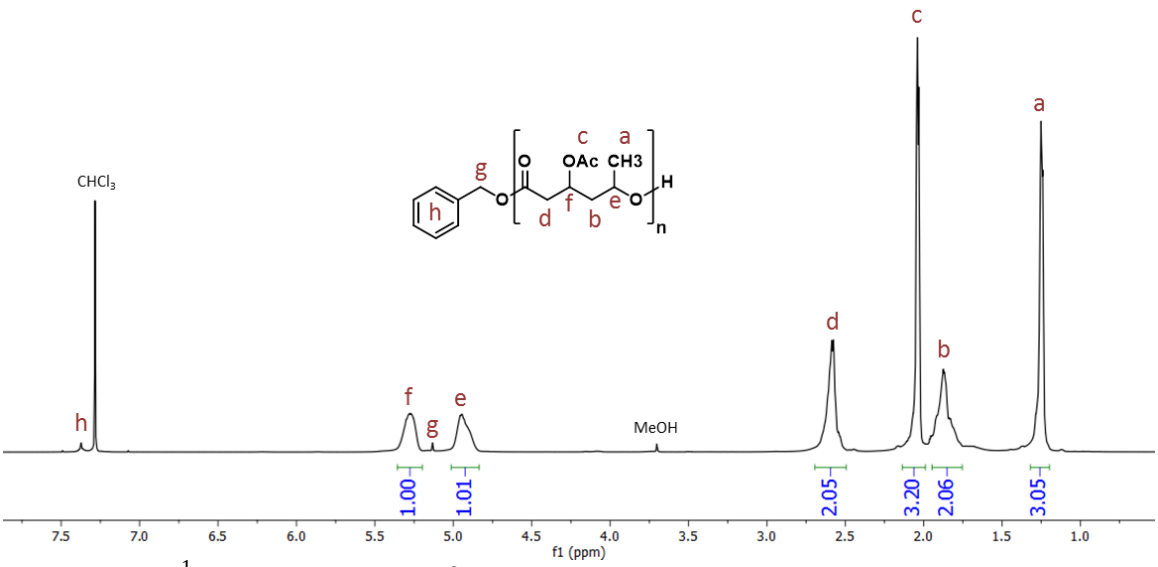

Figure 3. 12. ^{1}H NMR spectrum of poly(4) ($CDCl_3$, 500 MHz).

The molar mass of **poly(4)** was observed to be consistently lower than the targeted, theoretical value. As an example, starting with a 200:1 ratio of (**4**) to BnOH (theoretical M_n = 15.5 kDa based on a 45% monomer conversion), end group analysis via ^{1}H NMR indicated the molar mass to be 17 kDa. Analysis of the same sample via SEC-MALLS, however, revealed the M_n to be 10 kDa with a dispersity (Đ) of 1.2 (Figure 3.13). To elucidate the reason for the mismatched results from the two molar mass determination methods we carefully examined the ^{1}H NMR spectrum of **poly(4)** and observed the presence of small alkene resonances near the baseline (Figure 3.14). The ring opening of a molecule of (**4**) via cleavage of the ester bond produces a secondary alcohol as the propagating species, which, instead of propagating with the next monomer unit, can undergo an acid-catalyzed elimination reaction[136] to produce an olefin at the terminal end of the growing chain (Scheme 3.6). The olefin, unable to propagate, terminates the polymerization and causes a limiting effect on the molecular weight of the polymer chain. Additionally, the elimination reaction produces water as a byproduct, which can act as an adventitious initiator and leads to further attenuation of the achievable molar mass.

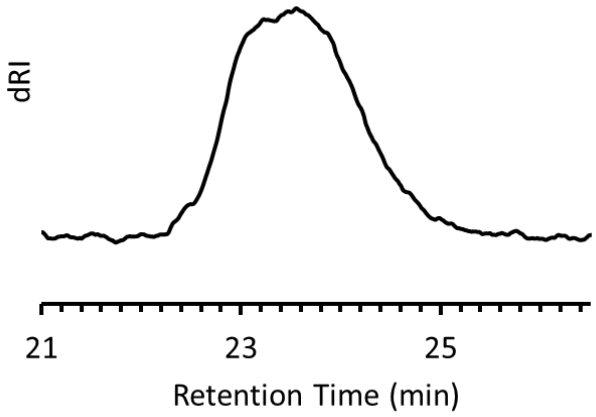

Figure 3. 13. THF SEC trace of poly(4) with differential refractive index (M_n = 10 kDa, (Đ) = 1.2).

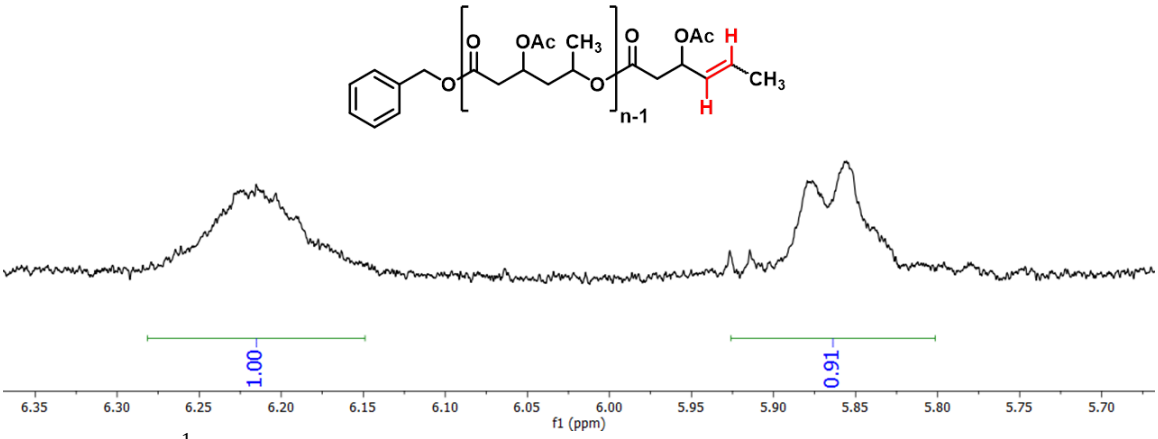

Figure 3. 14. ^{1}H NMR spectrum of poly(4), expanding the baseline in the alkene region, indicating the presence of terminal olefins formed through an elimination reaction of the secondary propagating alcohol during polymerization.

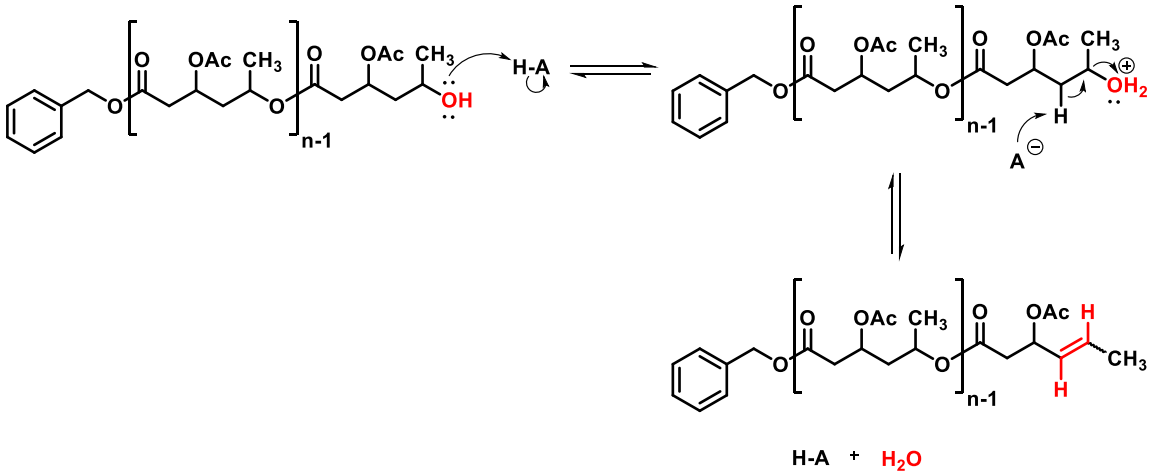

Scheme 3. 6. Proposed mechanism for the formation of a terminal alkene in the propagating chain of poly(4), catalyzed by DPP (denoted as a generic HA here), through an elimination reaction of the secondary alcohol.

The thermal properties of **poly(4)** were investigated by thermogravimetric analysis (TGA) and differential scanning calorimetry (DSC). The TGA thermogram shows a 5% weight loss occurring at 228 °C (Figure 3.15). The DSC thermogram of a 10 kDa sample of **poly(4)** shows it to be an amorphous material with a T_g of 25 °C, an exciting result for potential materials applications (Figure 3.16). Most poly(lactones), with the notable exception of poly(lactic acid) (T_g = 55 °C)[15] and poly(glycolide) (T_g = 36 °C),[137] exhibit T_g values below ambient temperature,[70,76,121,123,136,138–140] and thus, are typically only useful as soft, rubbery components in polymeric materials. The relatively higher T_g observed for **poly(4)** presents future opportunities to explore the effectiveness of the new poly(lactone) as the hard, glassy component in polymeric materials.

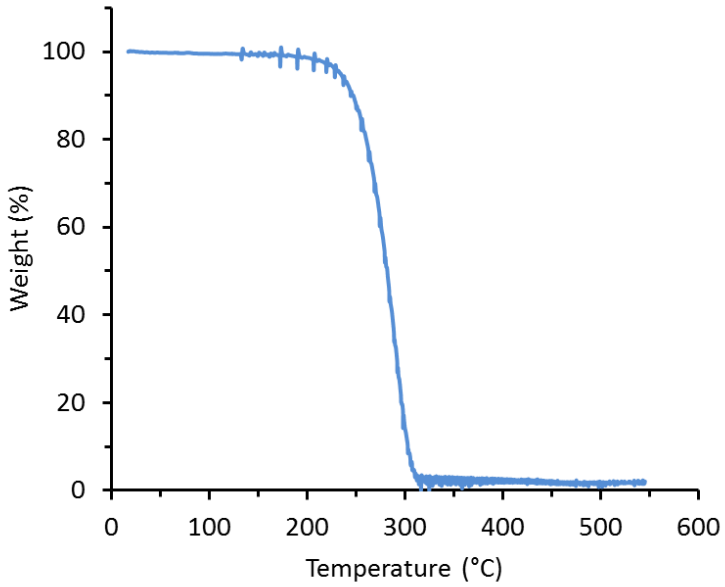

Figure 3. 15. TGA thermogram of poly(4) at a heating rate of 10 °C min^{-1}.

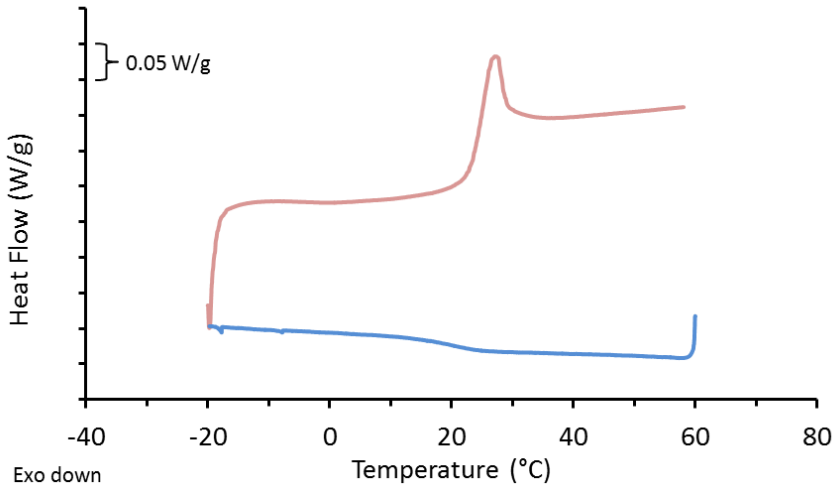

Figure 3. 16. DSC thermogram of poly(4) at a heating rate of 10 °C min^{-1} taken on the second heating (red) and cooling (blue) cycles. The thermogram shows a T_g = 25 °C for a 10 kDa sample.

To understand how monomer structure affects polymerization behavior of substituted δ-valerolactones, we determined the thermodynamics of polymerization for the disubstituted δ-valerolactone monomer (**4**) using a Van't Hoff analysis[141] (Equation 3.1), and compared the results to those previously published for δ-valerolactone (**9**), β-methyl-δ-valerolactone (**10**), and δ-methyl-δ-valerolactone (**11**) (Figures 3.17 – 3.18).[70] The bulk polymerization of (**4**) was monitored at 22 °C, 10 °C, and 0 °C (Figure 3.18) via ^{1}H NMR until apparent equilibrium (up to two months at 0 °C). The elimination of acetic acid from (**4**) in the presence of an acid catalyst such as DPP became a significant issue at elevated temperatures (Scheme 3.3), and thus, prevented us from measuring the equilibrium monomer concentrations at temperatures above ambient conditions.

$$\ln\left(\frac{[M]_{eq}}{[M]_0}\right) = \frac{\Delta H^\circ_p}{RT} - \frac{\Delta S^\circ_p}{R} \qquad \text{Equation 3.1}$$

The enthalpy ($\Delta H_p°$) and entropy ($\Delta S_p°$) of polymerization were calculated to be --25 ± 2 kJ mol^{-1} and -81 ± 5 mol^{-1} K^{-1}, respectively. By comparing the thermodynamics of polymerization of (**4**) to the values reported for (**9**) – (**11**), we observe a trend of increasing ring strain with the degree of substitution, indicated by $\Delta H_p°$ for the isodesmic reaction of ROP of lactones. This is in disagreement with the trend perceived from the theoretical calculations given in Table 3.1. Additionally, the value of $\Delta S_p°$ is also observed to significantly increase with degree of substitution. These results suggest that the bulk polymerization of substituted δ-valerolactones becomes increasingly exothermic and entropically disfavored with increasing degree of substitution. By further appending

substituents on the lactone ring (e.g. tri- and tetrasubstituted), the increased order of the system upon polymerization ($\Delta S_p°$) will eventually negate the ring strain ($\Delta H_p°$), and polymerizations will become thermodynamically disfavored.

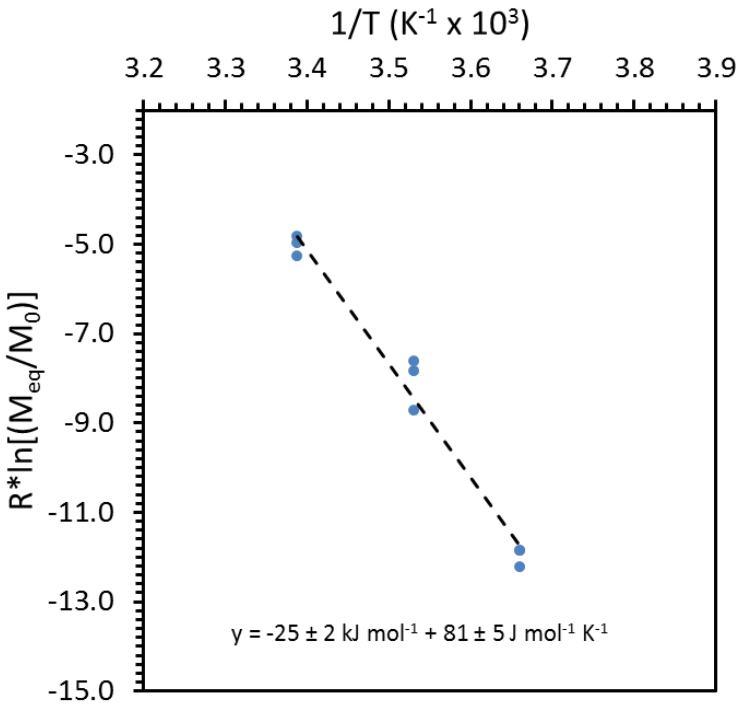

Figure 3. 17. Van't Hoff plot of the temperature dependency of the equilibrium monomer concentration for the ring opening polymerization of (4).

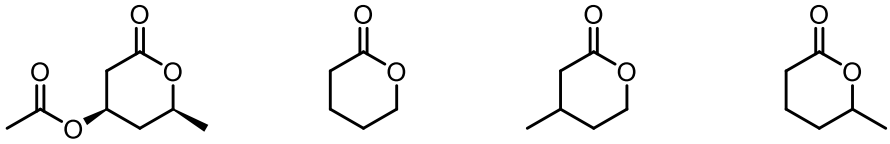

	4	**9**	**10**	**11**
$\Delta H_p°$ (kJ mol^{-1})	-25 ± 2	-10.5	-13.8 ± 0.3	-19.3 ± 0.5
$\Delta S_p°$ (J mol^{-1} K^{-1})	-81 ± 5	-15	-46 ± 1	-62 ± 2
k_{obs} (M/h)	0.012 ± 0.001	2.88 ± 0.33	2.46 ± 0.22	0.31 ± 0.04
$t_{1/2}$ (h)	276 ± 32	1.89 ± 0.22	1.86 ± 0.17	14.9 ± 2.1

Figure 3. 18. Thermodynamic and kinetic data comparing the polymerization of (4) to that of (9) – (11).[70]

The rate of polymerization of (**4**) was also studied in order to compare its reactivity to that of (**9**) – (**11**). The observed rate constants (k_{obs}) and half-lives ($t_{1/2}$) of (**9**) – (**11**) were previously reported for bulk polymerizations using a ratio of monomer to initiator (BnOH) to catalyst (DPP) of 200:1:1.[70] Under identical conditions, we measured the $t_{1/2}$ of conversion of (**4**) to be 276 ± 32 h with k_{obs} = 0.012 ± 0.001 M h^{-1} (Figure 3.19a. The observed rate constant was determined from the first 192 h (Figure 3.12b) using the zero-order rate equation:

$$[M] = [M]_o - k_{obs}t \qquad \text{Equation 3.2}$$

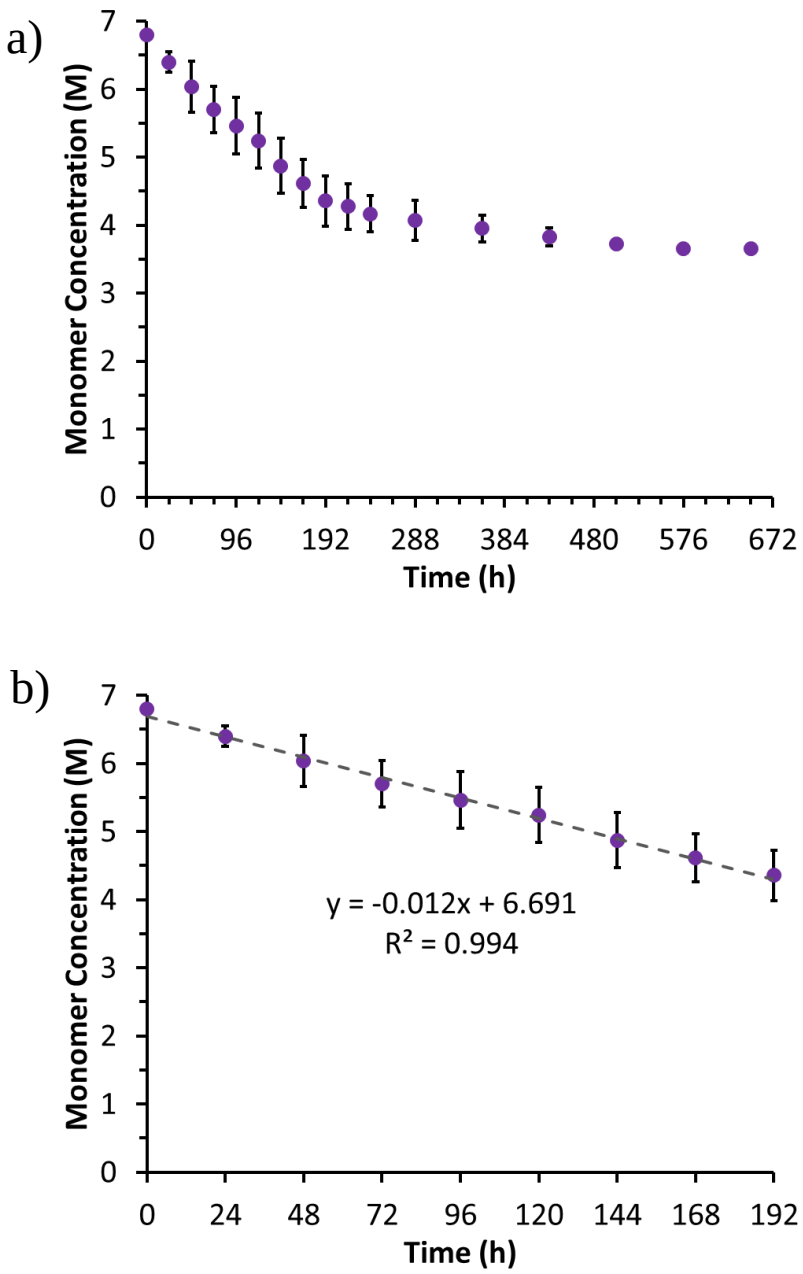

Figure 3. 19. Conversion of (4) during bulk polymerization conducted at 22 °C with BnOH as the initiator and DPP as the catalyst at a 200:1:1 monomer:initiator:catalyst ratio. Plot (A) shows the polymerization over the entire duration which the reaction was monitored and plot (B) shows the first 192 h of polymerization.

Overall, we observed the rate of polymerization (k_{obs}) of (**4**) to be two orders of magnitude slower than (**9**) and (**10**) and an order of magnitude slower than (**11**). Assuming that the rate-determining step in the ROP of lactones is cleavage of the C-O ester bond, we hypothesize that the proximity of the methyl substituent to the carbonyl group in (**4**) and (**11**) can hinder the nucleophilic attack of the hydroxyl end group of a polymer chain. Furthermore, ring opening of (**4**) and (**11**) results in a secondary alcohol as the propagating end group, which may itself by sterically hindered in reacting with other monomer molecules. These steric arguments offer a rationale for the slower kinetics observed for (**4**) and (**11**) in comparison to unsubstituted δ-valerolactone (**9**) and β-methyl-δ-valerolactone (**10**). In the case of (**4**), an additional carbonyl group is present (the β-acetoxy substituent) in the monomer structure. Under the assumption of an activated monomer mechanism (AMM) for the polymerization of lactones,[142] activation of the β-acetoxy carbonyl by DPP would be unproductive for propagation. In conjunction with the steric arguments presented for the methyl substituent in proximity to the ester carbonyl, the competitive nature of unproductive activation of the β-acetoxy carbonyl can rationalize the very slow polymerization rates observed for (**4**) compared to the monosubstituted δ-valerolactones (**10**) and **(11**).

3.3 Conclusions

In summary, this report demonstrates for the first time the successful ring opening polymerization of a disubstituted δ-valerolactone, β-acetoxy-δ-methylvalerolactone (**4**)**,** derived from the emerging platform chemical triacetic acid lactone. Using DPP as the organocatalyst the polymerization of (**4**) was observed to reach an equilibrium monomer conversion of 45% under ambient conditions. Differential scanning calorimetry analysis of a 10 kDa sample of **poly**(**4**) indicated the T_g of the resultant polyester to be 25 °C, a promising result for future materials applications. While a racemic mixture of (**4**) was used in this study, the influence of using an enantiomerically pure sample for polymerization on the T_g of the resultant polyester is under future consideration. The exclusive polymerization of either enantiomer (i.e. RS or SR) would yield a polymer with an isotactic sequence, which can lead to an increase the T_g of the material and may also impart a certain degree of crystallinity.[143,144] We established the kinetic and thermodynamic parameters for the polymerization of (**4**), and the results suggest that the polymerization of δ-valerolactones becomes increasingly exothermic and entropically disfavored with an increasing degree of substitution. Future studies are focused on assessing the mechanical properties of **poly(4)**, as well as discovering other disubstituted δ-valerolactones derived from TAL that can be polymerized.

3.4 Experimental

Materials. 4-Hydroxy-6-methyl-2-pyrone ("Triacetic Acid Lactone" (TAL)) was purchased from Oakwood Chemical and used without further purification. Pd/C (10 wt% loading) was purchased from Sigma-Aldrich and dried under vacuum prior to use. 4-(dimethylamino)pyridine (DMAP), acetic anhydride, and vinylmagnesium bromide (1M, THF solution) were obtained from Millipore-Sigma and used without further purification.

Characterization. All reported ^{1}H NMR and ^{13}C NMR spectra were collected on Bruker Avance III HD 500 MHz and Bruker Avance III HD 400 MHz spectrometers in deuterated chloroform ($CDCl_3$). ^{1}H NMR chemical shifts are referenced to tetramethylsilane (TMS) at 0.00 ppm and ^{13}C NMR spectra are referenced to the $CDCl_3$ carbon resonance at 77.16 ppm Spectra of small molecules were collected at 22 °C with a D1 = 1s (16 scans) and spectra of polymers were collected at 22 °C with a D1= 10s (64 scans).

THF size-exclusion chromatography (SEC) was performed in uninhibited THF utilizing a Waters Styragel guard column and three consecutive Waters Styragel columns at a flow rate of 1 mL min^{-1} at 22 °C. The instrument was equipped with an Agilent 1260 Infinity liquid chromatography coupled with a Wyatt Dawn Heleos II multiangle light scattering detector (18 angles from 10° to 160° and a 662.6 nm laser) and a Wyatt Optilab T-rEX refractive index detector. Reported dn/dc values were calculated from the RI signal using a known sample concentration and assuming 100% mass recovery from the column and used for molar mass determination.

Thermal gravimetric analysis (TGA) was performed on a TA Instruments Q500 series at a heating rate of 10 °C min^{-1} under 60/40 nitrogen/oxygen flow.

Differential scanning calorimetry (DSC) experiments were conducted with a TA Instruments Discovery DSC, using samples hermetically sealed in aluminum pans, at a heating/cooling rate of 10 °C min^{-1}. Reported T_g values are from the second heating/cooling ramps.

Hydrogenation of 4-hydroxy-6-methyl-2-pyrone (Triacetic Acid Lactone (TAL, 1)). Uninhibited THF was stirred over activated 3Å molecular sieves for 24 hours and filtered through a bed of Celite prior to use. A 300 mL high-pressure reactor vessel was charged with TAL (**1**) (20.0 g, 159 mmol), Pd/C (2.0 g, 10% by mass), and 200 mL of THF. The reactor was sealed, and first pressurized and de-pressurized with Argon (3X) to remove O_2, then pressurized with gaseous H_2 to 100 PSI, heated to 50 °C, then pressurized to 500 PSI. Over the next 48 h, the reactor vessel was periodically re-pressurized to 500 PSI, after which time the vessel was cooled to room temperature and purged with Argon to remove H_2. The reaction mixture was then filtered through a bed of Celite to remove the Pd/C. The THF was removed under vacuum and the resultant liquid was crystallized using ethyl acetate and hexanes to afford 4-hydroxy-6-methyl-2-lactone (**3**) (14 g, 68% isolated yield). ^{1}H NMR (500 MHz, Chloroform-d) δ 4.44 – 4.29 (m, 1H), 4.25 (ddt, J = 9.3, 7.8, 5.7 Hz, 1H), 2.97 (s, 1H), 2.91 – 2.83 (m, 1H), 2.45 (ddd, J = 17.1, 5.9, 1.3 Hz,

1H), 2.28 (dddd, J = 13.8, 5.6, 3.0, 1.3 Hz, 1H), 1.63 – 1.52 (m, 1H), 1.41 (d, J = 6.3, 1.8 Hz, 3H).

Synthesis of β-acetoxy-δ-methylvalerolactone (4). (**3**) (10.0 g, 76.8 mmol) and 4-(dimethylamino)pyridine (DMAP) (0.94 g, 7.7 mmol) were dissolved in 40 mL of anhydrous ethyl acetate in an oven-dried 100 mL round bottom flask. The flask was sealed with a rubber septum and submerged in an ice-bath, then acetic anhydride (11.0 mL, 11.9 g, 116.4 mmol) was added drop-wise via needle/syringe to the stirring solution over a period of 10 minutes. After 12 h, the reaction mixture was concentrated under vacuum to yield a yellow liquid. The yellow liquid was loaded on to a column of basic alumina (2" diameter x 10" length) and a mixture of ethyl acetate/hexanes (3:1) was used as the eluent. The desired compound eluted from the column first and DMAP, the acetic acid byproduct, and excess acetic anhydride were left behind on the column. The solvents were then removed under vacuum to afford (**3**) and a small impurity of parasorbic acid (**7**) (ca. 5% by ^{1}H NMR analysis). The parasorbic acid impurity was removed from the sample by applying high vacuum for 2 – 3 days, or until it undetectable by ^{1}H NMR analysis, to yield (**3**) (6.5 g, 49% isolated yield). ^{1}H NMR (500 MHz, Chloroform-*d*) δ 5.22 (dq, *J* = 8.6, 6.4 Hz, 1H), 4.40 (dqd, *J* = 11.6, 6.3, 2.9 Hz, 1H), 2.93 (ddd, *J* = 17.3, 6.4, 0.9 Hz, 1H), 2.59 (dd, *J* = 17.3, 6.7 Hz, 1H), 2.40 (dddd, *J* = 14.0, 6.2, 2.9, 0.9 Hz, 1H), 2.08 (s, 3H), 1.64 (dddd, *J* = 14.0, 6.2, 2.9, 0.9 Hz, 1H), 1.44 (d, *J* = 6.3 Hz, 3H).

Synthesis of 4-methoxy-6-methyl-2H-pyran-2-one (5). TAL (**1**) (10.0 g, 79.3 mmol) and potassium carbonate (K_2CO_3) (13.2 g, 95.5 mmol) were added to an oven-dried 250 mL round bottom flask with a side arm. Trimethylphosphate (19.4 mL, 23.2 g, 165.8 mmol) was added to the mixture under Argon flow and the flask was then submerged in a preheated oil bath at 140 °C. An air condenser leading to an oil bubbler was attached to the flask and the mixture was stirred under Argon using a large stir bar. After 1 h of heating, 50 mL of DI water and 100 mL of ethyl acetate were added to the flask, and the reaction mixture was then transferred to a large separatory funnel. The organic layer was separated, and an extraction was performed from the aqueous layer using 50 mL of ethyl acetate. The organic layers were combined, washed once with 50 mL of DI water, once with 50 mL of a brine solution, dried over magnesium sulfate ($MgSO_4$), then filtered through a bed of celite to yield a yellow solution. The ethyl acetate was removed under vacuum to yield a yellow solid, which was crystallized by dissolving in a minimal amount of ethyl acetate and adding hexanes until a precipitate was seen. The flask was then placed in a freezer for 6 h and the off-white, fine needles were collected on a fritted filter flask, washed with cold hexanes, and dried under vacuum to yield 4-methoxy-6-methyl-2H-pyran-2-one (**5**) (6.2 g, 56% isolated yield). ^{1}H NMR (400 MHz, Chloroform-*d*) δ 5.75 (dt, *J* = 2.0, 1.0 Hz, 1H), 5.37 (d, *J* = 2.2 Hz, 1H), 3.76 (s, 3H), 2.18 (s, 3H).

Synthesis of β-methoxy-δ-methylvalerolactone (6). Uninhibited THF was stirred over activated 3Å molecular sieves for 24 hours and filtered through a bed of Celite prior to use. A 300 mL high-pressure reactor vessel was charged with (**5**) (4.0 g, 28.5 mmol),

Pd/C (0.4 g, 10% by mass), and 150 mL of THF. The reactor was sealed, and first pressurized and de-pressurized with Argon (3X) to remove O_2, then pressurized with gaseous H_2 to 500 PSI. After 24 h the vessel was cooled to room temperature and purged with Argon to remove H_2. The reaction mixture was then filtered through a bed of Celite to remove the Pd/C. The THF was removed under vacuum to yield β-methoxy-δ-methylvalerolactone (**6**) as a clear, colorless liquid (3.6 g, 88% isolated yield). ^{1}H NMR (400 MHz, Chloroform-*d*) δ 4.35 (dqd, *J* = 11.6, 6.3, 2.9 Hz, 1H), 3.80 – 3.72 (m, *J* = 8.9, 7.3, 5.7, 5.7 Hz, 1H), 3.39 (s, 3H), 2.91 – 2.82 (dd, *J* = 17.1, 7.3 1H), 2.52 (ddd, *J* = 17.1, 5.9, 1.2 Hz, 1H), 2.32 (dddd, *J* = 13.9, 5.6, 2.9, 1.2 Hz, 1H), 1.58 – 1.48 (ddd, *J* = 13.9, 11.6, 8.9 Hz, 1H), 1.43 (s, 3H).

Synthesis of parasorbic acid (7). (**3**) (5.0 g, 38.4 mmol) and 1 mL of $CHCl_3$ were added to a 50 mL bomb flask. The flask was submerged in preheated oil bath at 150 °C for 24 h and then cooled to room temperature. The solution was transferred to an Erlenmeyer flask and dried over $MgSO_4$ to remove the water byproduct, filtered, and then concentrated under vacuum to yield parasorbic acid (**7**). Purification of (**7**) was performed via vacuum distillation using a short-path distillation column at 90 °C, 200 mTorr (4.0 g, 93% isolated yield). ^{1}H NMR (500 MHz, Chloroform-d) δ 6.89 (ddd, J = 9.8, 5.8, 2.6 Hz, 1H), 6.03 (ddd, J = 9.8, 2.7, 1.2 Hz, 1H), 4.58 (dtd, J = 10.8, 6.3, 4.4 Hz, 1H), 2.42 – 2.27 (m, 2H), 1.46 (d, J = 6.3 Hz, 3H).

Synthesis of β-vinyl-δ-methylvalerolactone (8). CuI (900 mg, 4.7 mmol) and 20 mL of anhydrous THF were added to a 100 mL round bottom flask, which was then sealed with a rubber septum. The flask was cooled to -78 °C using a dry ice/acetone bath for 10 minutes while sparging with nitrogen gas. Under a flow of nitrogen, 20 mL vinylmagnesium bromide solution (1.0 M in THF, 20 mmol) was added via needle/syringe over 10 minutes. Parasorbic acid (**7**) (1.0 g, 8.9 mmol) was dissolved in 10 mL of anhydride THF, and the solution was added drop-wise to the reaction flask via needle/syringe over 5 minutes. After stirring for 2 h at -78 °C, 15 mL of DI water was added to quench the reaction and the mixture was then warmed to room temperature. The organics were extracted with 50 mL of ether (3X), washed with 50 mL of brine (2X), dried over $MgSO_4$, filtered, and concentrated under vacuum to yield (**8**) as a slight yellow liquid. Purification of (**8**) was performed via vacuum distillation using a short-path distillation column at 80 °C, 200 mTorr (500 mg, 40% isolated yield). ^{1}H NMR (500 MHz, Chloroform-*d*) δ 5.88 – 5.81 (m, 1H), 5.17 – 5.08 (m, 2H), 4.60 – 4.53 (m, 1H), 2.83 – 2.75 (m, 1H), 2.62 (ddd, *J* = 16.9, 6.0, 0.8 Hz, 1H), 2.48 (dd, *J* = 16.9, 7.8 Hz, 1H), 1.84 – 1.80 (m, 2H), 1.39 (dd, *J* = 6.5, 0.8 Hz, 3H).

General procedure for the synthesis of Poly(4). The following is a representative example: β-acetoxy-δ-methylvalerolactone (**4)** (200 mg, 1.16 mmol, 200 equiv), benzyl alcohol (0.63 mg, 5.82 µmol, 1 equiv), and diphenyl phosphate (DPP) (14.5 mg, 0.058 mmol, 5 equiv) were combined together in a 5 mL vial and the contents were thoroughly mixed using a vortex mixer until the DPP was fully dissolved. The solution was stirred

for 14 days (during which time the conversion was periodically monitored via ^{1}H NMR spectroscopy) and then quenched by the addition of a solution of NEt_3 in THF (ca. 2 μL/mL). The polymer was precipitated from the THF solution into a 50/50 mixture of H_2O/methanol. The majority of the supernatant liquid was decanted from the suspension and the remaining solvents were removed on a rotary evaporator. The polymer was re-dissolved in THF and the precipitation procedure was repeated twice more (i.e. precipitated a total of 3 times). Drying in a vacuum oven at 40 °C for 12 h yielded **poly(4)** as a slightly tacky solid.

Poly(4): Thermodynamics of Polymerization. β-acetoxy-δ-methylvalerolactone (**4**) (600 mg, 3.48 mmol, 50 equiv), benzyl alcohol (7.8 mg, 0.072 mmol, 1 equiv), and diphenyl phosphate (DPP, 44.6 mg, 0.167 mmol, 2.5 equiv) were combined together in a 5 mL vial. The contents were thoroughly mixed using a vortex mixer and then separated into 3, separate, 5 mL vials. After 10 days at 22 °C (RT), an aliquot was removed from one sample and immediately quenched by the addition of a solution of NEt_3 in $CDCl_3$ (ca. 2 μL/mL). The conversion was analyzed using ^{1}H NMR spectroscopy. Aliquots were periodically removed everyday over the next 7 days, and in each case, the conversion had not increased; therefore, the other two vials were quenched and analyzed by the same method. This entire process was repeated to measure the equilibrium conversion of polymerization of (**4**) at 10 °C in an oil bath which was chilled using a Thermo Neslab 100-C immersion cooler; aliquots were periodically analyzed over the course of 30 days using ^{1}H NMR until apparent equilibrium. The process was repeated again to measure the

equilibrium conversion of polymerization at 0 °C; aliquots were periodically analyzed over the course of 60 days using ^{1}H NMR until apparent equilibrium. The data was plotted in Microsoft Excel and the LINEST function was used to calculate the uncertainty associated with the slope and Y-intercept of the best-fit line.

Poly(4): Kinetics of Polymerization. Benzyl alcohol (2.2 mg, 0.020 mmol) and β-acetoxy-δ-methylvalerolactone (**4**) (700 mg, 4.07 mmol) were mixed together in a 5 mL vial. Diphenyl phosphate (DPP, 1.5 mg, 6.0 μmol) was added to three separate 5 mL vials (i.e. each vial containing 1.5 mg DPP). 200 mg aliquot of the benzyl alcohol/(**4**) mixture was added to each vial and stirred until homogenous. Aliquots were removed from the stirred reaction mixture every 24 h and quenched by the addition of a solution of NEt_3 in $CDCl_3$ (ca. 2 μL/mL). Analysis by ^{1}H NMR spectroscopy was used to determine monomer conversion at the given time point. K_{obs} was determined from the first 192 h of polymerization using the rate equation $[M] = [M]_0 - k_{obs}t$. β-acetoxy-δ-methylvalerolactone (**4**) has a ρ = 1.16 g/mL, MW = 172.18 g/mol; thus, a neat $[M]_0$ = 6.75 M.

Chapter 4.

Degradable Polyanhydride Networks Derived from Itaconic Acid

Reproduced in part with permission from Sajjad, H.; Lillie, L. M.; Lau, C. M.; Ellison, C. J.; Tolman, W. B.; Reineke, T. M.; Degradable Polyanhydride Networks Derived from Itaconic Acid. *Polym. Chem*. **2021**. DOI: 10.1039/d0py01388a

4.1 Overview

The development of tunable and degradable crosslinked-polyanhydride networks from renewably derived itaconic anhydrides and multifunctional thiols is presented. Itaconic acid was initially converted to ethyl itaconic anhydride and isoamyl itaconic anhydride via a two-step synthetic procedure on hundred-gram scale with minimal purification. Dinorbornene-functionalized derivatives were prepared via cycloaddition chemistry, and photoinitiated thiol-ene polymerization reactions were explored using commercially available tetra- and hexa-functional thiols, all using solvent-free syntheses. The thiol-ene reaction kinetics of different monomer compositions were characterized by real-time Fourier transform infrared (RT-FTIR) spectroscopy, with the norbornene functionalized derivatives exhibiting the highest reactivity towards thiol-ene photopolymerizations. The thermal and mechanical characteristics of the thermosets were analyzed and the viscoelastic behavior was investigated by dynamic mechanical analysis to understand the influence of the ester functionality and choice of crosslinker on the material properties. The anhydride backbone was found to be susceptible to controlled degradation under physiologically- (phosphate-buffered saline) and environmentally-relevant (artificial seawater) testing conditions over a period of 60 days at 50 °C. This work demonstrates that itaconic acid may be a useful feedstock in the generation of degradable polyanhydride networks via thiol-ene photopolymerization.

4.2 Introduction

Degradable polymers are an important class of materials that have found use in many applications such as drug carriers for controlled dosage release from within a biological matrix, implants for medical devices, and temporary scaffolds for regenerative tissue engineering systems.[145–149] Beyond biomedical applications, there is significant interest in using such polymers to create thermoplastic and networked materials that degrade in environmental conditions to reduce the accumulation of plastic waste.[13] Typically, the degradation profiles of such polymers are controlled by the presence of hydrolytically sensitive functionalities distributed throughout the material. For example, esters, hemiacetals, ortho esters, amides, disulfides, or glycosidic bonds are commonly employed to create degradable polymers.[150–154] Materials made from such polymers typically degrade via a bulk erosion mechanism, whereby hydrolytic degradation occurs throughout the entire polymer sample because the rate of water diffusion into the matrix is faster than the rate of bond hydrolysis.[155,156]

Polyanhydride materials exhibit fast rates of degradation over a wide range of conditions owing to the instability of the anhydride bonds relative to other functional groups.[157,158] As a consequence of their shorter hydrolysis half-lives, polyanhydrides also typically undergo a surface erosion mechanism because the rate of water diffusion into the matrix is slower than the rate of bond cleavage at the interface. This property makes them ideal candidates for applications that require the controlled, steady release of bioactive compounds while maintaining their thermomechanical properties over the course of the degradation period. The commercial potential of such materials has been

illustrated through the clinical use of the GLIADEL® wafer, a polyanhydride comprised of 1,3-bis(p-carboxyphenoxy)propane (CPP) and sebacic acid (SA), as an implantable release agent for brain cancer treatment.[159] Among the important benefits of polyanhydride materials for in vivo applications is their decomposition into non-toxic diacids.[157]

Despite these appealing advantages, polyanhydride use has been deterred by inconveniences in synthetic protocols and instability toward moisture, which complicates the logistics of transportation and storage.[160] Traditional synthetic routes for polyanhydrides have relied on condensation polymerizations, which require the use of harmful reagents or stringent conditions such as high heat and vacuum to remove condensates in order to achieve appreciable molecular weights.[161,162] More recent syntheses have used acrylic anhydride monomers for the production of photoinitiated, crosslinked polyanhydride networks.[163–166] However, such polymerizations are inhibited by oxygen, and the chain growth reaction results in the formation of materials with non-uniform crosslink densities. A significant improvement to this strategy relies on thiol-ene "click" chemistry to synthesize polyanhydride networks using vinyl anhydride monomers and multifunctional thiols.[167–171] Thiol-ene reactions are not oxygen inhibited and thus can be performed under ambient conditions.[172,173] The polymerizations can reach high conversions in relatively shorter timeframes, can be done without organic solvents, and can lead to more uniform crosslink densities due to the step-growth mechanism.

In addition to degradability, another goal for sustainable materials synthesis is to integrate renewable feedstocks in the production of materials with similar mechanical

properties to petroleum-based counterparts.[13,174] In pursuit of novel anhydride monomers that are useful for the synthesis of polyanhydride networks via thiol-ene polymerizations, we thus sought renewable feedstocks that can offer rich chemical functionalities for control over application-dependent properties. Towards this end, we aimed to produce tunable crosslinked polyanhydride networks from itaconic acid, a bio-derived feedstock. Itaconic acid, an unsaturated dicarboxylic acid, is currently obtained from the fermentation of biomass by *Aspergillus terreus*.[175] It is produced on an ever-expanding industrial scale (80 kiloton/yr) and is presently commercially available at $1.8-2/kg.[176,177] Itaconic acid is analogous to vinyl monomers such as methacrylic acid, and has been applied to myriad applications ranging from resins, acrylate latexes, dispersants, to super-absorbent materials.[48,49] Notably, the acrylic functionality of itaconic acid has been previously used in post-polymerization modifications via thiol-ene chemistry.[58]

A challenge that must be overcome to use itaconic acid for radical-type polymerizations, however, is the low reactivity of its vinyl group, which is akin to bulky α-substituted acrylates observed to undergo sluggish radical polymerizations.[178,179] To address this limitation, we sought to transform the relatively unreactive vinyl bond of itaconic acid into a functional group that is more amenable towards thiol-ene chemistry. Thiol-norbornene systems are known to follow a thiol-ene step-growth mechanism and at polymerization rates that are faster than various stoichiometric monomer systems.[180] The conversion of the vinyl group of itaconic acid to norbornene-functionalized monomers for use in ring-opening-metathesis polymerizations was previously established via cycloaddition chemistry with cylopentadiene (CPD).[58]

Herein, we report the readily scalable synthesis of the linear itaconic anhydrides ethyl itaconic anhydride (**1**) and isoamyl itaconic anhydride (**2**), and subsequent conversion to dinorbornene-functionalized anhydrides (**3** and **4**) via efficient, solvent-free cycloaddition chemistry. Photoinitiated thiol-ene polymerizations of **1 - 4** with commercially available multifunctional thiols were conducted under ambient conditions to form polyanhydride networks, and the relative rates and network conversions were examined by real-time FTIR. The thermal and mechanical characteristics of the networks were analyzed to elucidate structure-property relationships, and the hydrolytic stability of these materials was assessed under physiologically- and environmentally-relevant aqueous conditions. Here, we highlight itaconic acid as a valuable feedstock to create tunable and degradable polyanhydride networks via thiol-ene photopolymerization.

4.3 Results and Discussion

The initial inspiration for this work stems from the advantageously selective and high yielding monoesterification of itaconic acid.[181] This chemistry has been performed with a variety of alcohols, enabling facile modification of thermal and mechanical properties of the resultant materials. We postulated that these itaconic monoesters could be transformed to linear itaconic anhydrides using chemistry we previously used to make a monomer precursor, 10-undecenoic anhydride.[182] To the best of our knowledge, these itaconic acid-based anhydride structures are unexplored in the literature. The synthesis of itaconic anhydrides, (**1**) and (**2**) was accomplished from itaconic acid through a two-step synthesis by Dr. Leon M. Lillie (Figure 4.1). The first step in the procedure involved the chemoselective esterification of itaconic acid with ethanol or isoamyl alcohol to produce ethyl itaconic acid (**1'**) and isoamyl itaconic acid (**2'**), respectively. The reactions were performed on large scales (100-200 g) with a single recrystallization step for purification. Both monoesters were then transformed into linear itaconic anhydrides by dehydration with acetic anhydride. The resultant anhydrides, ethyl itaconic anhydride (**1**) and isoamyl itaconic anhydride (**2**), were obtained as viscous oils with a slight yellow coloring. Although we focused on the ethyl and isoamyl variants for this work, this methodology can be expanded to produce other linear ester itaconic anhydrides to modulate the physical and thermal properties, as well as the aqueous degradability profiles, of the polyanhydride networks.

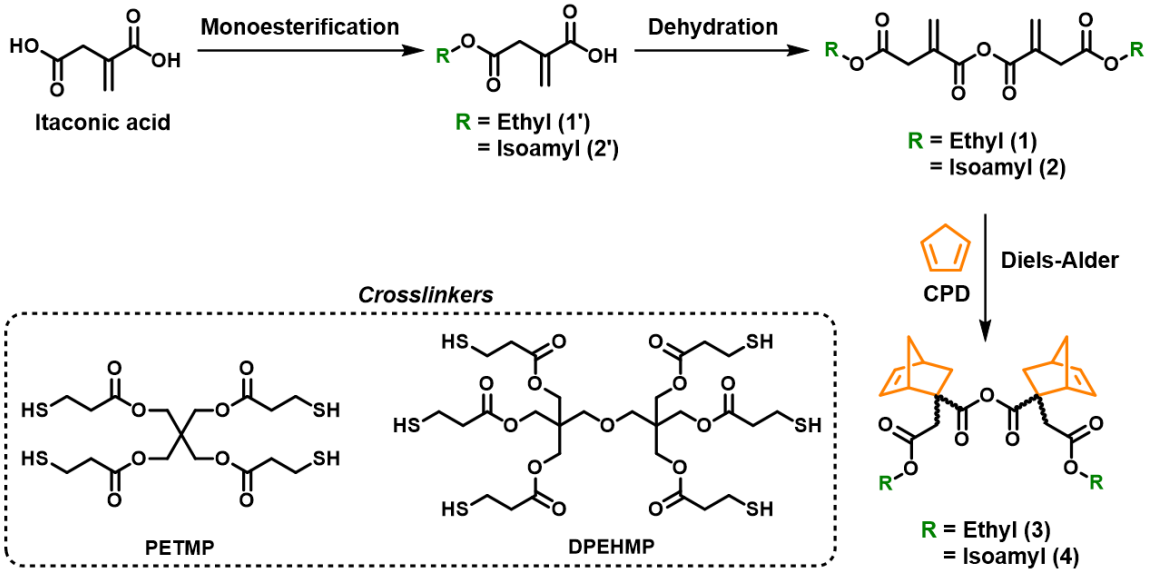

Figure 4. 1. Synthetic scheme for the transformation of itaconic acid into the anhydride monomers used in this study (1 – 4) and multifunctional thiol crosslinkers pentaerythritol tetrakis(3-mercaptopropionate) (PETMP) and dipentaerythritol hexakis(3-mercaptopropionate) (DPEHMP) used in the formation of polyanhydride networks via thiol-ene chemistry.

Efficient cycloaddition reactions with cyclopentadiene were then used to convert **1** and **2** into the dinorbornene-functionalized anhydride monomers **3** and **4**. The reactions were performed without the use of organic solvents and with a small excess of CPD, and the products were purified in a single step to remove the excess CPD and dicyclopentadiene byproduct via vacuum distillation.

The monomers **3** and **4** were produced as two sets of endo/exo diastereomers for each molecule, and these various possible endo/exo combinations convoluted the ^{1}H NMR spectra, making it challenging to integrate individual peaks in order to assess the purity of the monomer samples. To circumvent this issue and enable determination of the

endo:exo ratios, the anhydride moieties in samples of **3** and **4** were hydrolyzed with trifluoroacetic acid at 100 °C to yield only one set of diastereomers (Figure 4.2). The resultant ^{1}H NMR spectra, with signals that could be individually integrated, showed the samples to comprise pure monomers lacking any significant side-products. Integrations of the signals for the alkene protons showed an approximate 70:30 endo:exo ratio for both dinorbornene monomers, with the peaks assigned for the endo isomer on the basis of comparison to a similar norbornene monomer synthesized from itaconic acid reported in the literature.[58]

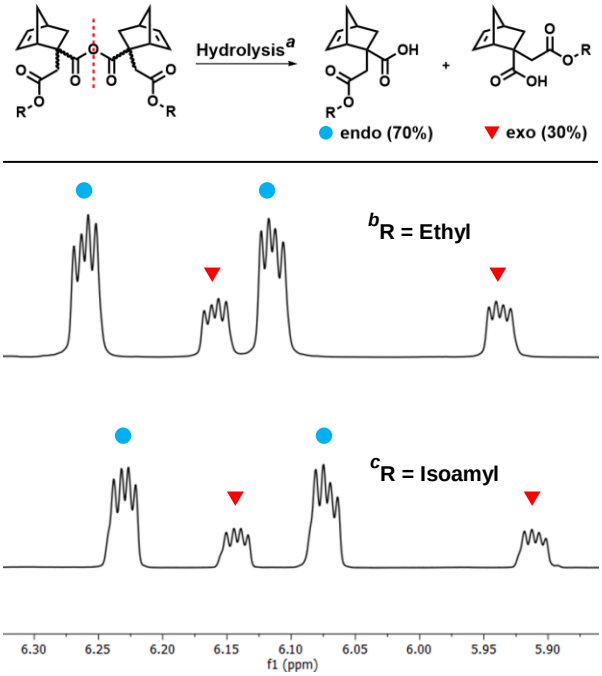

Figure 4. 2. Acid-catalyzed hydrolysis of the dinorbornene-functionalized monomers to cleave the anhydride linkages. a) Samples of the anhydride monomers were dissolved in acetone-d_6 in NMR tubes with 100uL each of D_2O and trifluoroacetic acid. The sealed tubes were then heated at 100 °C for ~2 h until complete hydrolysis of the anhydrides as monitored by ^{1}H NMR. b) ^{1}H NMR spectrum in the alkene region of the hydrolysis products of 3 and c) ^{1}H NMR spectrum in the alkene region of the hydrolysis products of 4. The blue circles indicate the alkene signals of the endo isomers and the red triangles indicate the alkene signals of the exo isomers.

The thiol-ene polymerization of the anhydride monomers **1** – **4** with multifunctional, commercially available thiols was monitored by real-time Fourier transform infrared (RT-FTIR) spectroscopy (Figure 4.3). The RT-FTIR spectroscopy studies were performed in collaboration with C. Maggie Lau, a graduate student of Dr. Christopher J. Ellison. Ensuring a 1:1 molar ratio of the ene:thiol end groups, the anhydride and thiol monomers were mixed together with 5 wt% of OMNIRAD TPO-L photoinitiator until a homogeneous solution was formed, and the samples were then placed between two polished NaCl plates. The Flory-Stockmayer theory (Equation 4.1) can be used to estimate the gel point (p_c) of step-growth thiol-ene crosslinked networks, which is the point at which an infinite network is first established. In the equation, r is defined as the ratio of the thiol to ene functional groups and f is defined as the functionality of the thiol crosslinker component. With r = 1 for all reaction mixtures (i.e. a 1:1 thiol:ene functionality ratio), f = 4 for PETMP, and f = 6 for DPEHMP, p_c was calculated to be 57.7% for networks using PETMP (indicated as a dashed red line) and 44.7% for networks using DPEHMP (indicated as a dotted red line). The reactions of **1** and **2** with pentaerythritol tetrakis(3-mercaptopropionate) (PETMP), following the conversion of the thiol group at 2572 cm^{-1} as a function of irradiation time, were observed to be sluggish, approaching equilibrium at less than 10% conversion after 95 s.

$$p_c = \frac{1}{\sqrt{r[1+(f-2)]}} \qquad \text{(Equation 4.1)}$$

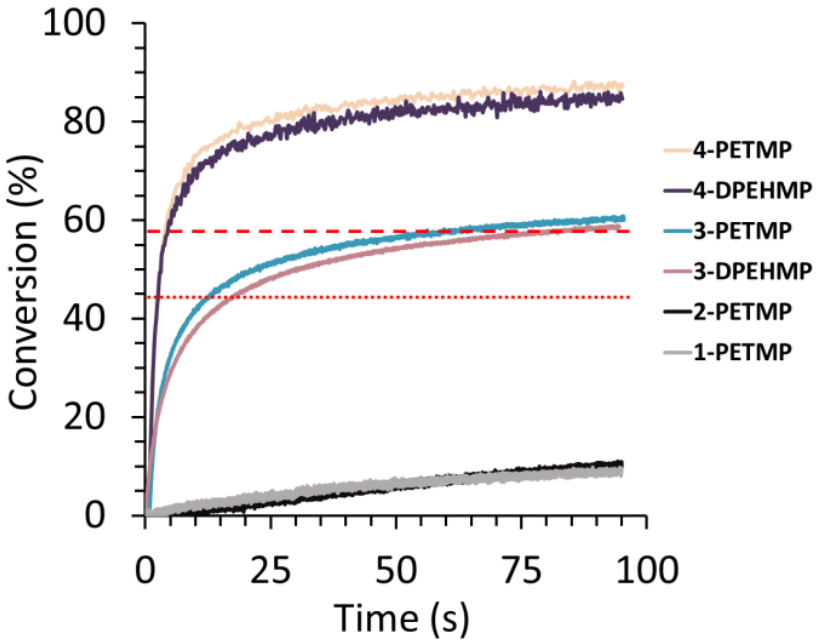

Figure 4. 3. Conversions of the S-H functional groups in PETMP or DPEHMP determined by following the S-H signal at 2572 cm^{-1} in RT-FTIR experiments during photopolymerization reactions with anhydride monomers 1 – 4. The dashed red line denotes the theoretical conversion at the gel point for thiol-ene step-growth networks formed with PETMP (57.7%) and similarly for the dotted red line with DPEHMP (44.7%).

Additionally, the kinetic data based on the conversion of the C=C signal of **1** and **2** did not match that of the thiol signal (Figures 4.4 and 4.5, respectively). Theoretically, the conversion of the ene and thiol functional groups should be identical for a step-growth thiol-ene polymerization; instead, the conversion of alkene groups in **1** and **2** were higher at 40 – 45%. This observation implies that free-radical homopolymerization reactions of **1** and **2** complicate the desired thiol-ene reactions and lead to the formation of inhomogeneous network structures. Using a modified equation (Equation 4.2) for mixed chain- and step-growth thiol-ene polymerizations to calculate the gel point

conversion for reactions of **1** and **2** with PETMP resulted in a C=C conversion of 21.6%.[183] Although the results from the RT-FTIR experiments show C=C conversions for **1**-PETMP and **2**-PETMP above the theoretical polymerization gel point, we observed only the formation of viscous liquids following irradiation. While it is possible that the viscous liquids were "infinite" networks with conversions close to or above the theoretical gel point, it would be necessary to perform rheological measurements on the monomer mixture during the photopolymerization process to support that conclusion. Furthermore, the gel point conversion value is calculated based on an idealized theory that does not account for defects, such as loops and/or dangling ends, which may exist within the network. Regardless, use of monomers **1** and **2** in the thiol-ene photopolymerizations did not produce solidified materials, and we therefore focused our attention on the norbornene-functionalized monomers **3** and **4** for further studies.

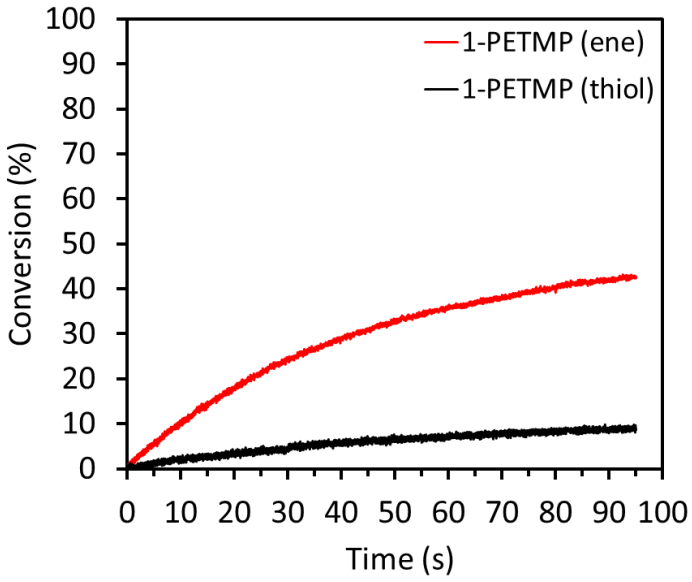

Figure 4. 4. Photopolymerization kinetic curves of the alkene (red) and thiol (black) conversion in 1-PETMP. The mismatch in overall conversions of the functional groups indicate that a thiol-ene mechanism is not exclusively obeyed during polymerizations.

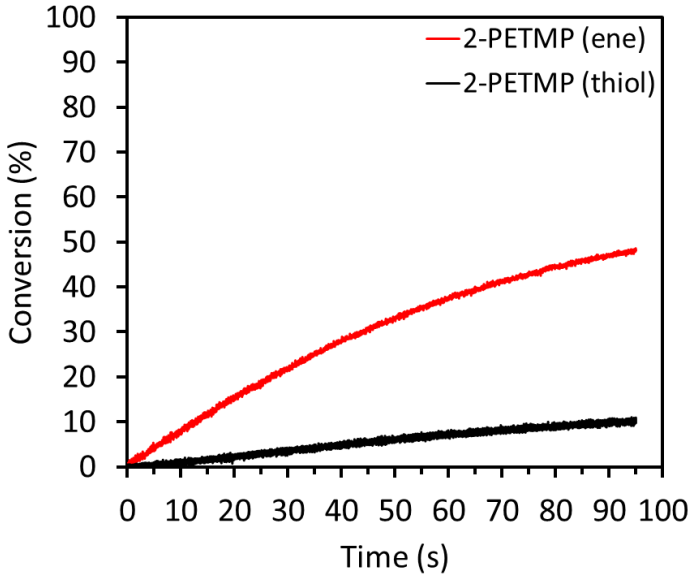

Figure 4. 5. Photopolymerization kinetic curves of the alkene (red) and thiol (black) conversion in 2-PETMP. The mismatch in overall conversions of the functional groups indicate that a thiol-ene mechanism is not exclusively obeyed during polymerizations.

$$\left(\overline{f_{ene}}-1\right)\frac{k_p}{k_{ct}}\frac{2}{r}p_\alpha+p_\alpha^2\left(\overline{f_{th}}-1\right)\left(\overline{f_{ene}}-1\right)\left(1+\frac{k_p}{k_{ct}}\frac{1}{r}\right)=1 \qquad \text{(Equation 4.2)}$$

The polymerization kinetic profiles of **3** and **4** with PETMP and dipentaerythritol hexakis(3-mercaptopropionate) (DPEHMP) show faster relative rates and higher conversions when compared to the profiles of **1** and **2**. It should be noted that the C=C vibrational frequency of the norbornene functional group was superimposed with other signals in the IR spectrum and thus S-H was monitored in the RT-FTIR experiments. The theoretical gel times (i.e. time to reach gel point) are 60 s and 3.9 s for **3**-PETMP and **4**-PETMP, respectively, and 18 s and 2.6 s, for **3**-DPEHMP and **4**-DPEHMP, respectively.

Monitoring the thiol peak as a function of irradiation time, **3**-PETMP reached a maximum conversion of 60% while **4**-PETMP reached 87% after 95 s. **3**-DPEHMP reached a maximum conversion of 59% while **4**-DPEHMP reached 85% after 95 s. As the enthalpy of reaction is expected to be similar for the two monomers (i.e. identical bonds are breaking and forming), the variations in conversion between **3** and **4** with PETMP and DPEHMP is attributed to the differences in mobility of the reactive functional groups within the polymer matrix during the reaction. Monomer mixtures that vitrify during polymerization are restricted in their molecular mobility at high conversions and, therefore, limited in the highest conversion that can be attained (i.e. a polymerization induced glass transition). Materials made with **4** exhibited glass transition temperatures (T_g) below room temperature (discussed below), and thus, the materials were above their T_g during the polymerization and reached higher conversions. In the

case of the materials made with **3**, the T_g values of the networks were above room temperature and, thus, these materials became vitrified during polymerization and could no longer react after that point. The improved reaction kinetics for the norbornene functionalized monomers **3** and **4** is a consequence of the thiol-ene reaction with norbornenes, which provides a significant relief in ring strain to the bicyclic structure. The carbon-centered radical that subsequently forms then undergoes rapid hydrogen abstraction from thiols.[184] Norbornenes better adhere to stoichiometric step-growth polymerizations with thiols, resulting in greater consumption of reactive functional groups and, thus, higher conversions.[180] The results from the FT-IR studies demonstrate that conversion of the α, β unsaturated double bond of itaconic acid to norbornene groups was crucial in improving the reaction kinetics to form solid, crosslinked networks.

The thermal stability of the norbornene polyanhydride networks (**3**-PETMP, **3**-DPEHMP, **4**-PETMP, and **4**-DPEHMP**)** was analyzed via thermogravimetric analysis (TGA) at a heating rate of 10 °C min^{-1} under a N_2 atmosphere up to 550 °C. The thermal decompositions of all four thermosets show nearly identical profiles, with decomposition temperatures (at 5% mass loss) in a narrow 230 – 242 °C range (Figure 4.6).

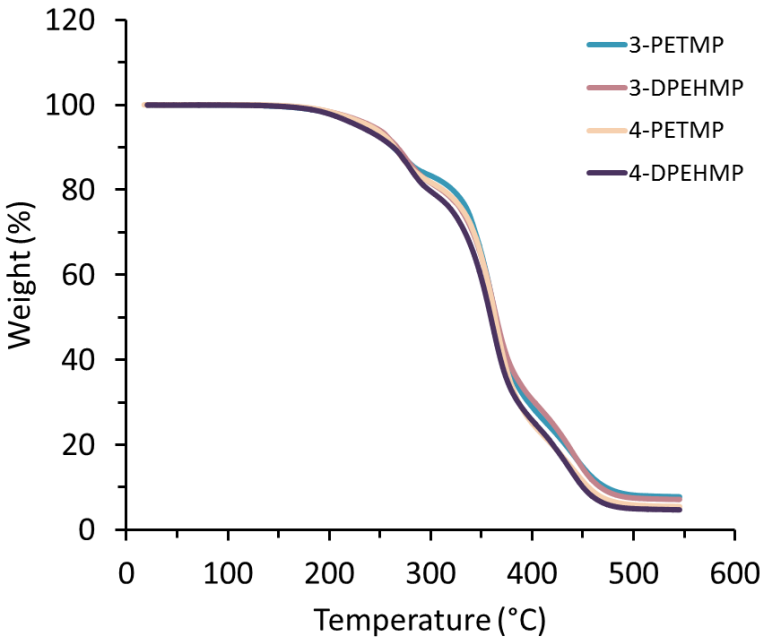

Figure 4. 6. TGA thermograms of anyhydride networks at a heating rate of 10 °C·min^{-1}.

The glass transition temperatures (T_g) of the thermoset materials were determined by differential scanning calorimetry (DSC) at a heating ramp rate of 10 °C, and the reported thermograms were obtained from the second heating cycle to erase any thermal history (Figures 4.7 – 4.10). It is evident from the thermograms that all of the thermosets are amorphous, without any endothermic or exothermic peaks indicating the presence of crystalline domains. The T_g values of **3**-PETMP, **3**-DPEHMP, **4**-PETMP, and **4**-DPEHMP, are 26, 32, 16, and 21 °C, respectively. The T_g values of the thermosets formed from ethyl-based anhydrides were consistently higher than those formed from bulkier isoamyl-based anhydrides with the same thiol crosslinker, exemplifying how the thermal properties of the materials can be tuned by modifying the R group functionality of the ester bonds. Additionally, thermosets formed from DPEHMP showed higher T_g

values than those formed from PETMP due to higher crosslinking densities. In comparison to similar polyanhydride networks made with 4-pentenoic acid and PETMP[24,28], higher T_g polyanhydride networks were obtained with **3**-PETMP and **4**-PETMP. Incorporation of the rigid norbornene functionality within thiol-ene networks has previously been shown to result high T_g materials.[45] The introduction of the norbornene moiety in monomers **3** and **4** is likely to be responsible for the comparatively higher T_g materials synthesized in this work.

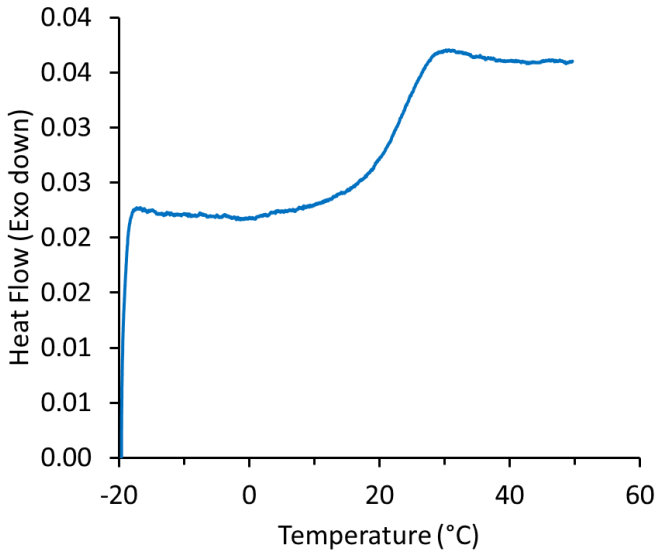

Figure 4. 7. DSC thermogram of 3-PETMP at a heating rate of 10 °C·min^{-1}.

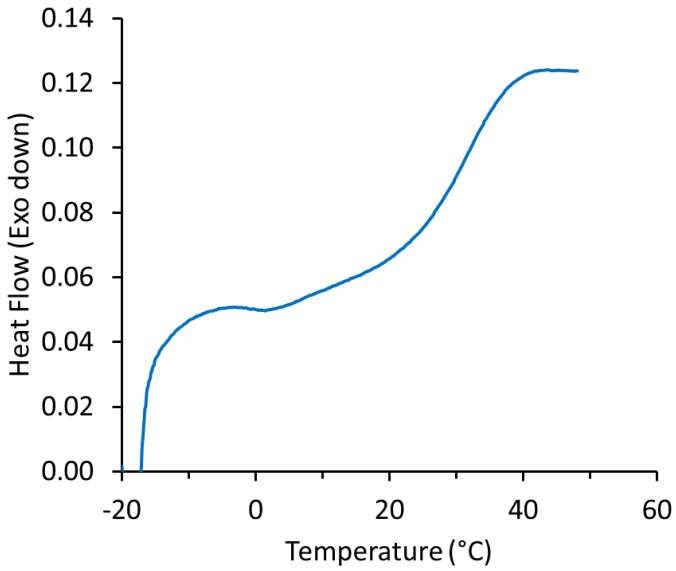

Figure 4. 8. DSC thermogram of 3-DPEHMP at a heating rate of 10 °C·min^{-1}.

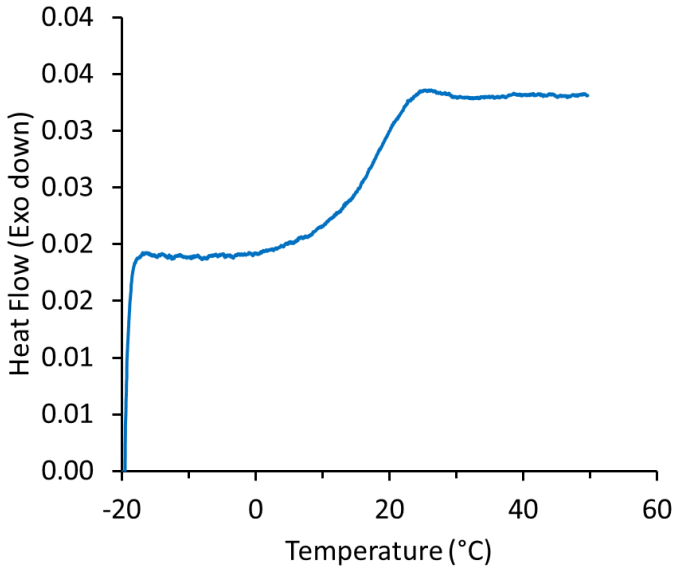

Figure 4. 9. DSC thermogram of 4-PETMP at a heating rate of 10 °C·min^{-1}.

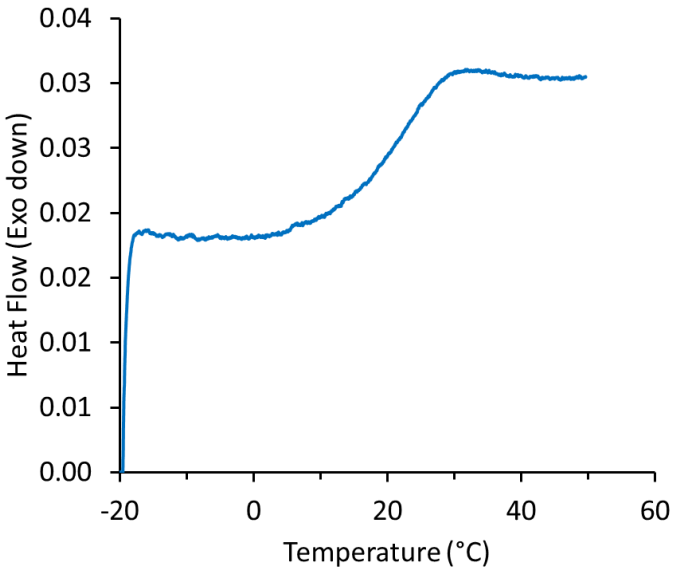

Figure 4. 10. DSC thermogram of 4-DPEHMP at a heating rate of 10 °C·min^{-1}.

Dynamic mechanical analysis (DMA) was performed on the thermosets to investigate their viscoelastic behavior as a function of temperature. The storage moduli and loss moduli are shown in Figure 4.11. The T_g of a crosslinked network can be recorded as the peak of the loss modulus as a function of temperature, identified as 26, 35, 17, and 23 °C, for **3**-PETMP, **3**-DPEHMP, **4**-PETMP, and **4**-DPEHMP, respectively. The plateau modulus in the rubbery plateau region was used to calculate the theoretical average molecular weight between points of crosslinking (M_c) and crosslink density (ν) with Equations 4.3 and 4.4, where ρ is the mass density of the thermoset, E' is the plateau modulus at temperature T, and R is the universal gas constant. The results are summarized in Table 4.1, and the ν values for **3**-PETMP, **3**-DPEHMP, **4**-PETMP, and **4**-DPEHMP were found to be 1.5, 3.5, 1.6, and 4.5 x 10^{-4} mol cm^{-3}. The calculated values only allow for a qualitative comparison among highly crosslinked networks,[46] which

indicate that the crosslink densities of the materials are within the same order of magnitude.

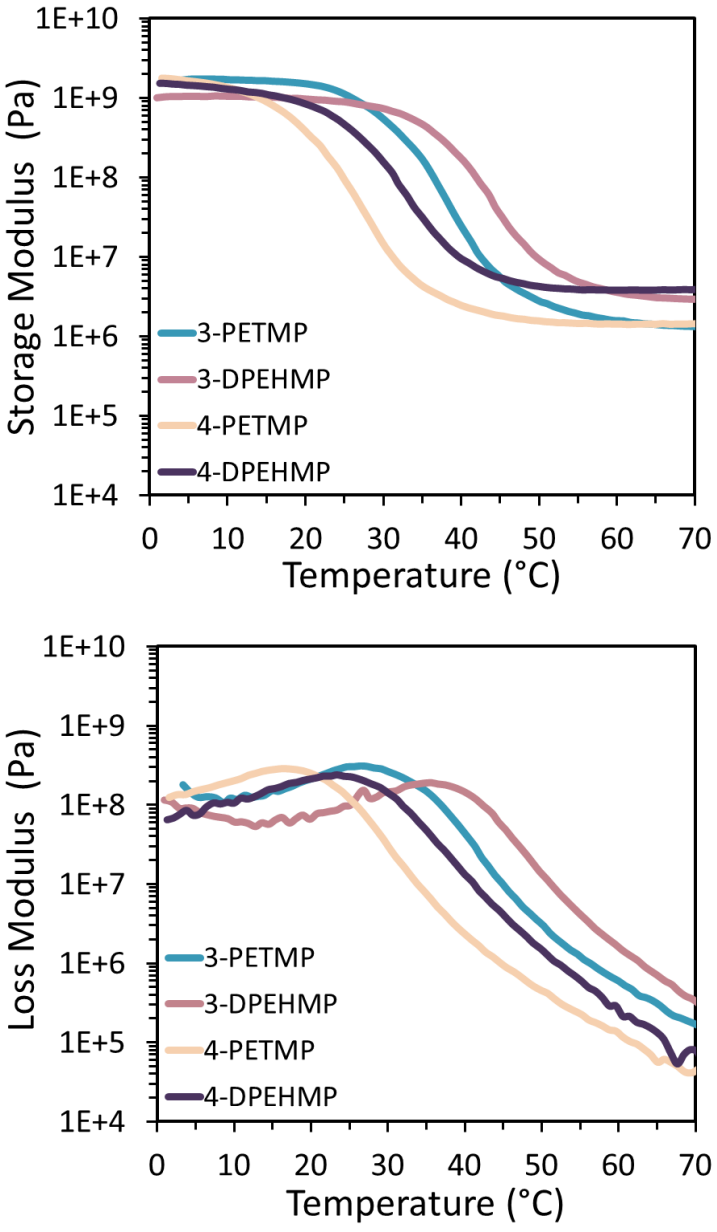

Figure 4. 11. DMA data showing the storage moduli (top) and loss moduli (bottom) of the polyanhydride networks as a function of temperature.

$$M_c = \frac{3\rho RT}{E'} \quad \text{(Equation 4.3)}$$

$$\nu = \frac{\rho}{M_c} \quad \text{(Equation 4.4)}$$

Table 4. 1. Summary of the characterization data for the polyanhydride networks studied in this work.

	3-PETMP	**3**-DPEHMP	**4**-PETMP	**4**-DPEHMP
T_d (°C)[a]	236	242	240	230
$T_{g,DSC}$ (°C)[b]	23	32	17	21
$T_{g,DMA}$ (°C)[c]	26	35	17	23
E (MPa)[d]	300 ± 36	560 ± 64	70 ± 10	260 ± 30
E' (MPa)[e]	1.3	3.0	1.4	3.9
ρ (g cm^{-3})[f]	1.26	1.25	1.19	1.18
M_c (g mol^{-1})[g]	8300	3600	7300	2600
ν (mol cm^{-3})[h]	1.5 x 10^{-4}	3.5 x 10^{-4}	1.6 x 10^{-4}	4.5 x 10^{-4}

[a]Degradation temperature at 5% weight loss. [b]Determined from the mid-point of the glass transition during the second heating ramp at 10 °C min^{-1}. [c]Recorded as the temperature at the peak of the loss modulus data. [d]Young's modulus calculated from the first 2% elongation during uniaxial tensile testing. [e]Plateau modulus taken at 70 °C. [f]Mass density of the thermoset materials determined by Archimedes' principle with a density determination kit. [g]Calculated from eq 4.3 with T = 343 K. [h]Calculated from eq 4.4.

The influence of the glass transition temperatures and crosslink densities on the mechanical behavior of the polyanhydride materials was assessed via uniaxial tensile analysis (Figure 4.12). Overall, the influence of both the glass transition temperature and crosslink densities must be considered in concert to understand the mechanical behavior of the materials. The stress at break and strain at break values, respectively, for the networks are as follows: 6.1 ± 0.8 MPa and 74 ± 9% for **3**-PETMP; 8.8 ± 1.1 MPa and 22 ± 5% for **3**-DPEHMP; 4.7 ± 0.5 MPa for **4**-PETMP; and 8.7 ± 0.6 and 60 ± 4% for **4**-DPEHMP. **4**-PETMP, with a T_g below ambient temperature (ca. 22 °C) and a low crosslink density displayed the most elastomeric-like behavior with the lowest Young's modulus of 70 ± 10 MPa. **3**-PETMP and **4**-DPEHMP exhibited similar Young's modulus values of 300 ± 36 MPa and 260 ± 30 MPa, respectively. Although **3**-PETMP had a lower crosslink density compared to **4**-DPEHMP, the fact that it has a higher T_g meant that the samples were in a vitrified state during tensile analysis. **4**-DPEHMP, comparatively, had a higher crosslink density but exhibited a T_g close to ambient temperature. **3**-DPEHMP, possessing the highest T_g and high crosslink density, displayed the most brittle behavior showing the highest ultimate tensile strength and largest Young's modulus value.

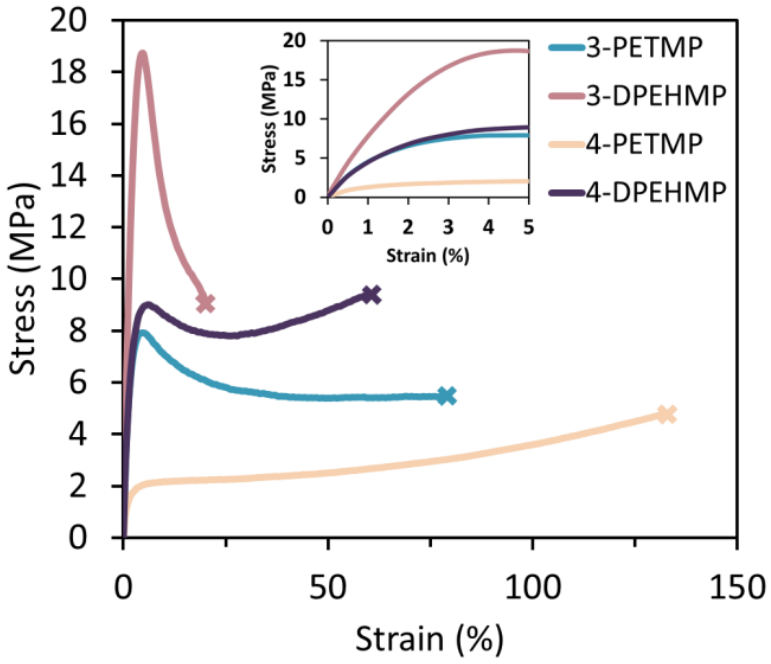

Figure 4. 12. Representative engineering stress vs strain data for the polyanhydride networks. Samples were elongated at a rate of 5 mm min^{-1} until break (denoted with *X*). The inset shows the initial tensile behavior from 0 - 5% strain.

Interestingly, in our handling and testing of the polyanhydride networks, we observed that the materials gradually became brittle over the course of a week. In light of this observation, thermal and physical characterization of the networks, discussed above, were performed immediately following photopolymerization (i.e. the same day). We hypothesized that the gradual change in material properties was due to chemical aging, where residual radicals in the crosslinked materials continue to react after photopolymerization.[47-50] Previous reports have demonstrated changes in physical properties after thermal curing following photopolymerization as a result of increased

monomer consumption within the photocured materials.[47-50] Under this assumption, a sample of **3**-PETMP was photopolymerized in a quartz capillary tube and immediately subjected to electron paramagnetic resonance (EPR) spectroscopy. The acquired EPR spectrum (Figure 4.13) showed a signal that indicated the presence of radicals in the polymer matrix. It is uncertain at this time which radical species (e.g. thiyl radicals and/or carbon-based radicals) gave rise to the EPR signal. The sample was then thermally treated at 100 °C for 24 h to accelerate the consumption of the residual radicals, and then again subjected to EPR spectroscopy. The newly acquired EPR spectrum was observed to be silent (Figure 4.14), indicating that the radical species were quenched. In a parallel experiment, a photopolymerized sample was left to anneal at ambient temperature (22 °C) for three days and then also subjected to EPR spectroscopy. The acquired EPR spectrum was nearly silent.

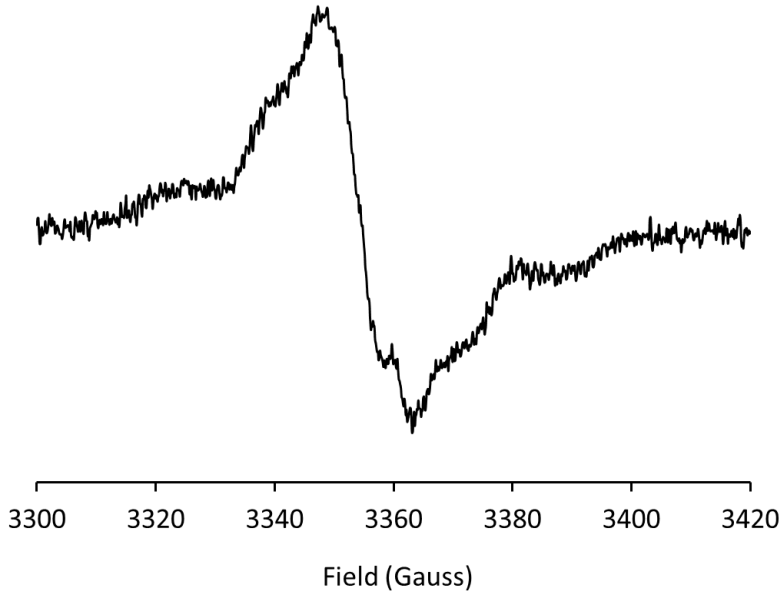

Figure 4. 13. EPR spectrum acquired immediately after the photopolymerization of 3-PETMP indicating the presence of "trapped" radicals in the polymer matrix**.** Operation conditions for the acquisition: microwave frequency, 9.40 GHz; modulation frequency, 100 kHz; modulation amplitude, 1.0 G.

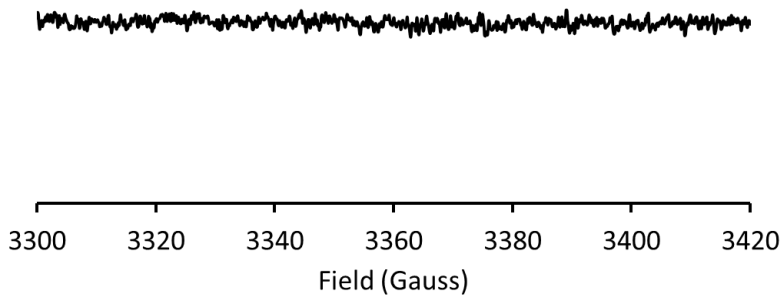

Figure 4. 14. EPR spectrum of 3-PETMP with post-curing thermal treatment at 100 °C for 24 hours. Operation conditions for the acquisition: microwave frequency, 9.40 GHz; modulation frequency, 100 kHz; modulation amplitude, 1.0 G.

In order to determine the ultimate thermal and viscoelastic properties, samples of the polyanhydride networks were thermally treated at 100 °C for 24 after photopolymerization and then analyzed via DSC (Figures 4.15 – 4.18) and DMA (Figures 4.19 – 4.22). The results, summarized in Table 4.2, showed an increase in T_g for **3**-PETMP, **3**-DPEHMP, **4**-PETMP, and **4**-DPEHMP to 34, 38, 24, and 29 °C, respectively. While DMA indicated an increase in the plateau moduli of the materials, the ultimate ν values for **3**-PETMP, **3**-DPEHMP, **4**-PETMP, and **4**-DPEHMP were calculated to be 1.9, 4.4, 2.1, and 6.4 x 10^{-4} mol cm^{-3}, which are on the same order of magnitude as the samples before thermal treatment. Reiterating that only a qualitative analysis can be made for highly crosslinked materials, the results indicate that the crosslink densities do not significantly increase as a result of chemical aging. Tensile analysis after the thermal treatment could not be performed due to the brittle nature of the materials.

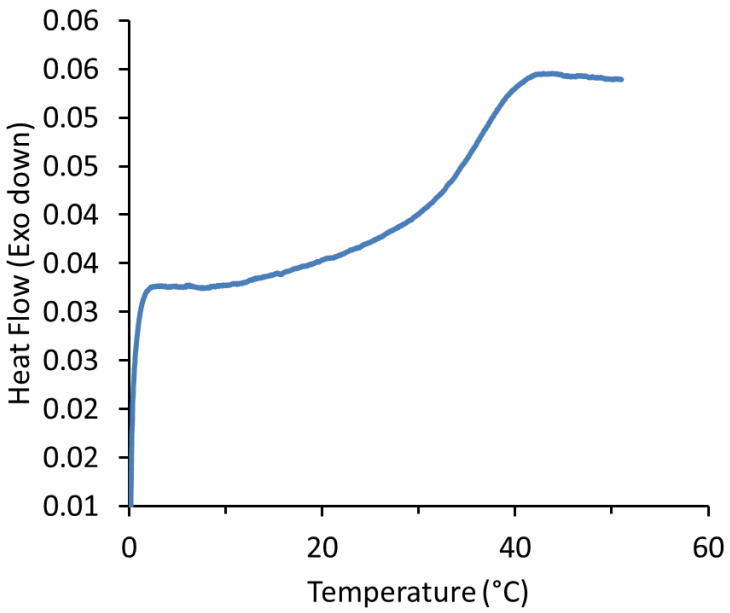

Figure 4. 15. DSC thermogram (heating rate of 10 °C·min-1) of 3-PETMP with post-curing thermal treatment at 100 °C for 24 h**.**

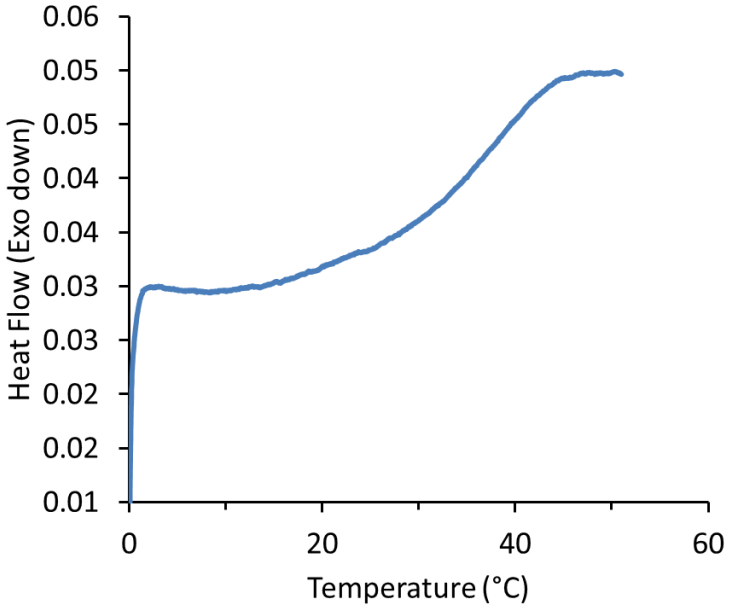

Figure 4. 16. DSC thermogram (heating rate of 10 °C·min-1) of 3-DPEHMP with post-curing thermal treatment at 100 °C for 24 h.

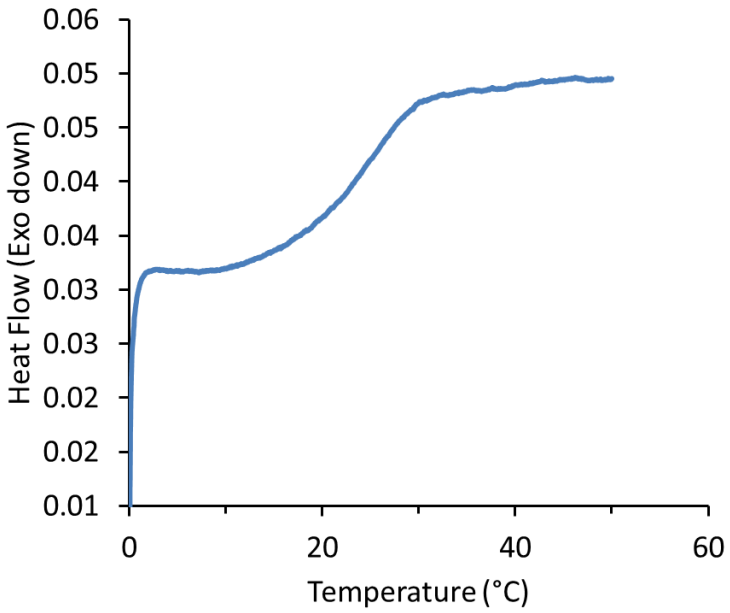

Figure 4. 17. DSC thermogram (heating rate of 10 °C·min-1) of 4-PETMP with post-curing thermal treatment at 100 °C for 24 h.

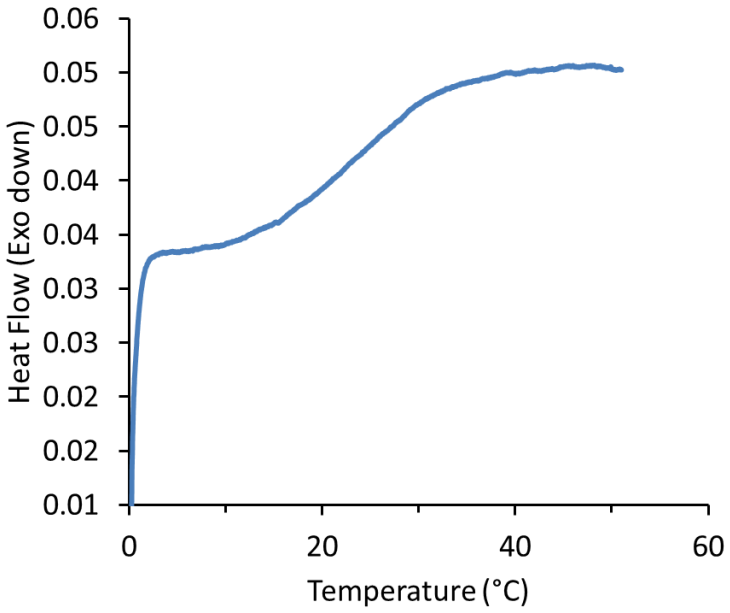

Figure 4. 18. DSC thermogram (heating rate of 10 °C·min-1) of 4-DPEHMP with post-curing thermal treatment at 100 °C for 24 h.

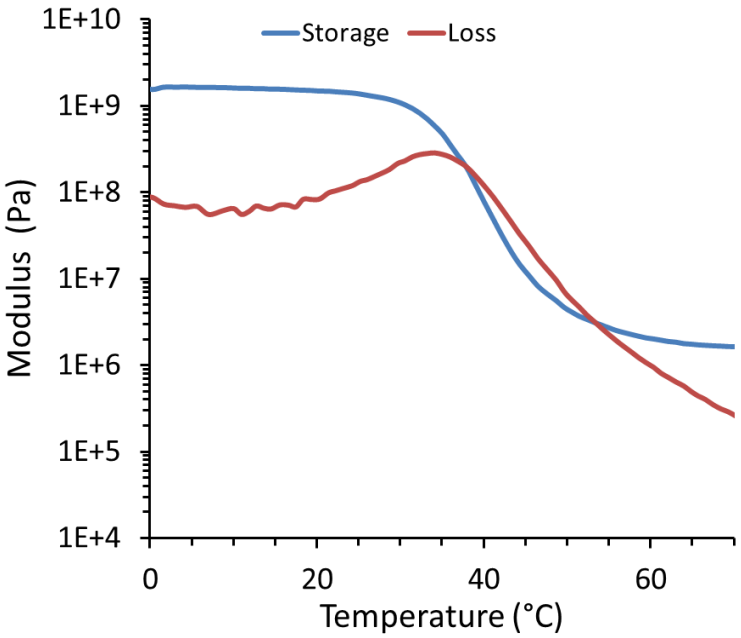

Figure 4. 19. Storage and loss moduli measured via DMA of 3-PETMP with post-curing thermal treatment at 100 °C for 24 h.

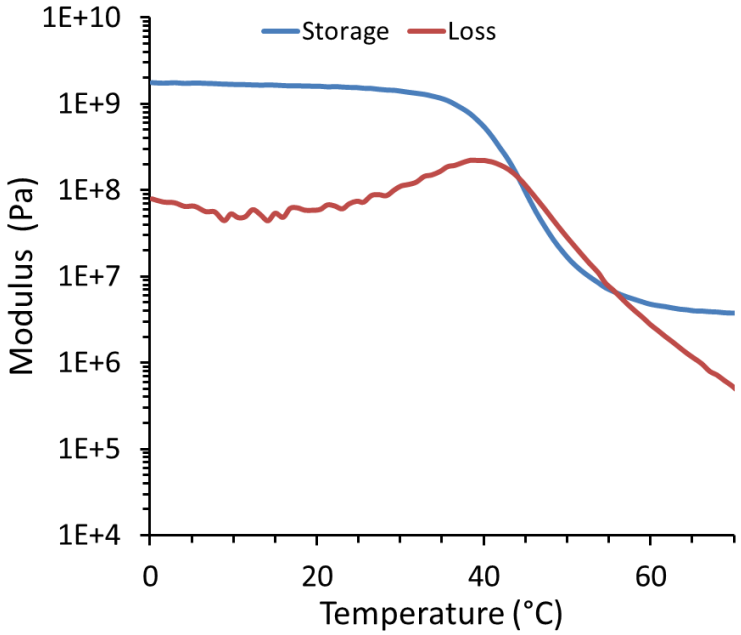

Figure 4. 20. Storage and loss moduli measured via DMA of 3-DPEHMP with post-curing thermal treatment at 100 °C for 24 h.

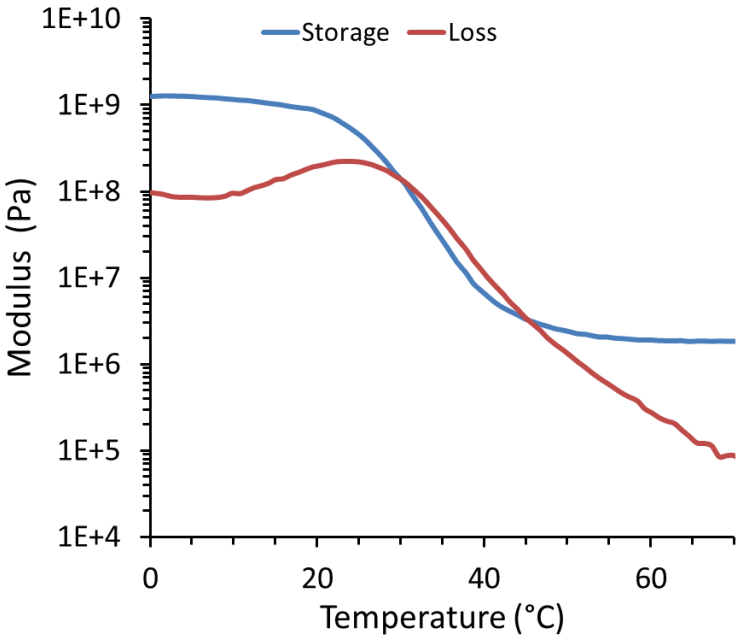

Figure 4. 21. Storage and loss moduli measured via DMA of 4-PETMP with post-curing thermal treatment at 100 °C for 24 h

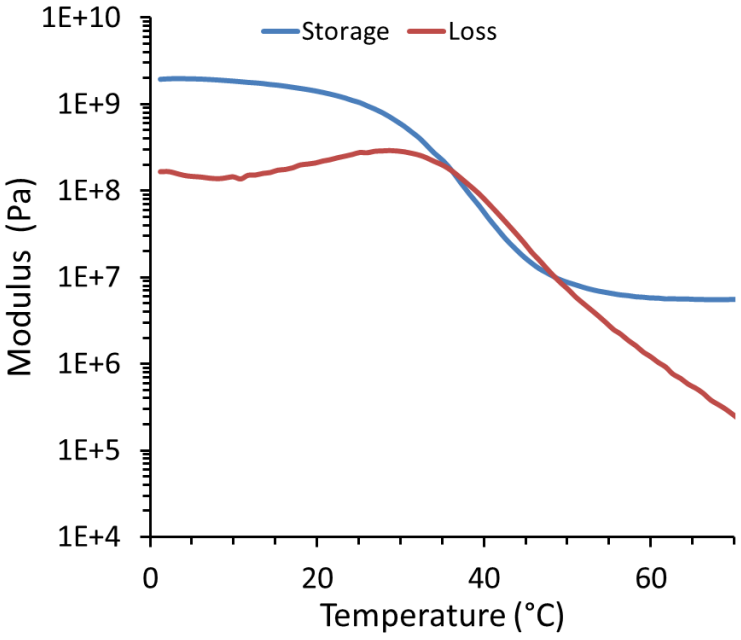

Figure 4. 22. Storage and loss moduli measured via DMA of 4-DPEHMP with post-curing thermal treatment at 100 °C for 24 h.

Table 4. 2. Summary of the characterization data for the polyanhydride networks after thermal treatment.

	3-PETMP[a]	**3**-DPEHMP[a]	**4**-PETMP[a]	**4**-DPEHMP[a]
$T_{g,DSC}$ (°C)[b]	34	37	23	27
$T_{g,DMA}$ (°C)[c]	34	38	24	29
E' (MPa)[d]	1.6	3.8	1.8	5.5
ρ (g cm^{-3})[e]	1.26	1.25	1.19	1.18
M_c (g mol^{-1})[f]	6700	2800	5600	1800
ν (mol cm^{-3})[g]	1.9 x 10^{-4}	4.4 x 10^{-4}	2.1 x 10^{-4}	6.4 x 10^{-4}

[a]Thermal data and viscoelastic properties measured after thermal treatment at 100 °C for 24 h. [b]Determined from the mid-point of the glass transition in DSC during the second heating ramp at 10 °C min^{-1}. [c]Recorded as the temperature at the peak of the loss modulus data. [d]Plateau modulus at taken at 70 °C. [e]Mass density of the thermoset materials. [f]Calculated from eq 4.3 with T = 343 K. [g]Calculated from eq 4.4.

Finally, the aqueous degradation profiles of the polyanhydride networks were assessed in deionized (DI) water (pH 7.0) as well as biologically-relevant (phosphate buffered salt (PBS) solution, pH 7.4) and environmentally-relevant (artificial sea water (SW), pH 7.8) conditions. Initial degradation studies conducted at room temperature revealed that the materials were stable in all tested aqueous environments, with less than 10% mass loss occurring after a month of testing (Figure 4.23). Similar polyanhydride networks, such as those made from 4-pentenoic anhydride and PETMP[24-28], have been reported to degrade in aqueous environments within 1 – 3 days under ambient or physiological conditions (≤ 37 °C, DI water or PBS solution). The more hydrophobic molecular structure of the itaconic acid-based anhydride monomers synthesized in this

work, containing dinorbornene units and alkyl ester substituents, is likely responsible for the comparatively prolonged stability to moisture and aqueous environments we have observed.

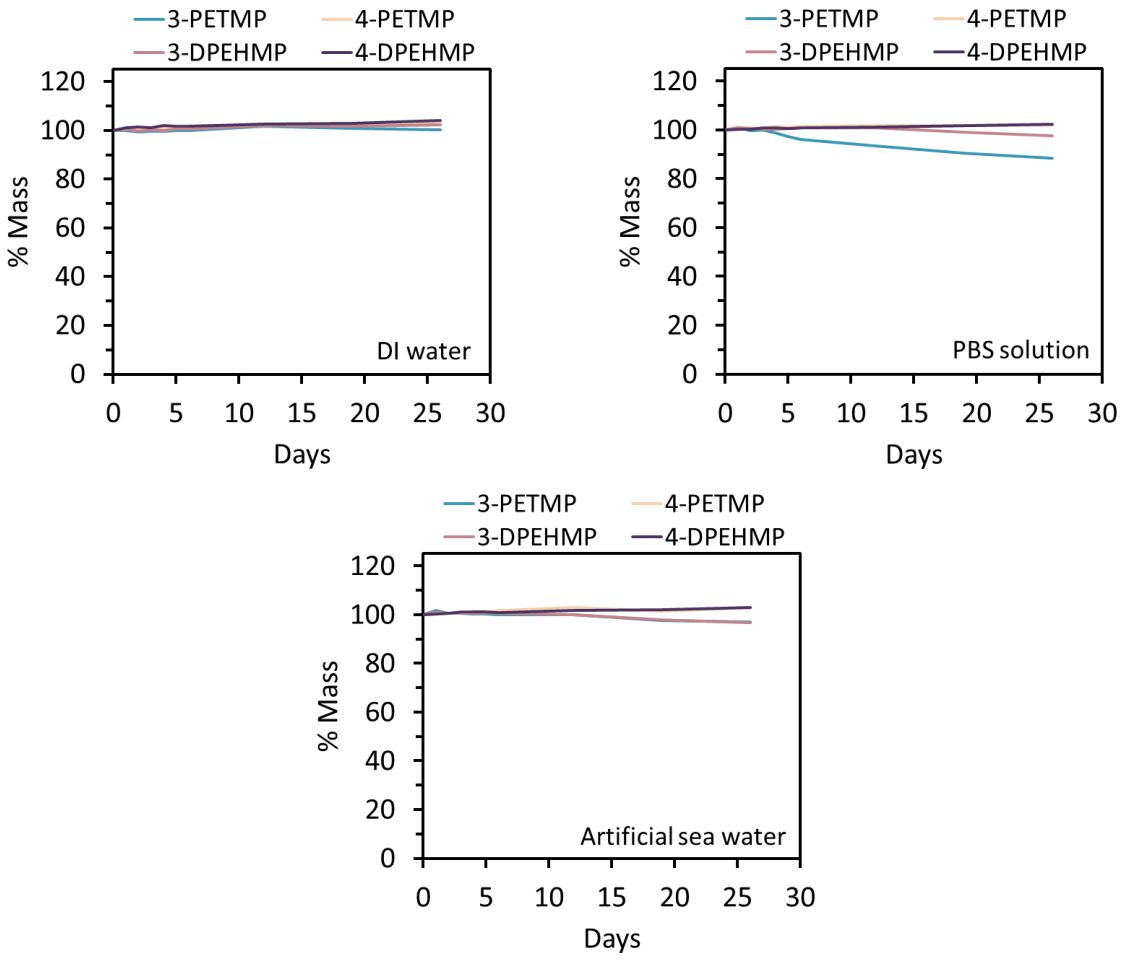

Figure 4. 23. Hydrolytic stability tests of the polyanhydride networks at 22 °C in DI water (pH 7.0), phosphate buffer saline (PBS) solution (pH 7.4), and artificial sea water (pH 7.8).

At elevated temperatures (e.g. 50 °C), however, the degradation processes was accelerated (Figure 4.24). The materials were found to slowly degrade in DI water at 50 °C, with approximately 20% mass loss for **4**-PETMP and **4**-DPEHMP and approximately 50% mass loss for **3**-PETMP and **4**-DPEHMP occurring after 51 days. Faster rates of degradation were observed in the buffered conditions of PBS solution and artificial SW at 50 °C. Complete degradation of the materials in PBS solution occurred within 24 – 37 days, and longer exposure times of 37 – 51 days were required to completely degrade the materials in artificial SW. We attribute the difference in rates of degradation between the PBS solution and artificial SW to the difference in buffering capacity of the aqueous media. While artificial SW had a higher initial pH than the PBS solution (7.8 vs 7.4), pH measurements of the solutions after complete degradation of the materials revealed that the PBS solutions maintained the highest pH (Table 4.3). The higher buffering capacity of the PBS solution can allow for better neutralization and solubilization of the network decomposition products while maintaining higher pH values, resulting in faster degradation rates. The prolonged stability of the anhydride networks under ambient conditions and aqueous environments is advantageous as it can allow for storage of these materials under ambient conditions without significant deterioration, and then can be degraded at elevated temperatures. Additionally, the materials were observed to degrade via a surface erosion mechanism, exhibiting a gradual loss in size during the course of the degradation experiments. It should be emphasized that while we focused on the ethyl and isoamyl variants of the anhydride monomers for this study, the ester functionality can be tuned with other substituents with varying degrees of hydrophobicity or hydrophilicity

with the potential to allow for control over the rate of degradation. Additionally, the effects of thiol and thio-ester degradation byproducts on the environment must be taken into consideration when designing degradable materials. While toxicological studies were outside the scope of the current work, future studies will assess the environmental impacts of such products.

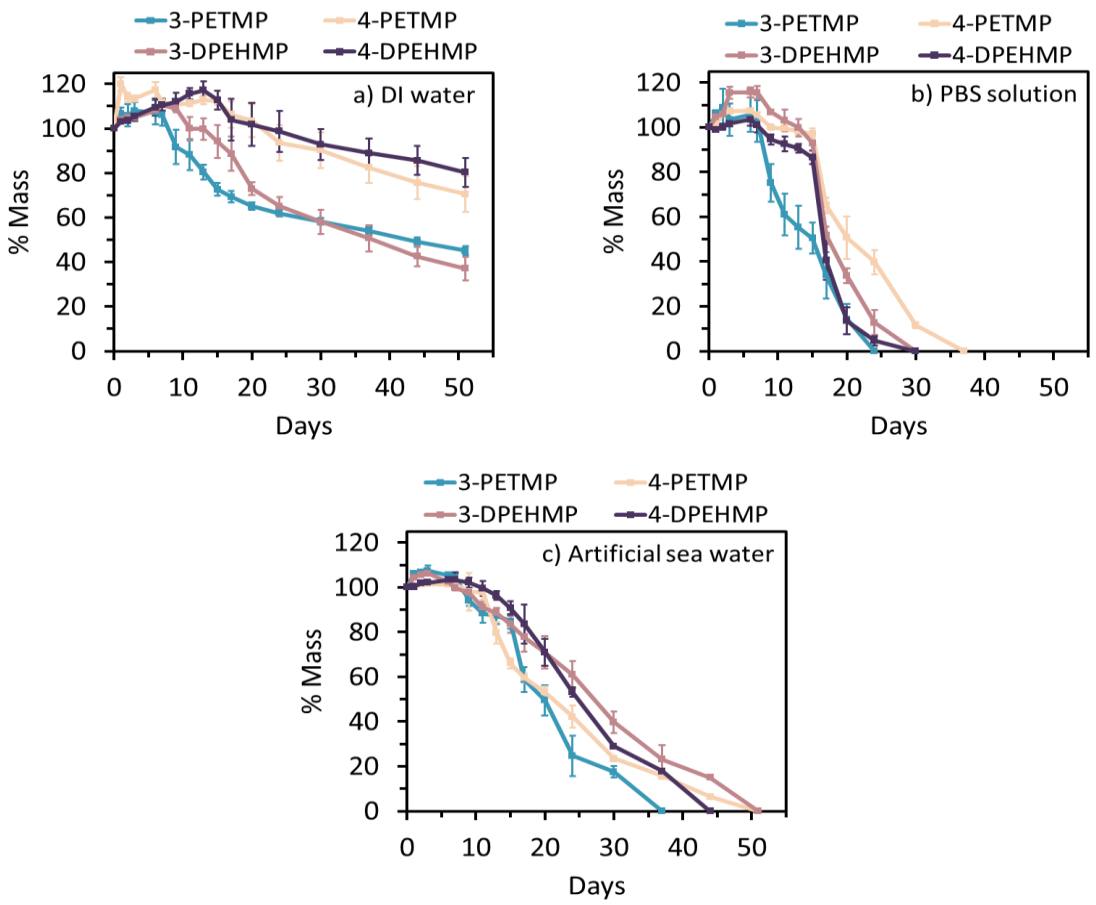

Figure 4. 24. Hydrolytic stability tests of the polyanhydride networks at 50 °C in a) DI water (pH 7.0), b) phosphate buffer saline (PBS) solution (pH 7.4), and c) artificial sea water (7.8). Each vertex in the degradation profiles represents the average mass of samples in triplicate.

Table 4. 3. pH values of the degradation solutions after completion of degradation studies at 50 °C.

	DI Water*	PBS solution	Artificial SW
3-PETMP	3.5	5.6	3.4
3-DPEHMP	3.1	5.0	3.4
4-PETMP	3.3	5.1	4.3
4-DPEHMP	3.2	5.6	3.7

4.4 Conclusions

In summary, we described the facile and scalable synthesis of novel linear anhydrides with tunable ester functionalities from itaconic acid. The photoinitiated thiol-ene polymerization of the anhydrides to form crosslinked polyanhydride networks was accomplished with commercially available tetrafunctional and hexafunctional thiols. The ester functionality of the anhydride monomers was found to have an influence on the degree of polymerization, with the bulkier isoamyl variant reaching higher conversions than the ethyl variant possibly as a consequence of greater free volume within the polymer matrix during polymerization. Use of the higher functionality hexathiol crosslinker DPEHMP yielded stiffer, higher T_g materials than those made with the tetrafunctional thiol PETMP. The polyanhydride networks were susceptible to degradation in aqueous environments, and the results indicated that buffered solutions that are able to maintain a more basic environment resulted in faster degradation rates. Future studies are aimed at investigating the effect of hydrophobic and hydrophilic ester substituents on the rates of degradation, as we postulate that degradation profiles of the networks can also be controlled by modulating the structure of the anhydride monomers. Findings from this work demonstrate a viable strategy to potentially address micro-plastics pollution through the development of renewable polyanhydride networks from itaconic acid that degrade in aqueous environments.

4.5 Experimental

Materials. Anhydrous ethanol was obtained from Pharmco-AAPER (Shelbyville, KY, USA). Acetic anhydride was obtained from Fisher Scientific (Hampton, NH, USA). OMNIRAD TPO-L was obtained from IGM Resins USA, Inc. (Charlotte, NC, USA). Itaconic acid and all other reagents were obtained from Sigma-Aldrich (St. Louis, MO, USA). Cyclopentadiene was obtained via "cracking" and fractional distillation of dicylopentadiene at 180 - 190 °C. Deuterated chloroform ($CDCl_3$) was obtained from Cambridge Isotope Laboratories (Tewksbury, MA, USA). Phosphate-buffered saline was prepared with a phosphate-buffered saline powder packet from Sigma-Aldrich (St. Louis, MO, USA), with pH of 7.4. Artificial seawater was prepared by combining 24.53 g NaCl, 5.20 g $MgCl_2$, 4.09 g Na_2SO_4, 1.16 g $CaCl_2$, 0.695 g KCl, 0.201 g $NaHCO_3$, and 0.101 g KBr in 1 L of DI water. All purchased compounds were used directly without further purification.

Characterization. Nuclear Magnetic Resonance (NMR) spectra were obtained on a Bruker Avance HD-500 in deuterated chloroform (CDCl3) using tetramethylsilane (TMS) as an internal reference. High-resolution mass spectrometry (HRMS) was performed on samples dissolved in methanol using a Bruker Bio-TOF II in positive mode with a PEG400 standard. Fourier-transform infrared (FT-IR) spectroscopy was performed on a Nicolet 6700 FT-IR spectrometer equipped with a KBr beam splitter, an MCT-A detector (Thermo Fisher Scientific, Waltham, MA), and a horizontal transmission accessory (Harrick Scientific Products, Inc., Pleasantville, NY) was used for studying the

reaction conversion of the monomer mixtures. The spectrometer and horizontal transmission accessory were continuously purged with dry, CO_2-free air. The monomer mixtures were irradiated using a UV light source (OmniCure S1500 Spot UV Light Curing System, Excelitas Technologies) with an intensity of 50 mW/cm^2. The spectra were recorded with an average of 1 scan every 20 ms and a resolution of 32 cm-1 for a total of 100 s. The samples were placed between two polished NaCl plates (diameter: 25 mm; thickness: 4 mm). The reaction was monitored based on the C=C acrylate peak of iAIAH and EtIAH at 1636 cm−1, the C=C norbornene peak of NBiAIAH and NBEtIAH at 713 cm-1, and the S-H peak of PETMP and DPEHMP at 2572 cm−1. The peak heights were normalized in reference to the C=O stretch. The reaction conversion was calculated based on the initial peak intensity, I0, and the peak intensity at time t, It, (i.e. Conversion = $(I0 - It)/I0$ *100%). Thermogravimetric analysis (TGA) was performed on a TA Instruments Q500. TGA analyses were performed on 4-10 mg of sample under a nitrogen atmosphere with a heating rate of 10 °C/min from room temperature to 550 °C. Differential Scanning Calorimetry (DSC) was performed on a TA Instruments Q-1000 on samples in hermetically sealed aluminum pans. The samples were heated and cooled at 2 °C/min and the reported spectra are from the second heating ramp. Dynamic mechanical analysis (DMA) was performed with an RSA-G2 solid analyzer (RAS-G2, TA Instruments, USA) equipped with a film tension clamp. The temperature was controlled by a force convection oven attached with a liquid N2 cooling device, and the measurement was conducted by applying a frequency of 1 Hz and a strain of 0.05%. The specimen was cooled down to 0 °C by liquid N2 prior to the acquisition of data, and the

temperature was ramped to 70 °C at 5 °C min-1. Electron paramagnetic resonance (EPR) spectroscopy was performed on a Bruker EleXsys E500 X-band spectrometer. Spectra of 1-PETMP were acquired in the R4122 SHQ spherical resonator at 22 °C. Sweep width was 120 G with 1,024 points per spectrum, microwave frequency of 9.40 GHz; modulation frequency of 100 kHz, and modulation amplitude of 1.0 G. Tensile testing was performed on a Shimadzu AFS-X at room temperature on dogbone shaped samples with the approximate gauge dimensions, 2.7 mm x 13.5 mm x 0.7 mm (W x L x T). Polyanhydride samples were extended at 5 mm/min and 5 replicate runs were averaged for analysis. pH measurements were conducted using a Accumet Basic AB15 pH meter.

Syntheses of Ethyl Itaconic Acid (1'), Isoamyl Itaconic Acid (2'), Ethyl Itaconic Anhydride (1), and Isoamyl Itaconic Anhydride (2). Synthetic procedures and characterization methods (1H NMR, 13C NMR, and high resolution mass spectrometry) of compounds 1', 2', 1, and 2 are reported in the Ph.D. dissertation of Leon M. Lillie.

Synthesis of Norbornene-Ethyl Itaconic Anhydride (3). Ethyl Itaconic Anhydride (10 g, 33.5 mmol) and freshly distilled cyclopentadiene (5.54 g, 83.8 mmol) were added to a 25 mL round bottom flask. The flask was sealed with a glass stopcock and the reagents were stirred at 50 °C for 16 h. The flask was then connected to a Schlenk line and the excess cyclopentadiene and dicylopentadiene byproduct were removed under reduced pressure at 50 °C (monitored via ^{1}H NMR spectroscopy). The resultant yellow viscous

liquid was used without further purification (14.3 g quantitative yield). HRMS (ESI-TOF, *m/z*) calculated for $C_{24}H_{30}O_7Na^+$: 453.1883; Observed: 453.1902.

Synthesis of Norbornene-Isoamyl Itaconic Anhydride (4). Isoamyl Itaconic Anhydride (10 g, 26.1 mmol) and freshly distilled cyclopentadiene (4.32 g, 65.4 mmol) were added to a 25 mL round bottom flask. The flask was sealed with a glass stopcock and the reagents were stirred at 50 °C for 16 h. The flask was then connected to a Schlenk line and the excess cyclopentadiene and dicylopentadiene byproduct were removed under reduced pressure at 50 °C (monitored via ^{1}H NMR spectroscopy). The resultant yellow viscous liquid was used without further purification (13.3 g quantitative yield). HRMS (ESI-TOF, *m/z*) calculated for $C_{30}H_{42}O_7Na^+$: 537.2823; Observed: 537.2847.

Representative Thiol-ene Polymerization of Itaconic Anhydrides. Itaconic acid anhydride and thiol monomers were mixed such that the ratio of the [ene]:[thiol] end groups was kept at 1:1. **3** (0.50 g, 1.16 mmol), PETMP (0.28 g, 0.58 mmol.), and TPO-L (39 mg, 5 wt%) were added to a 5 mL glass scintillation vial and shaken using a vortex device for 5 -10 minutes to ensure solution homogeneity. This mixture was then pipetted into silicon dog-bone molds (2.7 mm x 13.5 mm x 0.7 mm (W x L x T))) for curing with a 36 W MelodySusie® UV Nail Dryer. Samples were exposed to UV light for 2 minutes, flipped over, and exposed for an additional 2 minutes and then stored in a desiccator until use.

Hydrolytic Stability Testing. Samples of the anhydride networks (~30 mg) were added to 5 mL scintillation vials and used for hydrolytic stability testing in triplicate in DI water

(pH ~7), phosphate-buffered saline (PBS) solution (pH 7.4), and artificial seawater (pH 7.8). The vials were placed in a dish filled with aluminum beads heated to 50 °C. Mass measurements were performed by removing the submerged sample from the vials, blotting them dry with a KimWipe, and recording the mass using a balance. The solutions were changed every two weeks.

Chapter 5.

Summary

Dissertation Summary

In summary, this thesis detailed work focused on the utilization of emerging renewable feedstocks as alternatives to petroleum-derived compounds for the synthesis of novel polymeric materials.

Chapter 2 employed lauryl acrylate, readily available from vegetable oil derivatives, as the rubbery midblock in triblock copolymers for pressure-sensitive adhesive applications. Triacetic acid lactone (TAL) was found to be a suitable candidate to serve as the glassy endblocks in the acrylate-based system. The resultant triblock copolymers were of high molecular weights and narrow dispersities, specific component ratios were targeted, and the adhesives demonstrated comparable performance to commercial products.

Chapter 3 investigated the ring opening polymerization of a disubstituted δ-valerolactone, β-acetoxy-δ-methylvalerolactone, derived from TAL. Using DPP as the organocatalyst the polymerization of the disubstituted lactone was observed to reach an equilibrium monomer conversion of 45% under ambient conditions. We established the kinetic and thermodynamic parameters for the ring opening polymerization, and the results suggested that the polymerization of δ-valerolactones becomes increasingly exothermic and entropically disfavored with an increasing degree of substitution. This report is the first to demonstrate successful ROP of a derivative of TAL and provides valuable insight towards the thermodynamics of ROP of substituted valerolactones.

Chapter 4 detailed the synthesis of novel polyanhydride networks derived from itaconic acid. Itaconic acid was modified into anhydride monomers and polymerized with

commercially available thiols via photo-initiated thiol-ene chemistry. The resultant polyanhydride networks were found to be bench-stable, rigid materials which degraded relatively slowly in aqueous environments due to their hydrophobic nature. Such materials could find potential use as implants for the controlled release of pharmaceutical compounds and other therapeutics.

The demand and utility for plastics is ever-increasing in our society. If we wish to continue using plastics to improve our daily lives and the lives of future generations, we must establish alternative, sustainable ways to produce them before the finite supplies of fossil fuels are inevitably exhausted. The work described in this thesis represents an important step forward in realizing a sustainable model for the synthesis and use of polymeric materials, and by extension, will aid in the preservation of our planet.

References

(1) Harmand, S.; Lewis, J. E.; Feibel, C. S.; Lepre, C. J.; Prat, S.; Lenoble, A.; Boës, X.; Quinn, R. L.; Brenet, M.; Arroyo, A.; Taylor, N.; Clement, S.; Daver, G.; Brugal, J-P.; Leakey, L.; Mortlock, R. A.; Wright, J. D.; Lokorodi, S.; Kirwa, C.; Kent, D. V.; Roche, H. 3.3-Million-Year-Old Stone Tools from Lomekwi 3, West Turkana, Kenya. *Nature* **2015**, *521*, 310 – 315.

(2) Kipfer, B. A. *Encyclopedic Dictionary of Archaeology*, Second Edition, Springer International Publishing, 2021.

(3) Andrady, A. L.; Neal, M. A. Applications and Societal Benefits of Plastics. *Philos. Trans. R. Soc. B Biol. Sci.* **2009**, *364*, 1977 – 1984.

(4) Geyer, R.; Jambeck, J. R.; Law, K. L. Production, Use, and Fate of All Plastics Ever Made. *Sci. Adv.* **2017,** *3*, 1 – 5.

(5) Zalasiewicz, J.; Waters, C. N.; Ivar do Sul, J. A.; Corcoran, P. L.; Barnosky, A. D.; Cearreta, A.; Edgeworth, M.; Gałuszka, A.; Jeandel, C.; Leinfelder, R.; McNeill, J. R.; Steffen, W.; Summerhayes, C.; Wagreich, M.; Williams, M.; Wolfe, A. P.; Yonan, Y. The Geological Cycle of Plastics and Their Use as a Stratigraphic Indicator of the Anthropocene. *Anthropocene*, **2016**, *13*, 4 – 17.

(6) Hopewell, J.; Dvorak, R.; Kosior, E. Plastics Recycling: Challenges and Opportunities. *Philosophical Transactions of the Royal Society B: Biological Sciences*. **2009**, *364*, 2115 – 2126.

(7) Mann, P.; Gahagan, L.; Gordon, M. B. Tectonic Setting of the World's Giant Oil and Gas Fields, In *AAPG Memoir*, 2003, American Association of Petroleum Geologists.

(8) British Petroleum (BP), *Statistical Review of World Energy*, 2020, 69th edition.

(9) Environmental Protection Agency, *Inventory of U.S. Greenhouse Gas Emissions and Sinks 1990-2018*, 2020.

(10) Pecl, G. T.; Araújo, M. B.; Bell, J. D.; Blanchard, J.; Bonebrake, T. C.; Chen, I. C.; Clark, T. D.; Colwell, R. K.; Danielsen, F.; Evengård, B.; Falconi, L.; Ferrier, S.; Frusher, Sw.; Garcia, R. A.; Griffis, R. B.; Hobday, A. J.; Janion-Scheepers, C.; Jarzyna, M. A.; Jennings, S.; Lenoir, J.; Linnetved, H I.; Martin, V. Y.; McCormack, P. C.; McDonald, J.; Mitchell, N. J.; Mustonen, T.; Pandolfi, J. M.; Pettorelli, N.; Popova, E.; Robinson, S. A.; Scheffers, B. R.; Shaw, J. D.; Sorte, C. J. B.; Strugnell, J. M.; Sunday, J. M.; Tuanm, M.; Verges, A.; Villaneuva, C.; Wernberg, T.; Wapstra, E.; Williams. S. E. Biodiversity Redistribution under Climate Change: Impacts on Ecosystems and Human Well-Being. *Science*. **2017**, *355*, 1 -11.

(11) Zhao, C.; Liu, B.; Piao, S.; Wang, X.; Lobell, D. B.; Huang, Y.; Huang, M.; Yao, Y.; Bassu, S.; Ciais, P.; Durand, J.; Elliot, J.; Ewert, F.; Janssens, I. A.; Li, T.; Lin, E.; Liu, Q.; Martre, P.; Muller, C.; Peng, S.; Penuelas, J.; Ruane, A. C.; Wallach, D.; Wang, T.; Wu, D.; Liu, Z.; Zhu, Y.; Zhu, Z.; Asseng, S. Temperature Increase Reduces Global Yields of Major Crops in Four Independent Estimates. *Proc. Natl.*

Acad. Sci. U. S. A. **2017**, *114*, 9326 – 9331.

(12) IPCC. *Global Warming of 1.5°C*, 2018.

(13) Zhu, Y.; Romain, C.; Williams, C. K. Sustainable Polymers from Renewable Resources. *Nature* **2016**, *540*, 354–362.

(14) Schneiderman, D. K.; Hillmyer, M. A. 50th Anniversary Perspective: There Is a Great Future in Sustainable Polymers. *Macromolecules* **2017**, *50*, 3733 – 3749.

(15) Garlotta, D. A Literature Review of Poly(Lactic Acid). *J. Polym. Environ.* **2001**, *9*, 63 – 84.

(16) Miller, S. A. Sustainable Polymers: Replacing Polymers Derived from Fossil Fuels. *Polym. Chem.*, **2014**, *5*, 3117 – 3118.

(17) Nagarajan, V.; Mohanty, A. K.; Misra, M. Perspective on Polylactic Acid (PLA) Based Sustainable Materials for Durable Applications: Focus on Toughness and Heat Resistance. *ACS Sustainable Chem. Eng*., **2016**, *4*, 2899 – 2916.

(18) Miller, S. A. Sustainable Polymers: Opportunities for the next Decade. *ACS Macro Lett.* **2013**, *2*, 550 – 554.

(19) Collie, J. N. The Lactone of Triacetic Acid. *J. Chem. Soc. Trans.* **1891**, *59*, 607–617.

(20) Obydennov, D. L.; El-Tantawy, A. I.; Sosnovskikh, V. Y. Triacetic Acid Lactone as a Bioprivileged Molecule in Organic Synthesis. *Mendeleev Communications*

2019, *29*, 1-10.

(21) Shanks, B. H.; Keeling, P. L. Bioprivileged Molecules: Creating Value from Biomass. *Green Chem.* **2017**, *19*, 3177–3185.

(22) Xie, D.; Shao, Z.; Achkar, J.; Zha, W.; Frost, J. W.; Zhao, H. Microbial Synthesis of Triacetic Acid Lactone. *Biotechnol. Bioeng.* **2006**, *94*, 727–736.

(23) Goel, A.; Ram, V. J. Natural and Synthetic 2H-Pyran-2-Ones and Their Versatility in Organic Synthesis. *Tetrahedron* **2009**, *65*, 7865–7913.

(24) Eckermann, S.; Schröder, G.; Schmidt, J.; Strack, D.; Edrada, R. A.; Helariutta, Y.; Elomaa, P.; Kotilainen, M.; Kilpeläinen, I.; Proksch, P.; Teeri, T. H.; Schröder, J. New Pathway to Polyketides in Plants. *Nature* **1998**, *396*, 387–390

(25) Tang, S. Y.; Qian, S.; Akinterinwa, O.; Frei, C. S.; Gredell, J. A.; Cirino, P. C. Screening for Enhanced Triacetic Acid Lactone Production by Recombinant Escherichia Coli Expressing a Designed Triacetic Acid Lactone Reporter. *J. Am. Chem. Soc.* **2013**, *153*, 10099–10103.

(26) Cardenas, J.; Da Silva, N. A. Metabolic Engineering of Saccharomyces Cerevisiae for the Production of Triacetic Acid Lactone. *Metab. Eng.* **2014**, *25*, 194–203.

(27) Saunders, L. P.; Bowman, M. J.; Mertens, J. A.; Da Silva, N. A.; Hector, R. E. Triacetic Acid Lactone Production in Industrial Saccharomyces Yeast Strains. *J. Ind. Microbiol. Biotechnol.* **2015**, *42*, 711–721.

(28) Yu, J.; Landberg, J.; Shavarebi, F.; Bilanchone, V.; Okerlund, A.; Wanninayake, U.; Zhao, L.; Kraus, G.; Sandmeyer, S. Bioengineering Triacetic Acid Lactone Production in Yarrowia Lipolytica for Pogostone Synthesis. *Biotechnol. Bioeng.* **2018**, *115*, 2383–2388.

(29) Markham, K. A.; Palmer, C. M.; Chwatko, M.; Wagner, J. M.; Murray, C.; Vazquez, S.; Swaminathan, A.; Chakravarty, I.; Lynd, N. A.; Alper, H. S. Rewiring Yarrowia Lipolytica toward Triacetic Acid Lactone for Materials Generation. *Proc. Natl. Acad. Sci.* **2018**, *115*, 2096–2101.

(30) Chia, M.; Schwartz, T. J.; Shanks, B. H.; Dumesic, J. A. Triacetic Acid Lactone as a Potential Biorenewable Platform Chemical. *Green Chem.* **2012**, *14*, 1850–1853.

(31) Kraus, G. A.; Basemann, K.; Guney, T. Selective Pyrone Functionalization: Reductive Alkylation of Triacetic Acid Lactone. *Tetrahedron Lett.* **2015**, *56*, 3494 – 3496.

(32) Kraus, G. A.; Wanninayake, U. K. An Improved Aldol Protocol for the Preparation of 6-Styrenylpyrones. *Tetrahedron Lett.* **2015**, *56*, 7112 – 7114.

(33) Kraus, G. A.; Wanninayake, U. K.; Bottoms, J. Triacetic Acid Lactone as a Common Intermediate for the Synthesis of 4-Hydroxy-2-Pyridones and 4-Amino-2-Pyrones. *Tetrahedron Lett.* **2016**, *57*, 1293 – 1295.

(34) Schwartz, T. J.; O'Neill, B. J.; Shanks, B. H.; Dumesic, J. A. Bridging the Chemical and Biological Catalysis Gap: Challenges and Outlooks for Producing

Sustainable Chemicals. *ACS Catal*. **2014**, *4*, 2060 – 2069.

(35) Williams, C. K.; Hillmyer, M. A. Polymers from Renewable Resources: A Perspective for a Special Issue of Polymer Reviews. *Polym. Rev.* **2008**, *48*, 1 – 11.

(36) Liu, H.; Cheng, T.; Xian, M.; Cao, Y.; Fang, F.; Zou, H. Fatty Acid from the Renewable Sources: A Promising Feedstock for the Production of Biofuels and Biobased Chemicals. *Biotechnology Advances* **2014**, *32*, 382 – 389.

(37) Ford, S. G.; Marvel, C. S. Lauryl Alcohol. In *Organic Syntheses*; 2003.

(38) Klaus, N.; Grafahend, W. Fatty Alcohols. *Ullman's Encyclopedia of Industrial Chemistry*; 2006, 114–141.

(39) Yee, G. M.; Hillmyer, M. A.; Tonks, I. A. Bioderived Acrylates from Alkyl Lactates via Pd-Catalyzed Hydroesterification. *ACS Sustain. Chem. Eng.* **2018**, *6*, 9579 – 9584.

(40) Beers, K. L.; Matyjaszewski, K. The Atom Transfer Radical Polymerization of Lauryl Acrylate. *J. Macromol. Sci. - Pure Appl. Chem.* **2001**, 731 – 739.

(41) Coelho, J. F. J.; Carvalho, E. Y.; Marques, D. S.; Popov, A. V.; Goncalves, P. M.; Gil, M. H. Synthesis of Poly(Lauryl Acrylate) by Single-Electron Transfer/Degenerative Chain Transfer Living Radical Polymerization Catalyzed by $Na_2S_2O_4$ in Water. *Macromol. Chem. Phys.* **2007**, *208*, 1218 – 1227.

(42) Konaganti, V. K.; Madras, G. Photocatalytic and Thermal Degradation of

Poly(Methyl Methacrylate), Poly(Butyl Acrylate), and Their Copolymers. *Ind. Eng. Chem. Res.* **2009**.

(43) Mahalik, J. P.; Madras, G. Effect of Alkyl Group Substituants, Temperature, and Solvents on the Ultrasonic Degradation of Poly(n-Alkyl Acrylates). *Ind. Eng. Chem. Res.* **2005**, *48*, 1712 – 1718.

(44) Gupta, J.; Keddie, D. J.; Wan, C.; Haddleton, D. M.; McNally, T. Functionalisation of MWCNTs with Poly(Lauryl Acrylate) Polymerised by Cu(0)-Mediated and RAFT Methods. *Polym. Chem.* **2016**, *7*, 3884 – 3896.

(45) Wang, S.; Vajjala Kesava, S.; Gomez, E. D.; Robertson, M. L. Sustainable Thermoplastic Elastomers Derived from Fatty Acids. *Macromolecules* **2013**, *46*, 7202–7212.

(46) Baup, S. Ueber eine neue Pyrogen-Citronensäure, und über Benennung der Pyrogen-Säuren überhaupt. *Annalen der Pharmacie* **1836,** *19*, 29.

(47) Steiger, M. G.; Blumhoff, M. L.; Mattanovich, D.; Sauer, M. Biochemistry of microbial itaconic acid production. *Front Microbiol.* **2013,** *4*, 23.

(48) Robert, T.; Friebel, S. Itaconic Acid-a Versatile Building Block for Renewable Polyesters with Enhanced Functionality. *Green Chem.* **2016**, *18*, 2922 – 2934.

(49) Kumar, S.; Krishnan, S.; Samal, S. K.; Mohanty, S.; Nayak, S. K. Itaconic Acid Used as a Versatile Building Block for the Synthesis of Renewable Resource-Based Resins and Polyesters for Future Prospective: A Review. *Polymer*

International **2017**, *66*, 1349 – 1363.

(50) Durant, Y. G. Development of Integrated Production of Polyitaconic Acid from Northeast Hardwood Biomass. 2009.

(51) Ma, S.; Liu, X.; Jiang, Y.; Fan, L.; Feng, J.; Zhu, J. Synthesis and Properties of Phosphorus-Containing Bio-Based Epoxy Resin from Itaconic Acid. *Sci. China Chem.* **2014**, *57*, 379 – 388.

(52) Ma, S.; Liu, X.; Jiang, Y.; Tang, Z.; Zhang, C.; Zhu, J. Bio-Based Epoxy Resin from Itaconic Acid and Its Thermosets Cured with Anhydride and Comonomers. *Green Chem.* **2013**, *15*, 245 – 254.

(53) Ali, M. A.; Kaneko, T. Microbe-Derived Itaconic Acid: Novel Route to Biopolyamides. In *Microbial Applications*, Vol. 2., 2017.

(54) Wang, Z.; Wei, T.; Xue, X.; He, M. M.; Xue, J. J.; Song, M.; Wu, S. Z.; Kang, H. L.; Zhang, L. Q.; Jia, Q. X. Synthesis of fully bio-based polyamides with tunable properties by employing itaconic acid. *Polymer* **2014,** *55*, 4846.

(55) Wang, R.; Ma, J.; Zhou, X.; Wang, Z.; Kang, H.; Zhang, L.; Hua, K. C.; Kulig, J. Design and Preparation of a Novel Cross-Linkable, High Molecular Weight, and Bio-Based Elastomer by Emulsion Polymerization. *Macromolecules* **2012**, *45*, 6830 – 6839.

(56) Barrett, D. G.; Merkel, T. J.; Luft, J. C.; Yousaf, M. N. One-Step Syntheses of Photocurable Polyesters Based on a Renewable Resource. *Macromolecules* **2010**, *43*, 9660 – 9667.

(57) Goerz, O.; Ritter, H. Polymers with Shape Memory Effect from Renewable Resources: Crosslinking of Polyesters Based on Isosorbide, Itaconic Acid and Succinic Acid. *Polym. Int.* **2013**, *62*, 709 – 712.

(58) Winkler, M.; Lacerda, T. M.; Mack, F.; Meier, M. A. R. Renewable Polymers from Itaconic Acid by Polycondensation and Ring-Opening-Metathesis Polymerization. *Macromolecules* **2015**, *48*, 1398 - 1403.

(59) Legge, N. R.; Holden, G.; Schroeder, H. E. *Thermoplastic Elastomers: A Comprehensive Review*; Hanser Publishers: Munich, 1987.

(60) Holden, G. Thermoplastic Elastomers and Their Applications. In *Applied Polymer Science: 21st Century*; Craver, C. D.; Carraher, C. E. Jr. Eds.; Elsevier: Oxford, 2007; 231-256.

(61) Bates, F. S.; Fredrickson, G. H. Block Copolymers-Designer Soft Materials. *Phys. Today* **1999**, *2*, 32-38.

(62) Nagpal, U.; Detcheverry, F. A.; Nealey, P. F.; De Pablo, J. J. Morphologies of Linear Triblock Copolymers from Monte Carlo Simulations. *Macromolecules* **2011**, *44*, 5490–5497.

(63) Weisz, P. B. Basic Choices and Constraints on Long-Term Energy Supplies. *Phys.*

Today **2004**, *47*, 47–52.

(64) Wang, Z.; Yuan, L.; Tang, C. Sustainable Elastomers from Renewable Biomass. *Acc. Chem. Res.* **2017**, *50*, 1762–1773.

(65) Watts, A.; Kurokawa, N.; Hillmyer, M. A. Strong, Resilient, and Sustainable Aliphatic Polyester Thermoplastic Elastomers. *Biomacromolecules* **2017**, *18*, 1845-1854.

(66) Qian, H.; Bei, J.; Wang, S. Synthesis, Characterization and Degradation of ABA Block Copolymer of L-Lactide and ε-Caprolactone. *Polym. Degrad. Stab.* **2000**, *68*, 423-429.

(67) Lee, S.; Lee, K.; Jang, J.; Choung, J. S.; Choi, W. J.; Kim, G. J.; Kim, Y. W.; Shin, J. Sustainable poly(ε-Decalactone)−poly(L-Lactide) Multiarm Star Copolymer Architectures for Thermoplastic Elastomers with Fixed Molar Mass and Block Ratio. *Polymer* **2017**, *112*, 306-317.

(68) Lee, S.; Lee, K.; Kim, Y. W.; Shin, J. Preparation and Characterization of a Renewable Pressure-Sensitive Adhesive System Derived from ε-Decalactone, L -Lactide, Epoxidized Soybean Oil, and Rosin Ester. *ACS Sustain. Chem. Eng.* **2015**, *3*, 2309-2320..

(69) Schneiderman, D. K.; Hill, E. M.; Martello, M. T.; Hillmyer, M. A. Poly(Lactide)-Block-Poly(ε-Caprolactone-Co-ε-Decalactone)-Block-Poly(Lactide) Copolymer Elastomers. *Polym. Chem.* **2015**, *6*, 3641-3651.

(70) Schneiderman, D. K.; Hillmyer, M. A. Aliphatic Polyester Block Polymer Design. *Macromolecules* **2016**, *49*, 2419-2428.

(71) Schneiderman, D. K.; Gilmer, C.; Wentzel, M. T.; Martello, M. T.; Kubo, T.; Wissinger, J. E. Sustainable Polymers in the Organic Chemistry Laboratory: Synthesis and Characterization of a Renewable Polymer from δ-Decalactone and l-Lactide. *J. Chem. Educ.* **2014**, *91*, 131-135.

(72) Arrington, K. J.; Waugh, J. B.; Radzinski, S. C.; Matson, J. B. Photo- and Biodegradable Thermoplastic Elastomers: Combining Ketone-Containing Polybutadiene with Polylactide Using Ring-Opening Polymerization and Ring-Opening Metathesis Polymerization. *Macromolecules* **2017**, *50*, 4180-4187.

(73) Wanamaker, C. L.; O'Leary, L. E.; Lynd, N. A.; Hillmeyer, M. A.; Tolman, W. B. Renewable-Resource Thermoplastic Elastomers Based on Polylactide and Polymenthide. *Biomacromolecules* **2007**, *8*, 3634-3640.

(74) Shin, J.; Martello, M. T.; Shrestha, M.; Wissinger, J. E.; Tolman, W. B.; Hillmyer, M. A. Pressure-Sensitive Adhesives from Renewable Triblock Copolymers. *Macromolecules* **2011**, *44*, 87–94.

(75) Cohn, D.; Hotovely-Salomon, A. Biodegradable Multiblock PEO/PLA Thermoplastic Elastomers: Molecular Design and Properties. *Polymer* **2005**, *46*, 2068-207.

(76) Hillmyer, M. A.; Tolman, W. B. Aliphatic Polyester Block Polymers: Renewable, Degradable, and Sustainable. *Acc. Chem. Res.* **2014**, *47*, 2390-2396..

(77) Lee, S.; Yuk, J. S.; Park, H.; Kim, Y. W.; Shin, J. Multiblock Thermoplastic Elastomers Derived from Biodiesel, Poly(Propylene Glycol), and L-Lactide. *ACS Sustain. Chem. Eng.* **2017**, *5*, 8148-8160

(78) Frick, E. M.; Zalusky, A. S.; Hillmyer, M. A. Characterization of Polylactide-b-Polyisoprene-b-Polylactide Thermoplastic Elastomers. *Biomacromolecules* **2003**, *4*, 216-223.

(79) Lebarbé, T.; Ibarboure, E.; Gadenne, B.; Alfos, C.; Cramail, H. Fully Bio-Based Poly(L-Lactide)-*b*-Poly(Ricinoleic Acid)-*b*-Poly(L-Lactide) Triblock Copolyesters: Investigation of Solid-State Morphology and Thermo-Mechanical Properties. *Polym. Chem.* **2013**, *4*, 3357-3369.

(80) Noppalit, S.; Simula, A.; Ballard, N.; Callies, X.; Asua, J. M.; Billon, L. Renewable Terpene Derivative as a Biosourced Elastomeric Building Block in the Design of Functional Acrylic Copolymers. *Biomacromolecules* **2019**, *20*, 2241-2251.

(81) Noppalit, S.; Simula, A.; Billon, L.; Asua, J. M. Paving the Way to Sustainable Waterborne Pressure-Sensitive Adhesives Using Terpene-Based Triblock Copolymers. *ACS Sustain. Chem. Eng.* **2019**, *7*, 17990-17998.

(82) Gallagher, J. J.; Hillmyer, M. A.; Reineke, T. M. Isosorbide-Based

Polymethacrylates. *ACS Sustain. Chem. Eng.* **2015**, *3*, 662–667.

(83) Gallagher, J. J.; Hillmyer, M. A.; Reineke, T. M. Acrylic Triblock Copolymers Incorporating Isosorbide for Pressure Sensitive Adhesives. *ACS Sustain. Chem. Eng.* **2016**, *4*, 3379–3387.

(84) Nasiri, M.; Reineke, T. M. Sustainable Glucose-Based Block Copolymers Exhibit Elastomeric and Adhesive Behavior. *Polym. Chem.* **2016**, *7*, 5233–5240.

(85) Nasiri, M.; Saxon, D. J.; Reineke, T. M. Enhanced Mechanical and Adhesion Properties in Sustainable Triblock Copolymers via Non-Covalent Interactions. *Macromolecules* **2018**, *51*, 2456–2465.

(86) Chiefari, J.; Chong, Y. K.; Ercole, F.; Krstina, J.; Jeffery, J.; Le, T. P. T.; Mayadunne, R. T. A.; Meijs, G. F.; Moad, C. L.; Moad, G.; Rizzardo, E.; Thang, S. H. Living Free-Radical Polymerization by Reversible Addition - Fragmentation Chain Transfer: The RAFT Process. *Macromolecules* **1998**, *31*, 5559–5562.

(87) Perrier, S. 50th Anniversary Perspective: RAFT Polymerization - A User Guide. *Macromolecules* **2017**, *50*, 7433–7447.

(88) Tong, J. D.; Jerôme, R. Dependence of the Ultimate Tensile Strength of Thermoplastic Elastomers of the Triblock Type on the Molecular Weight between Chain Entanglements of the Central Block. *Macromolecules* **2000**, *33*, 1479–1481.

(89) Tong, J. D.; Jerôme, R. Synthesis of poly(methyl methacrylate)-*b*-poly(n-butyl acrylate)-*b*- poly(methyl methacrylate) Triblocks and Their Potential as

Thermoplastic Elastomers. *Polymer* **2000**, *41*, 2499–2510.

(90) Creton, C. Pressure-Sensitive Adhesives: An Introductory Course. *MRS Bull.* **2003**, *28*, 434–439.

(91) Wang, S.; Shuai, L.; Saha, B.; Vlachos, D. G.; Epps, T. H. From Tree to Tape: Direct Synthesis of Pressure Sensitive Adhesives from Depolymerized Raw Lignocellulosic Biomass. *ACS Cent. Sci.* **2018**, *4*, 701–708.

(92) Vendamme, R.; Schüwer, N.; Eevers, W. Recent Synthetic Approaches and Emerging Bio-Inspired Strategies for the Development of Sustainable Pressure-Sensitive Adhesives Derived from Renewable Building Blocks. *J. Appl. Polym. Sci.* **2014**, *131*, 40669-40685.

(93) Ding, W.; Robertson, M. L. Sustainable Thermoplastic Elastomers with a Transient Network. *Eur. Polym. J.* **2019**, *113*, 411-423.

(94) Li, Y.; Qian, S.; Dunn, R.; Cirino, P. C. Engineering Escherichia Coli to Increase Triacetic Acid Lactone (TAL) Production Using an Optimized TAL Sensor-Reporter System. *J. Ind. Microbiol. Biotechnol.* **2018**, *45*, 789–793.

(95) Abbott, S. *Adhesion Science, Principles and Practice*; DEStech Publications: Lancaster, 2015.

(96) Rehberg, C. E.; Fisher, C. H. Preparation and Properties of the N-Alkyl Acrylates. *J. Am. Chem. Soc.* **1944**, *66*, 1203–1207.

(97) Mogri, Z.; Paul, D. R. Membrane Formation Techniques for Gas Permeation Measurements for Side-Chain Crystalline Polymers. *J. Memb. Sci.* **2000**, *175*, 253–265.

(98) O'Leary, K.; Paul, D. R. Copolymers of Poly(n-Alkyl Acrylates): Synthesis, Characterization, and Monomer Reactivity Ratios. *Polymer* **2004**, *19*, 6576–6585.

(99) Liu, C.; He, J.; Ruymbeke, E. van; Keunings, R.; Bailly, C. Evaluation of Different Methods for the Determination of the Plateau Modulus and the Entanglement Molecular Weight. *Polymer* **2006**, *13*, 4461–4479.

(100) Chatterjee, D. P.; Mandal, B. M. Triblock Thermoplastic Elastomers with Poly(Lauryl Methacrylate) as the Center Block and Poly (Methyl Methacrylate) or Poly(Tert-Butyl Methacrylate) as End Blocks. Morphology and Thermomechanical Properties. *Macromolecules* **2006**, *39*, 9192-9200.

(101) Mahalik, J. P.; Madras, G. Effect of the Alkyl Group Substituents on the Thermal and Enzymatic Degradation of Poly(n-Alkyl Acrylates). *Ind. Eng. Chem. Res.* **2005**, *44*, 4171–4177.

(102) Witkowski, A.; Stec, A. A.; Hull, T. R. Thermal Decomposition of Polymeric Materials. In *SFPE Handbook of Fire Protection Engineering*, 5; Gottuk, D., Hall, J. R. Jr., Harada, K., Kuligowski, E., Puchovsky, M., Torero, J., WAtts, J. M. Jr., Weiczorek, C., Eds.; Springer: New York, 2016; 1, 167-254.

(103) Chia, M.; Haider, M. A.; Pollock, G.; Kraus, G. A.; Neurock, M.; Dumesic, J. A.

Mechanistic Insights into Ring-Opening and Decarboxylation of 2-Pyrones in Liquid Water and Tetrahydrofuran. *J. Am. Chem. Soc.* **2013**, *135*, 5699–5708.

(104) Moad, G.; Rizzardo, E.; Thang, S. H. Living Radical Polymerization by the RAFT Process. *Aust. J. Chem.* **2005**, *58*, 379–410.

(105) Barner-Kowollik, C.; Perrier, S. The Future of Reversible Addition Fragmentation Chain Transfer Polymerization. *J. Polym. Sci. Part A Polym. Chem.* **2008**, *46*, 5715–5723.

(106) Keddie, D. J. A Guide to the Synthesis of Block Copolymers Using Reversible-Addition Fragmentation Chain Transfer (RAFT) Polymerization. *Chem. Soc. Rev.* **2014**, *43*, 496–505.

(107) Fox, T. G.; Flory, P. J. Second-Order Transition Temperatures and Related Properties of Polystyrene. I. Influence of Molecular Weight. *J. Appl. Phys.* **1950**, *21*, 581-591.

(108) Chang, E. P. Viscoelastic Properties of Pressure-Sensitive Adhesives. *J. Adhes.* **1997**, *60*, 233–248.

(109) Benedek, I. *Pressure-Sensitive Adhesives and Applications - Second Edition , Revised and Expanded*; Marcel Dekker: New York, 2004.

(110) Daoulas, K. C.; Theodorou, D. N.; Roos, A.; Creton, C. Experimental and Self-Consistent-Field Theoretical Study of Styrene Block Copolymer Self-Adhesive Materials. *Macromolecules* **2004**, *37*, 5093–5109.

(111) Nakajima, N.; Babrowicz, R.; Harrell, E. R. Rheology, Composition, and Peel-mechanism of Block Copolymer–Tackifier-based Pressure Sensitive Adhesives. *J. Appl. Polym. Sci.* **1992**, *44*, 1437–1456.

(112) Brown, K.; Hooker, J. C.; Creton, C. Micromechanisms of Tack of Soft Adhesives Based on Styrenic Block Copolymers. *Macromol. Mater. Eng.* **2002**, *287*, 163–179.

(113) Van Der Ploeg, F. Natural Resources: Curse or Blessing? *Journal of Economic Literature*. 2011, *49*, 366 – 420.

(114) Fagnani, D. E.; Tami, J. L.; Copley, G.; Clemons, M. N.; Getzler, Y. D. Y. L.; McNeil, A. J. 100th Anniversary of Macromolecular Science Viewpoint: Redefining Sustainable Polymers. *ACS Macro Lett.* **2021**, *10*, 41 – 53.

(115) Sajjad, H.; Tolman, W. B.; Reineke, T. M. Block Copolymer Pressure-Sensitive Adhesives Derived from Fatty Acids and Triacetic Acid Lactone. *ACS Appl. Polym. Mater.* **2020**, *2*, 2719 – 2728.

(116) Kamber, N. E.; Jeong, W.; Waymouth, R. M.; Pratt, R. C.; Lohmeijer, B. G. G.; Hedrick, J. L. Organocatalytic Ring-Opening Polymerization. *Chem. Rev.* **2007**, *107*, 5813 – 5840.

(117) Nuyken, O.; Pask, S. D. Ring-Opening Polymerization-An Introductory Review. *Polymers* **2013**, *5*, 361 – 403.

(118) Dubois, P.; Coulembier, O.; Raquez, J. M. *Handbook of Ring-Opening*

Polymerization; 2009.

(119) Olsén, P.; Odelius, K.; Albertsson, A. C. Thermodynamic Presynthetic Considerations for Ring-Opening Polymerization. *Biomacromolecules* **2016**, *17*, 699 – 709.

(120) Duda, A.; Kowalski, A.; Libiszowski, J.; Penczek, S. Thermodynamic and Kinetic Polymerizability of Cyclic Esters. *Macromolecular Symposia* **2005**, *224*, 71 – 84.

(121) Fahnhorst, G. W.; Hoye, T. R. A Carbomethoxylated Polyvalerolactone from Malic Acid: Synthesis and Divergent Chemical Recycling. *ACS Macro Lett.* **2018**, *7*, 143 – 147.

(122) Fahnhorst, G. W.; De Hoe, G. X.; Hillmyer, M. A.; Hoye, T. R. 4-Carboalkoxylated Polyvalerolactones from Malic Acid: Tough and Degradable Polyesters. *Macromolecules* **2020**.

(123) Xu, S.; Wang, Y.; Hoye, T. R. Poly(4-Ketovalerolactone) from Levulinic Acid: Synthesis and Hydrolytic Degradation. *Macromolecules* **2020**, *53*, 3194 – 3201.

(124) Hoye, T. R.; Hanson, P. R.; Vyvyan, J. R. A Practical Guide to First-Order Multiplet Analysis in 1H NMR Spectroscopy. *J. Org. Chem.* **1994**. *59*, 4096 – 4103.

(125) Hoye, T. R.; Zhao, H. A Method for Easily Determining Coupling Constant Values: An Addendum to "a Practical Guide to First-Order Multiplet Analysis in 1H NMR Spectroscopy." *J. Org. Chem.* **2002**, *67*, 4014 – 4016.

(126) Brandänge, S.; Färnbäck, M.; Leijonmarck, H.; Sundin, A. Highly Diastereoselective Hydrogenations Leading to β-Hydroxy δ-Lactones in Hydroxy-Protected Form. A Modified View of δ-Lactone Conformations. *J. Am. Chem. Soc.* **2003**, *125*, 11942 – 11955.

(127) Häusler, J. Synthese von Rac-Detoxinin. *Liebigs Ann. der Chemie* **1983**, *6*, 982 – 992.

(128) Bennett, F.; Knight, D. W.; Fenton, C. Methyl (3R)-3-Hydroxyhex-5-Enoate as a Precursor to Chiral Mevinic Acid Analogues. *J. Chem. Soc. Perkin Trans.* **1991**, 133 – 140.

(129) Hansen, C. A.; Frost, J. W. Deoxygenation of Polyhydroxybenzenes: An Alternative Strategy for the Benzene-Free Synthesis of Aromatic Chemicals. *J. Am. Chem. Soc.* **2002**, *124*, 5926 – 5927.

(130) Pirkle, W. H.; Adams, P. E. Enantiomerically Pure Lactones. 3. Synthesis of and Stereospecific Conjugate Additions to α,β-Unsaturated Lactones. *J. Org. Chem.* **1980**, *45*, 4117 – 4121.

(131) Kido, F.; Sinha, S. C.; Abiko, T.; Watanabe, M.; Yoshikoshi, A. New Entry to the Perhydrofuro[2,3-b]Furan Ring System. *J. Chem. Soc. Chem. Commun.* **1990**, 418 – 420.

(132) Makiguchi, K.; Satoh, T.; Kakuchi, T. Diphenyl Phosphate as an Efficient Cationic Organocatalyst for Controlled/Living Ring-Opening Polymerization of δ-

Valerolactone and ε-Caprolactone. *Macromolecules* **2011**, *44*, 1999 – 2005.

(133) Williams, C. K.; Breyfogle, L. E.; Choi, S. K.; Nam, W.; Young, V. G.; Hillmyer, M. A.; Tolman, W. B. A Highly Active Zinc Catalyst for the Controlled Polymerization of Lactide. *J. Am. Chem. Soc.* **2003**, *125*, 11350 – 11359.

(134) Macaranas, J. A.; Luke, A. M.; Mandal, M.; Neisen, B. D.; Marell, D. J.; Cramer, C. J.; Tolman, W. B. Sterically Induced Ligand Framework Distortion Effects on Catalytic Cyclic Ester Polymerizations. *Inorg. Chem.* **2018**, *57*, 3451 – 3457.

(135) Luke, A. M.; Peterson, A.; Chiniforoush, S.; Mandal, M.; Popowski, Y.; Sajjad, H.; Bouchey, C. J.; Shopov, D. Y.; Graziano, B. J.; Yao, L. J.; et al. Mechanism of Initiation Stereocontrol in Polymerization of Rac-Lactide by Aluminum Complexes Supported by Indolide-Imine Ligands. *Macromolecules* **2020**, *53*, 1809 – 1818.

(136) Batiste, D. C.; Meyersohn, M. S.; Watts, A.; Hillmyer, M. A. Efficient Polymerization of Methyl-ϵ-Caprolactone Mixtures to Access Sustainable Aliphatic Polyesters. *Macromolecules* **2020**, *53*, 1795 – 1808.

(137) Gilding, D. K.; Reed, A. M. Biodegradable Polymers for Use in Surgery-Polyglycolic/Poly(Actic Acid) Homo- and Copolymers: 1. *Polymer* **1979**, *20*, 1459 – 1464.

(138) Labet, M.; Thielemans, W. Synthesis of Polycaprolactone: A Review. *Chem. Soc. Rev.* **2009**, *38*, 3484 – 3504.

(139) Aubin, M.; Prud'homme, R. E. Preparation and Properties of Poly(Valerolactone). *Polymer* **1981**.

(140) Hong, M.; Chen, E. Y. X. Completely Recyclable Biopolymers with Linear and Cyclic Topologies via Ring-Opening Polymerization of γ-Butyrolactone. *Nat. Chem.* **2016**, *8*, 42 – 49.

(141) van't Hoff, M. J. H. Etudes de Dynamique Chimique. *Recl. des Trav. Chim. des Pays-Bas* **1884**.

(142) Baśko, M.; Kubisa, P. Cationic Copolymerization of ε-Caprolactone and L,L-Lactide by an Activated Monomer Mechanism. *J. Polym. Sci. Part A Polym. Chem.* **2006**, *44*, 7071 – 7081.

(143) Pang, X.; Zhuang, X.; Tang, Z.; Chen, X. Polylacic Acid (PLA): Research, Development and Industrialization. *Biotechnology Journal* **2010**, *5*, 1125 – 1136.

(144) Saeidlou, S.; Huneault, M. A.; Li, H.; Park, C. B. Poly(Lactic Acid) Crystallization. *Progress in Polymer Science* **2012**, *37*, 1657 – 1677.

(145) Lendlein, A.; Sisson, A. *Handbook of Biodegradable Polymers: Isolation, Synthesis, Characterization and Applications*; Wiley-VCH Verlag GmbH & Co. KGaA, 2011.

(146) Kamaly, N.; Yameen, B.; Wu, J.; Farokhzad, O. C. Degradable Controlled-Release Polymers and Polymeric Nanoparticles: Mechanisms of Controlling Drug Release. *Chem. Rev.* **2016**, *116*, 2602-2663.

(147) Uhrich, K. E.; Cannizzaro, S. M.; Langer, R. S.; Shakesheff, K. M. Polymeric Systems for Controlled Drug Release. *Chem. Rev.* **1999**, *99*, 3181-3198.

(148) Zhang, Z.; Ortiz, O.; Goyal, R.; Kohn, J. Biodegradable Polymers. In *Principles of Tissue Engineering: Fourth Edition*; Elsevier, 2013, 441-473.

(149) Jothimani, B.; Venkatachalapathy, B.; Karthikeyan, N. S.; Ravichandran, C. A Review on Versatile Applications of Degradable Polymers. In *Green Biopolymers and their Nanocomposites;* Springer, Singapore, 2019, 403-422.

(150) Vroman, I.; Tighzert, L. Biodegradable Polymers. *Materials* **2009**, *2*, 307-344.

(151) Luckachan, G. E.; Pillai, C. K. S. Biodegradable Polymers- A Review on Recent Trends and Emerging Perspectives. *J. Polym. Environ.* **2011**, *19*, 637-676.

(152) Jiang, L.; Zhang, J. Biodegradable Polymers and Polymer Blends. In *Handbook of Biopolymers and Biodegradable Plastics: Properties, Processing and Applications*; Elsevier, 2013, 109-128.

(153) Gunatillake, P. A.; Adhikari, R.; Gadegaard, N. Biodegradable Synthetic Polymers for Tissue Engineering. *Eur Cell Mater.* **2003**, *5*, 1-16.

(154) Herwig, G.; Dove, A. P. Synthesis of Rapidly Surface Eroding Polyorthoesters and Polyacetals Using Thiol-Ene Click Chemistry. *ACS Macro Lett.* **2019**, *8*, 1268-1274.

(155) Göpferich, A. Mechanisms of Polymer Degradation and Erosion. *Biomaterials*

1996, *17*, 103-114.

(156) Burkersroda, F. Von; Schedl, L.; Göpferich, A. Why Degradable Polymers Undergo Surface Erosion or Bulk Erosion. *Biomaterials* **2002**, *23*, 4221-4231.

(157) Kumar, N.; Langer, R. S.; Domb, A. J. Polyanhydrides: An Overview. *Adv. Drug Deliv. Rev.* **2002**, *54*, 889-910.

(158) Basu, A.; Domb, A. J. Recent Advances in Polyanhydride Based Biomaterials. *Adv. Mater*. **2018**, *30*, 1706815.

(159) Dang, W.; Daviau, T.; Ying, P.; Zhao, Y.; Nowotnik, D.; Clow, C. S.; Tyler, B.; Brem, H. Effects of GLIADEL® Wafer Initial Molecular Weight on the Erosion of Wafer and Release of BCNU. *J. Control. Release* **1996**, *42*, 83-92.

(160) Deronde, B. M.; Carbone, A. L.; Uhrich, K. Storage Stability Study of Salicylate-Based Poly(Anhydride-Esters). *Polym. Degrad. Stab.* **2010**, *95*, 1778-1782.

(161) Leong, K. W.; Simonte, V.; Langer, R. Synthesis of Polyanhydrides: Melt-Polycondensation, Dehydrochlorination, and Dehydrative Coupling. *Macromolecules* **1987**, *20*, 705-712.

(162) Uhrich, K. E.; Gupta, A.; Thomas, T. T.; Laurencin, C. T.; Langer, R. Synthesis and Characterization of Degradable Poly(Anhydride-Co-Imides). *Macromolecules* **1995**, *28*, 2184-2193.

(163) Muggli, D. S.; Burkoth, A. K.; Keyser, S. A.; Lee, H. R.; Anseth, K. S. Reaction

Behavior of Biodegradable, Photo-Cross-Linkable Polyanhydrides. *Macromolecules* **1998**, *31*, 4120-4125.

(164) Anseth, K. S.; Shastri, V. R.; Langer, R. Photopolymerizable Degradable Polyanhydrides with Osteocompatibility. *Nat. Biotechnol.* **1999**, *17*, 156-159.

(165) Tarcha, P. J.; Su, L.; Baker, T.; Langridge, D.; Shastri, V.; Langer, R. Stability of Photocurable Anhydrides: Methacrylic Acid Mixed Anhydrides of Nontoxic Diacids. *J. Polym. Sci. Part A Polym. Chem.* **2001**, *39*, 4189-4195.

(166) Burkoth, A. K.; Anseth, K. S. A Review of Photocrosslinked Polyanhydrides: In Situ Forming Degradable Networks. *Biomaterials* **2000**, *21*, 2395-2404.

(167) Rutherglen, B. G.; McBath, R. A.; Huang, Y. L.; Shipp, D. A. Polyanhydride Networks from Thiol-Ene Polymerizations. *Macromolecules* **2010**, *43*, 10297-10303.

(168) Shipp, D. A.; McQuinn, C. W.; Rutherglen, B. G.; McBath, R. A. Elastomeric and Degradable Polyanhydride Network Polymers by Step-Growth Thiol-Ene Photopolymerization. *Chem. Commun.* **2009**, *42*, 6415-6417.

(169) Poetz, K. L.; Mohammed, H. S.; Snyder, B. L.; Liddil, G.; Samways, D. S. K.; Shipp, D. A. Photopolymerized Cross-Linked Thiol-Ene Polyanhydrides: Erosion, Release, and Toxicity Studies. *Biomacromolecules* **2014**, *15*, 2573-2582.

(170) Poetz, K. L.; Durham, O. Z.; Shipp, D. A. Polyanhydride Nanoparticles by “click” Thiol-Ene Polymerization. *Polym. Chem.* **2015**, *6*, 5464-5469.

(171) Poetz, K. L.; Mohammed, H. S.; Shipp, D. A. Surface Eroding, Semicrystalline Polyanhydrides via Thiol-Ene "Click" Photopolymerization. *Biomacromolecules* **2015**, *16*, 1650-1659.

(172) Hoyle, C. E.; Bowman, C. N. Thiol-Ene Click Chemistry. *Angew. Chem. Int. Ed.* **2010**, *49*, 1540-1573.

(173) Lowe, A. B. Thiol-Ene "Click" Reactions and Recent Applications in Polymer and Materials Synthesis: A First Update. *Polym. Chem*. **2014**, *5*, 4820-4870.

(174) Lambert, S.; Wagner, M. Environmental Performance of Bio-Based and Biodegradable Plastics: The Road Ahead. *Chem. Soc. Rev.* **2017**, *46*, 6855-6871.

(175) Okabe, M.; Lies, D.; Kanamasa, S.; Park, E. Y. Biotechnological Production of Itaconic Acid and Its Biosynthesis in Aspergillus Terreus. *Appl Microbiol Biotechnol*. **2009**, *84*, 597-606.

(176) Werpy, T.; Petersen, G. *Top Value Added Chemicals from Biomass: Volume I -- Results of Screening for Potential Candidates from Sugars and Synthesis Gas*. United States, 2004.

(177) Bafana, R.; Pandey, R. A. New Approaches for Itaconic Acid Production: Bottlenecks and Possible Remedies. *Critical Reviews in Biotechnology*. **2018**, *38*, 68-82.

(178) Penelle, J.; Collot, J.; Rufflard, G. Kinetic and Thermodynamic Analysis of Methyl Ethacrylate Radical Polymerization. *J. Polym. Sci. Part A Polym. Chem.*

1993, *31*, 2407-2412.

(179) Trotta, J. T.; Jin, M.; Stawiasz, K. J.; Michaudel, Q.; Chen, W. L.; Fors, B. P. Synthesis of Methylene Butyrolactone Polymers from Itaconic Acid. *J. Polym. Sci. Part A Polym. Chem.* **2017**, *55*, 2730-2737.

(180) Cramer, N. B.; Reddy, S. K.; O'Brien, A. K.; Bowman, C. N. Thiol - Ene Photopolymerization Mechanism and Rate Limiting Step Changes for Various Vinyl Functional Group Chemistries. *Macromolecules* **2003**, *36*, 7964-7969.

(181) Cowie, J. M. G.; Hag, Z. Poly(mono n-alkyl itaconic acid esters): Their preparation and some physical properties. Polym. Inter. **1977**, *9*, 241-245.

(182) Lillie, L. M.; Tolman, W. B.; Reineke, T. M. Structure/Property Relationships in Copolymers Comprising Renewable Isosorbide, Glucarodilactone, and 2,5-Bis(Hydroxymethyl)Furan Subunits. *Polym. Chem.* **2017**, *8*, 3746-3754.

(183) Reddy, S. K.; Okay, O.; Bowman, C. N. Network Development in Mixed Step-Chain Growth Thiol-Vinyl Photopolymerizations. *Macromolecules* **2006**, *39*, 8832-8843.

(184) Hoyle, C. E.; Lee, T. Y.; Roper, T. Thiol-Enes: Chemistry of the Past with Promise for the Future. *J. Polym. Sci. Part A Polym. Chem.* **2004**, *42*, 5301-5338.